

Loughborough University Institutional Repository

Photoplethysmography in noninvasive cardiovascular assessment

This item was submitted to Loughborough University's Institutional Repository by the/an author.

Additional Information:

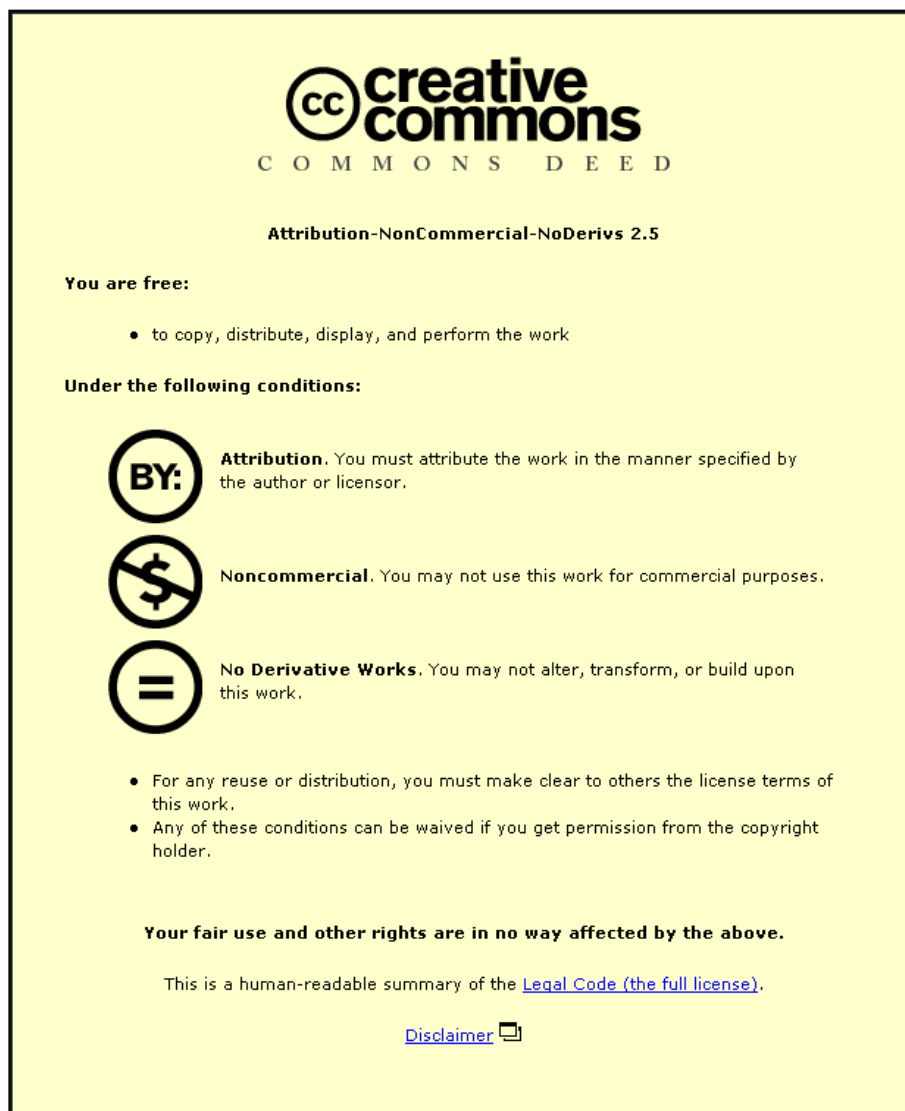
- A Doctoral Thesis. Submitted in partial fulfillment of the requirements for the award of Doctor of Philosophy of Loughborough University.

Metadata Record: <https://dspace.lboro.ac.uk/2134/5399>

Publisher: © Ping Shi

Please cite the published version.

This item was submitted to Loughborough's Institutional Repository (<https://dspace.lboro.ac.uk/>) by the author and is made available under the following Creative Commons Licence conditions.



For the full text of this licence, please go to:
<http://creativecommons.org/licenses/by-nc-nd/2.5/>

Thesis Access Form

Copy No.....Location.....

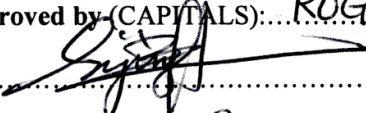
Author PING SHI

Title PHOTOPLETHYSMOGRAPHY IN NONINVASIVE CARDIOVASCULAR ASSESSMENT

Status of access OPEN / RESTRICTED / CONFIDENTIAL

Moratorium Period:.....years, ending...../.....200.....

Conditions of access approved by (CAPITALS): ROGER GOODALL

Supervisor (Signature).....

Department of ELECTRONIC & ELECTRICAL ENGINEERING

Author's Declaration: *I agree the following conditions:*

Open access work shall be made available (in the University and externally) and reproduced as necessary at the discretion of the University Librarian or Head of Department. It may also be digitised by the British Library and made freely available on the Internet to registered users of the EThOS service subject to the EThOS supply agreements.

The statement itself shall apply to ALL copies including electronic copies:

This copy has been supplied on the understanding that it is copyright material and that no quotation from the thesis may be published without proper acknowledgement.

Restricted/confidential work: All access and any photocopying shall be strictly subject to written permission from the University Head of Department and any external sponsor, if any.

Author's signature Ping Shi Date 6/10/2009

users declaration: for signature during any Moratorium period (Not Open work): <i>I undertake to uphold the above conditions:</i>			
Date	Name (CAPITALS)	Signature	Address



CERTIFICATE OF ORIGINALITY

This is to certify that I am responsible for the work submitted in this thesis, that the original work is my own except as specified in acknowledgments or in footnotes, and that neither the thesis nor the original work contained therein has been submitted to this or any other institution for a degree.

.....*Ping Shi*..... (Signed)

.....*6/10/2009*..... (Date)

DEPARTMENT OF ELECTRICAL AND ELECTRONIC ENGINEERING

FACULTY OF ENGINEERING

LOUGHBOROUGH UNIVERSITY

PHOTOPLETHYSMOGRAPHY IN NONINVASIVE CARDIOVASCULAR ASSESSMENT

BY

PING SHI

A Doctoral Thesis

Submitted in partial fulfilment of the requirements for the award of
Doctor of Philosophy of Loughborough University

May 2009

Supervisor: Dr Sijung Hu

Co-supervisor: Professor Ron Summers

Department of Electronic and Electrical Engineering

© Copyright
Ping Shi, 2009

To my family

ABSTRACT

The electro-optic technique of measuring the cardiovascular pulse wave known as photoplethysmography (PPG) is clinically utilised for noninvasive characterisation of physiological components by dynamic monitoring of tissue optical absorption. There has been a resurgence of interest in this technique in recent years, driven by the demand for a low cost, compact, simple and portable technology for primary care and community-based clinical settings, and the advancement of computer-based pulse wave analysis techniques. PPG signal provides a means of determining cardiovascular properties during the cardiac cycle and changes with ageing and disease. This thesis focuses on the photoplethysmographic signal for cardiovascular assessment.

The contour of the PPG pulse wave is influenced by vascular ageing. Contour analysis of the PPG pulse wave provides a rapid means of assessing vascular tone and arterial stiffness. In this thesis, the parameters extracted from the PPG pulse wave are examined in young adults. The results indicate that the contour parameters of the PPG pulse wave could provide a simple and noninvasive means to study the characteristic change relating to arterial stiffness.

The pulsatile component of the PPG signal is due to the pumping action of the heart, and thus could reveal the circulation changes of a specific vascular bed. Heart rate variability (HRV) represents one of the most promising quantitative markers of cardiovascular control. Calculation of HRV from the peripheral pulse wave using PPG, called pulse rate variability (PRV), is investigated. The current work has confirmed that the PPG signal could provide basic information about heart rate (HR) and its variability, and highly suggests a good alternative to understanding dynamics pertaining to the autonomic nervous system (ANS) without the use of an

electrocardiogram (ECG) device. Hence, PPG measurement has the potential to be readily accepted in ambulatory cardiac monitoring due to its simplicity and comfort.

Noncontact PPG (NPPG) is introduced to overcome the current limitations of contact PPG. As a contactless device, NPPG is especially attractive for physiological monitoring in ambulatory units, NICUs, or trauma centres, where attaching electrodes is either inconvenient or unfeasible. In this research, a prototype for noncontact reflection PPG (NRPPG) with a vertical cavity surface emitting laser (VCSEL) as a light source and a high-speed PiN photodiode as a photodetector is developed. The results from physiological experiments suggest that NRPPG is reliable to extract clinically useful information about cardiac condition and function.

In summary, recent evidence demonstrates that PPG as a simple noninvasive measurement offers a fruitful avenue for noninvasive cardiovascular monitoring.

Key words: Photoplethysmography (PPG), Cardiovascular assessment, Pulse wave contour analysis, Arterial stiffness, Heart rate (HR), Heart rate variability (HRV), Pulse rate variability (PRV), Autonomic nervous system (ANS), Electrocardiogram (ECG).

ACKNOWLEDGEMENTS

I am extremely grateful to Dr *Sijung Hu*. Without his continual guidance and instruction this study would not have been possible. As my supervisor, he has been a source of direction. He encouraged me to independently thinking, build and experiment without any restriction. I would also particularly acknowledge my co-supervisor Professor *Ron Summers* for his assistance and guidance for completion of this thesis.

I would like to express my profound sense of gratitude to Professor *Yisheng Zhu*, Head of Department of Biomedical Engineering, Shanghai Jiao Tong University, for his advice, supervision and continuous support during all these years.

I gratefully thank Professor *Shanbao Tong* and Dr *Yihong Qiu*, Department of Biomedical Engineering, Shanghai Jiao Tong University, for supporting this work.

I appreciate all the help I have got from *Angelos Echiadis*, *Vicente Azorin-Peris*, *Jia Zheng* and *Dave Stevens*. I also want to express my thanks to all the volunteers who take part in the experiments and provide the valuable physiological data that lead to the new findings in this thesis.

I gratefully acknowledge the financial support of this work by Loughborough University and Shanghai Jiao Tong University.

I wish to express my deep gratitude to my mother and father for all their love, support and encouragement, which they have unselfishly given me all my lives. I owe my warmest thanks to my husband *Guoning*, whose understanding love and support has been irreplaceable.

LIST OF PUBLICATIONS AND COMMUNICATIONS

This thesis is based on the following original publications or communications:

P Shi, S Hu, Y Zhu, J Zheng, Y Qiu, S Tong and P Cheang, “Insight into the dicrotic notch in photoplethysmographic pulses from finger tip of young adults”, *Journal of Medical Engineering & Technology*, 2009, DOI: 10.1080/03091900903150980.

P Shi, Y Zhu, J Allen and S Hu, “Analysis of pulse rate variability derived from photoplethysmography with the combination of lagged Poincaré plots and spectral characteristics”, *Medical Engineering & Physics*, 2009, 31(7): 866-871.

P Shi, S Hu and Y Zhu, “A preliminary attempt to understand compatibility of photoplethysmographic pulse rate variability with electrocardiogram heart rate variability”, *Journal of Medical and Biological Engineering*, 2008, 28(4): 173-180.

P Shi, S Hu, A Echiadis, V Azorin-Peris, J Zheng and Y Zhu, “Development of a remote photoplethysmographic technique for human biometrics”, 2009, *Proceedings of SPIE: Design and Quality for Biomedical Technologies II*, Vol. 7170, 717006.

P Shi, V Azorin-Peris, A Echiadis, P Cheang, J Zheng, Y Zhu and S Hu, “Non-contact reflection photoplethysmography towards effective human physiological monitoring”, *IOP Photon08 Conference*, 26-29 August 2008, Herriot-Watt University, Edinburgh, UK.

P Shi, V Azorin-Peris, A Echiadis, J Zheng, Y Zhu and S Hu, “Non-contact reflection photoplethysmography towards effective human physiological monitoring”, submitted to *Journal of Medical and Biological Engineering*, revision.

TABLE OF CONTENTS

ABSTRACT.....	3
ACKNOWLEDGEMENTS.....	5
LIST OF PUBLICATIONS AND COMMUNICATIONS	6
TABLE OF CONTENTS.....	7
LIST OF TABLES	12
LIST OF FIGURES.....	14
ABBREVIATIONS.....	16

CHAPTER 1 INTRODUCTION

1.1 Background and motivation.....	20
1.2 Aim and objectives	22
1.3 Thesis overview.....	23

CHAPTER 2 PHOTOPLETHYSMOGRAPHY: PRINCIPLES AND MEASUREMENT SYSTEM

2.1 Introduction	26
2.2 Principles of photoplethysmography.....	26
2.2.1 The origins of the PPG waveform	26
2.2.2 PPG signal	31
2.3 History of PPG.....	32
2.4 PPG measurement system	33
2.4.1 PPG Instrumentation.....	33

2.4.2	Two modes of PPG operation.....	34
2.4.2.1	<i>Transmission mode</i>	35
2.4.2.2	<i>Reflection mode</i>	35
2.5	Practical applications of PPG.....	37
2.5.1	Measurement protocols.....	37
2.5.2	Limitations of current contact PPG	37
2.5.3	Noncontact PPG.....	38
2.6	Clinical applications of PPG	39
2.6.1	Clinical physiological monitoring	39
2.6.2	Vascular assessment	40
2.6.3	Autonomic function	41
2.7	Summary	41

CHAPTER 3

NONINVASIVE CARDIOVASCULAR ASSESSMENT

3.1	Contour analysis of PPG pulse wave.....	44
3.1.1	Interpretation of pulse wave changes	44
3.1.1.1	<i>Respiratory interaction</i>	44
3.1.1.2	<i>Amplitude</i>	44
3.1.1.3	<i>Area under the curve and the dicrotic notch</i>	45
3.1.1.4	<i>Baseline width</i>	45
3.1.2	Measurement and contour analysis of photoplethysmographic pulse	45
3.2	Heart rate variability and pulse rate variability	47
3.2.1	HRV from ECG	47
3.2.1.1	<i>ECG recording</i>	47
3.2.1.2	<i>Mechanisms of HRV</i>	50
3.2.2	PRV from PPG	51
3.2.2.1	<i>Mechanisms of PRV</i>	51
3.2.2.2	<i>Comparability of PRV and HRV</i>	51
3.2.3	Measurement of HRV	52
3.2.3.1	<i>Time domain methods</i>	53

3.2.3.2	<i>Frequency domain methods</i>	55
3.2.3.3	<i>Nonlinear analysis methods</i>	57
3.3	Summary	60

CHAPTER 4

CARDIOVASCULAR MONITORING SETUPS, PROTOCOLS AND APPROACHES

4.1	Engineering setups	62
4.1.1	Contact measurement.....	62
4.1.2	Noncontact measurement.....	64
4.1.2.1	<i>Noncontact reflection PPG model</i>	64
4.1.2.2	<i>Noncontact reflection PPG photonics engineering setup</i>	66
4.2	Protocols	67
4.3	Physiological parameter measurements	71
4.3.1	Contour analysis of PPG waveform	71
4.3.2	Measurement of HRV and PRV	73
4.3.2.1	<i>Time Domain measures</i>	73
4.3.2.2	<i>Frequency domain measures</i>	73
4.3.2.3	<i>Nonlinear measures</i>	74
4.4	Statistical analysis	75
4.5	Summary	77

CHAPTER 5

PHYSIOLOGICAL CHARACTERISTICS DERIVED FROM PHOTOPLETHYSMOGRAPHY SIGNALS

5.1	Dicrotic notch in PPG waveform from young adults	80
5.2	PPG technique for physiological monitoring	84
5.2.1	PPG PRV as a surrogate to ECG HRV.....	84
5.3	Combination of lagged Poincaré plot and spectral characteristics to analyse pulse rate variability	91
5.3.1	Frequency domain parameters	91

5.3.2	Lagged Poincaré plots indices	92
5.3.3	Correlation between lagged Poincaré plot indices and frequency domain parameters	93
5.4	Noncontact PPG as a substitute technique for contact PPG	95
5.4.1	Geometrical parameters for noncontact reflection PPG photonics engineering setup	95
5.4.2	The feature of synchronised PPG signals	96
5.4.3	The spectra of PPG signals	97
5.4.4	Results from recurrence plot	98
5.4.5	The agreement analysis of PPG signal for physiological parameters	100
5.5	The effectiveness of noncontact PPG for physiological monitoring ...	102
5.6	Summary	104

CHAPTER 6

DISCUSSION

6.1	Waveform analysis for arterial stiffness	106
6.2	PPG-derived PRV as a surrogate to ECG-derived HRV	109
6.3	Combination of lagged Poincaré plot and spectral characteristics to analyse pulse rate variability	111
6.4	Noncontact PPG as a substitute technique for contact PPG	113
6.4.1	Geometrical parameters in noncontact reflection PPG photonics engineering setup	113
6.4.2	Comparison of PPG signals between NRPPG and CPPG	114
6.5	The effectiveness of noncontact PPG for physiological monitoring ...	116

CHAPTER 7

CONCLUSIONS AND FURTHER WORK

7.1	Conclusions	118
7.1.1	Waveform analysis	118

7.1.2	Reliability of PPG in heart rate monitoring	118
7.1.3	Utility of PRV in heart activity assessment	119
7.1.4	Feasibility of noncontact PPG	119
7.2	Future work	119
7.2.1	Standardisation of measurements	119
7.2.2	Advanced signal processing	120
7.2.3	Understanding of physiology-related PPG	120
7.2.4	Multi-location utility.....	120
7.2.5	Engineering improvements on noncontact PPG	121
7.2.6	All-in-one monitoring.....	121
 APPENDIX A:		
AUTOCORRELATION AND AUTOCOVARIANCE.....		122
 APPENDIX B:		
RECURRENCE PLOT STRUCTURES.....		123
 APPENDIX C:		
DESIGN OF INFINITE IMPULSE RESPONSE DIGITAL FILTER...		129
 REFERENCES		135

LIST OF TABLES

Table No.	Title of Tables
2-1	Approximate depth for penetration of optical radiation in fair Caucasian skin to a value of $1/e$ (37%) of the incident energy density
3-1	Time domain measures of HRV
3-2	Frequency domain measures of HRV
4-1	Descriptive information of participants in Studies I-V
4-2	Overview of the protocols in Studies I-V
4-3	Descriptions of the PPG features
4-4	The measures in Studies I-V
5-1	Waveform information
5-2	Waveform characteristics
5-3	Agreement analysis between ePRV or fPRV from PPG and HRV from ECG.
5-4	Correlation coefficient (r) between ePRV or fPRV from PPG and HRV from ECG
5-5	Kurtosis and Skewness coefficients of RRI and PPI distribution
5-6	Time domain and frequency domain analyses for the first selected subject
5-7	Time domain and frequency domain analyses for the second selected subject
5-8	Comparisons from frequency domain between habitual smokers and non-smokers
5-9	Summary of lagged Poincaré plot indices in smoker group and non-smoker group

5-10	Three ranges depending on the quality of opto-electronic signal
5-11	The comparison and correlation relationship between CPPG and NRPPG for PR variables parameters
B-1	Typical patterns in RPs and their meanings

LIST OF FIGURES

Figure No.	Title of Figures
2-1	The structure of the skin showing the blood vessels
2-2	A tissue optical window exists between 600 and 1300 nm
2-3	Absorption spectra of Hb and HbO ₂
2-4	PPG signal
2-5	Electronic building blocks used in a typical PPG measurement system
2-6	Two modes of PPG operation
3-1	Classification of the digital volume pulse (DVP) waveform
3-2	The 12-lead ECG is formed by the 3 bipolar surface leads: I, II, and III; the augmented Wilson terminal referenced limb leads: aVR , aVL , and aVF ; and the Wilson terminal referenced chest leads: V1 , V2 , V3 , V4, V5 , and V6
3-3	A stylised version of a normal lead II recording showing the P wave, QRS complex, and the T and U waves
3-4	Scheme of the cardiovascular control mechanisms responsible for the main periodic fluctuations in heart rate
3-5	A typical Poincaré plot
4-1	Contact measurement setup
4-2	Simplified representation of light distribution
4-3	Instrumental hardware setup for NRPPG system illustrating the fundamental parameters
4-4	The schematic dicrotic notch and the associated parameters
5-1	Linear correlation analysis between relevant parameters

5-2	Linear correlation analysis between age and relevant parameters
5-3	Box-and-whisker plot for time domain variables and frequency domain variables from ePRV, fPRV and HRV
5-4	Poincaré plot of the PPI from ePRV, fPRV and RRI from HRV
5-5	Density distribution of NN interval from one subject
5-6	The correlations between SD1 _m and frequency domain indices
5-7	The correlations between SD2 _m and frequency domain indices
5-8	The correlation between SD1 _m /SD2 _m and LF/HF
5-9	Representative PPG signals captured from NRPPG photonics engineering setup
5-10	Comparison of CPPG and NRPPG signals
5-11	The spectra of PPG signals
5-12	Frequency spectrum of the PPG signal from a representative person
5-13	Recurrence plot is introduced as a graphical tool to tentatively study the (a) CPPG signal and (b) NRPPG signal
5-14	Bland-Altman plot is applied to agreement analysis between CPPG and NRPPG for Range of PPI
5-15	Illustrated individuals: (a) SD1, (b) SD2 and (c) their ratio SD1/SD2 from the physiological monitoring
5-16	Representative Poincaré plots demonstrated cardiovascular variations in morning and afternoon in same day
6-1	Separate waveforms with same RI and SI, and different PNL and PNRA
B-1	Three commonly used norms for the neighbourhood
B-2	Characteristic typology of recurrence plots
C-1	Sketches of frequency responses of Butterworth filter
C-2	Magnitude-frequency response for BZT
C-3	The original ECG signal and the filtered ECG signal
C-4	The spectrum of the original ECG signal and the filtered ECG signal

ABBREVIATIONS

ADC	Analogue-to-digital converter
AGC	Automatic gain control
ANS	Autonomic nervous system
BRS	Baroreflex sensitivity
BZT	Bilinear z-transform
CPPG	Contact PPG
CNS	Central nervous system
DI	Distribution index
DVP	Digital volume pulse
DNS	Dicrotic notch searching
ECG	Electrocardiography
ePRV	Ear pulse rate variability
ESC	European Society of Cardiology
FFT	Fast Fourier transform
FIR	Finite impulse response
fPRV	Finger pulse rate variability
HR	Heart rate
HRT	Heart rate turbulence
HRV	Heart rate variability
HF	high frequency component of HRV: 0.15-0.4 Hz
HF(n.u.)	HF expressed in normalised units (n.u.)
Hb	Haemoglobin
HbO₂	Oxyhaemoglobin
IIR	Infinite impulse response
IQR	Interquatile range

LA	Limits of agreement
LED	High-intensity light-emitting diodes
LF	Low frequency component of HRV: 0.04-0.15 Hz
LF(n.u.)	LF expressed in normalised units (n.u.)
MBS	Microprocessor-based system
MPM	Pairwise means
NASPE	North American Society of Pacing and Electrophysiology
NIBM	Noninvasive biomedical monitoring
NI	Notch index
NIR	near infrared
NIMD	Noninvasive medical diagnosis
NN	Normal-to-normal
NN50	Number of interval differences of successive NN intervals greater than 50 ms
NPPG	Noncontact PPG
NRPPG	Noncontact reflection PPG
PNL	PPG notch latency
PNRA	Notch relative amplitude
PPG	Photoplethysmography
PPL	PPG peak latency
PPI	Pulse-to-pulse interval
PRV	Pulse rate variability
PSD	Power spectral density
PTNL	Peak-to-notch Latency
pNN50	Proportion derived by dividing NN50 by the total number of NN intervals
pHF	High frequency component for PPG signal: 1.5-6 Hz
pLF	Low frequency component for PPG signal: 0.5-1.5 Hz
pTF	Total power
pVLF	Very low frequency component for PPG signal: 0.01-0.5 Hz,
PWV	Pulse wave velocity
RBC	Red blood cells
RIIV	Respiratory induced intensity variations

RP	Recurrence plot
RRI	R-wave to R-wave interval
SD	Standard deviation
SDANN	Standard deviation of the averages of NN intervals in all 5-minute segments of the entire recording.
SDNN	Standard deviation of all NN intervals
SD1	Poincaré width
SD2	Poincaré length
SI	Stiffness Index
STFT	Short time Fourier transform
RI	Reflection Index
RMSSD	Square root of the mean squared differences of successive NN intervals
TINN	The triangular interpolation of NN interval histogram
TWA	T-wave alternans
ULF	Ultra low frequency component of HRV: <0.003 Hz
VLF	Very low frequency component of HRV: 0.003-0.04 Hz
VCSEL	Vertical cavity surface emitting laser
WDN	Well-defined dicrotic notch
WT	Wavelet transform
WDNSA	Well-defined dicrotic notch searching algorithm

CHAPTER 1

INTRODUCTION

Optical assessment of physiological parameters is very attractive because they often provide simple, non-invasive, continuous physiological monitoring conditions. Photoplethysmography (PPG) is such a low-cost optical technique, and can simply and continuously record the light intensity scattered from a given source by the tissue and collected by a suitable photodetector. The arterial pulse waveform carries physiological information about mechanical properties of the peripheral arteries, and thus the PPG pulse wave could be used to noninvasively assess artery stiffness. A pulsatile PPG signal reveals the heart rate (HR) and could be used to study heart rate variability (HRV). The noncontact concept provides an innovative development for PPG technique.

1.1 Background and motivation

Noninvasive biomedical monitoring (NIBM) and noninvasive medical diagnosis (NIMD) are preferred whenever possible to avoid the risks and expense attendant to surgical opening of the body surface, e.g. infection; adverse systemic reactions to anaesthesia, dye injections, antibiotics and other medications; and surgical error. Optical assessments of physiological parameters are very attractive since they often provide simple, noninvasive, continuous physiological monitoring conditions. Nowadays, physiological signals can be accurately obtained and recorded by means of optical instruments, which supply researchers and doctors with important information as a basis for diagnosis and treatment. Photoplethysmography (PPG) is such a simple and low-cost optical technique that allows noninvasively detecting blood volume changes in the microvascular bed of tissue. The most recognised waveform feature is the peripheral pulse, and it is synchronised to each heartbeat. It is generally accepted that the PPG signal can provide valuable information about the cardiovascular system [1].

Arterial stiffness is recognised as a major determinant of cardiovascular risk [2]. Although pulse wave velocity (PWV) is accepted as the ‘gold standard’ measurement of arterial stiffness [3], it is solely a measure of large artery segments [4] and offers no insight into the status of smaller blood vessels. Assessment of smaller arteries may allow much earlier identification of cardiovascular events related to arterial stiffness [5], as is significant since structural changes in the aorta are probably a late manifestation of cardiovascular abnormalities. Although it is eminently feasible to study large central and peripheral arteries using catheterisation techniques or surface tonometers, it is currently impossible to use such technologies for the direct study of small vessels. The photoplethysmographic pulse wave, recorded from photoplethysmography (PPG), provides a “window” into the properties of small arteries. The appearance of the pulse was defined as two phases: the anacrotic phase concerned with systole, and the catacrotic phase concerned with diastole and wave reflections from the periphery [6]. Stiffening of the small arteries alters the magnitude and timing of reflected waves [7]. Thus, contour analysis of the PPG pulse wave is a promising method to obtain the information of artery stiffness. The second-derivative

contour analysis has been developed to study the peripheral pressure pulse, including the screening of arteriosclerotic disease and the evaluation of ageing effect in the cardiovascular system [8-11]. Artificial neural networks [12], the extraction of periodic components using frequency analysis [13] and nonlinear dynamic analysis [14] were also used to recognise features or patterns of pulse wave. Although these approaches facilitate the distinction of the PPG waves, the physiological and clinical characteristics relating to the derived parameters have not been clearly identified, and these available publications also have ignored specific characteristics existing in young adult. Actually, the process of hardening (“stiffening”) of the arteries has been shown to start from around the first or second decades of life in healthy subjects [15]. A dicrotic notch is prevalently seen in the catacrotic phase of the PPG pulse from young subjects with healthy compliant arteries [16]. Yet few, if any, studies have examined the characteristics of dicrotic notch from photoplethysmographic pulse wave to assess the arteries stiffening in young adults. Hence, it is meaningful to noninvasively investigate the arterial stiffness of young subjects through contour analysis of photoplethysmographic pulse wave.

In recent decades, statistical operations on the R-wave to R-wave intervals (RRI) (time domain analysis) or spectral analysis (frequency domain) of an array of RRI via noninvasive techniques based on the electrocardiography (ECG) have been widely employed as markers of autonomic modulation of the heart. These clinical techniques include heart rate variability (HRV) [17, 18], baroreflex sensitivity (BRS) [19], Q-T interval [20, 21], QT dispersion [22], T-wave alternans (TWA) [23] and heart rate turbulence (HRT) [24]. Among these techniques, HRV has been recognised as a simple and valuable tool to assess the regulation of heart rate (HR) behaviour. HRV reflects the homeostatic interplay between perturbations in cardiovascular functions and the dynamic responses of the cardiovascular regulatory systems [18, 25]. There is a considerable interest in HR fluctuations because their simple statistical measures, such as the standard deviation of the interbeat intervals (the RRI), have been shown to be some of the strongest independent predictors of mortality after myocardial infarction [26]. Moreover, other techniques such as spectral analysis and nonlinear analysis of the RRI have been widely applied in HRV studies. On some occasions, these techniques have been shown to discriminate between subjects with different cardiac conditions as well as to predict mortality in some groups of patients [27, 28].

As the rise and fall of the PPG signal reflects the fluctuations of the heartbeats, it is possible that PPG variability, so-called pulse rate variability (PRV), does reflect the dynamics of the cardiovascular system. In contrast to ECG, PPG pulse waves, the throbbing of the arteries as an effect of the heartbeat, can be traced with a single opto-electronic sensor without any electrode, and with neither the inconvenience of installation nor the need for subjects to unclothe. Some studies have directly used PRV as the alternative for HRV assessment of heart behaviour [29, 30], but none of these studies have provided a detailed and direct quantitative comparison between the PPG and ECG signals. It is intriguing to investigate whether PRV can serve as an alternative approach to obtain HRV information.

The noncontact PPG (NPPG) concept was introduced to overcome the limitations of current contact probe, such as restriction of measurement sites, contact force from probe and hygiene risk. The NPPG was initially explored by the researchers at Loughborough University [31, 32]. The feasibility of NPPG as a substitute technique for contact PPG (CPPG) has not been studied in detail, and the effectiveness of NPPG used for biomedical monitoring needs practical examination.

1.2 Aim and objectives

This thesis aims to make contributions to photoplethysmographic cardiovascular assessment in two aspects: the arterial stiffness of young adults and possibility of PPG signal to evaluate the cardiovascular dynamics. To that end, the specific objectives are:

- I. to evaluate arterial stiffness in a group of young adults using the PPG pulse wave containing stiffness information (Study I);
- II. to determine whether PRV can be used in lieu of HRV to extract cardiovascular dynamics (Study II);
- III. to practically study the PRV parameters for the assessment of the autonomic nervous system (ANS) function on smokers and non-smokers (Study III);

IV. to develop the noncontact reflection PPG (NRPPG) and study the possibility that NRPPG could be used as a physiological monitoring system instead of CPPG (Study IV);

V. to practically study the effectiveness of NRPPG for physiological monitoring (Study V).

1.3 Thesis overview

The thesis is divided into seven chapters. Chapter 1 begins by introducing research background, and includes research motivations, research aims and objectives.

Chapter 2 presents the basic aspects of the PPG technique. Interaction of light with tissue is provided as the basis for understanding the principle of PPG. A brief review of the early and recent history of PPG is included. Next, the PPG measurement system is described, and two modes of PPG operation, i.e. transmission mode and reflection mode, are compared with each other. The limitations of the CPPG probe are specifically addressed; then the noncontact PPG probe is introduced as an alternative use. Finally, photoplethysmographic applications in clinical physiological measurements are presented.

Chapter 3 is concerned primarily with different methods related to cardiovascular assessment based on the PPG technique. Contour analysis for the PPG pulse wave is described and presented. Time and frequency domain and a nonlinear method for analysing variability of heartbeats are discussed.

The experimental investigations into cardiovascular assessment by means of PPG are undertaken in Chapter 4. Experimental measurements were carried out at Shanghai Jiao Tong University and Loughborough University. The study population and protocols are presented. The pulse rate measurements were conducted with CPPG (Studies I-V) and NPPG (Studies IV and V). ECG is recorded to detect HR as a reference (Study II). The well-defined dicrotic notch searching algorithm (WDNSA)

is described for PPG pulse contour analysis (Study I). The lagged Poincaré plot is developed here to study PRV that is used to assess the ANS response (Study III). In this chapter, an optical model is established for NRPPG (Study IV). The relationship between quality of signal and sensor placement is experimentally tested (Study IV). Also, the agreement between CPPG and NRPPG is analysed (Study IV), and a physiological measurement is performed to confirm the prospect of the NRPPG (Study V).

Chapter 5 presents significant findings related to cardiovascular assessment based on the PPG technique. First, arterial stiffness issues associated with contour characteristic of PPG pulse wave are discussed. Then the detailed and direct quantitative comparison between the PPG-derived PRV and ECG-derived HRV is described. The findings from a practical study of PRV assessment on ANS response are illustrated. Finally, the experimental results from NRPPG as a substitute technique for CPPG are presented.

Chapter 6 discusses the findings of this work, while the final chapter, Chapter 7, briefly reiterates the major achievements of the work and provides concluding remarks. Recommendations are also made for future studies in this area.

Appendices are included to give theoretical detail of autocorrelation and autocovariance and recurrence plots used in this work. The references are listed in the final part.

CHAPTER 2

PHOTOPLETHYSMOGRAPHY: PRINCIPLES AND MEASUREMENT SYSTEM

PPG allows the recording of pulsatile changes in the dermal vasculature and is synchronised with the heartbeat. The apparatus consists of a transducer which shines red/infrared light onto the skin. The light is absorbed by haemoglobin, and the backscattered radiation is detected and recorded. The PPG technique has been found a wide range of applications although the origin of the PPG signal is not completely understood. The basic principles of the PPG technique, together with its hardware and relevant aspects for practical use, are examined in this chapter.

2.1 Introduction

Photoplethysmography (PPG) is an optical means to detect blood volume changes in the microvascular bed of tissue. Hertzman and Spielman were the first to use the term ‘photoplethysmography’ and suggested that the resultant ‘plethysmogram’ represented volumetric changes in the blood vessels [6]. PPG is most often employed noninvasively and operates at a red or a near infrared (NIR) wavelength. The basic form of PPG technology requires only a few opto-electronic components: a light source to illuminate the tissue, and a photodetector to measure the small variations in light intensity associated with changes in blood perfusion. PPG has widespread clinical application. This technique will be discussed in detail in this chapter.

2.2 Principles of photoplethysmography

2.2.1 The origins of the PPG waveform

PPG is based on the determination of the optical properties of a selected skin area. Although without complete knowledge of the optical structure of tissue, a general understanding of the optical behaviour of skin has been formulated through experiments on excised tissue and the theoretical models which have been proposed. The basic anatomy of the skin with the blood vessels is shown in Figure 2-1 [33]. The diagram is representative but there are considerable variations from one site on the body to another. The skin consists of three main visible layers from the surface: epidermis, dermis and subcutaneous fat. The epidermis (100 μm thick), outside, contains no blood vessels and dead cells are continually being shed from its surface. Less numerous cells called melanocytes located near the base of the epidermis produce a dark-brown pigment called melanin, which is responsible for the protection of the skin against harmful radiation by means of absorption. The dermis (1–4 mm thick), inside, contains an extensive network of arterioles, capillaries and venules. Capillaries are very thin, fragile blood vessels that receive oxygen-rich blood from arterioles, exchange oxygen and carbon dioxide and then deliver the waste-rich blood to the venules. The capillaries are usually oriented perpendicular to the surface in most skin areas, but in the skin bordering the nails, the nailfold, the capillary loops are

parallel to the surface. The subcutaneous tissue (from 1 to 6 mm thick, in dependence from the body site) is a layer of fat and connective tissue that houses larger blood vessels and nerves. This layer plays a big role in the regulation of skin and body temperature.

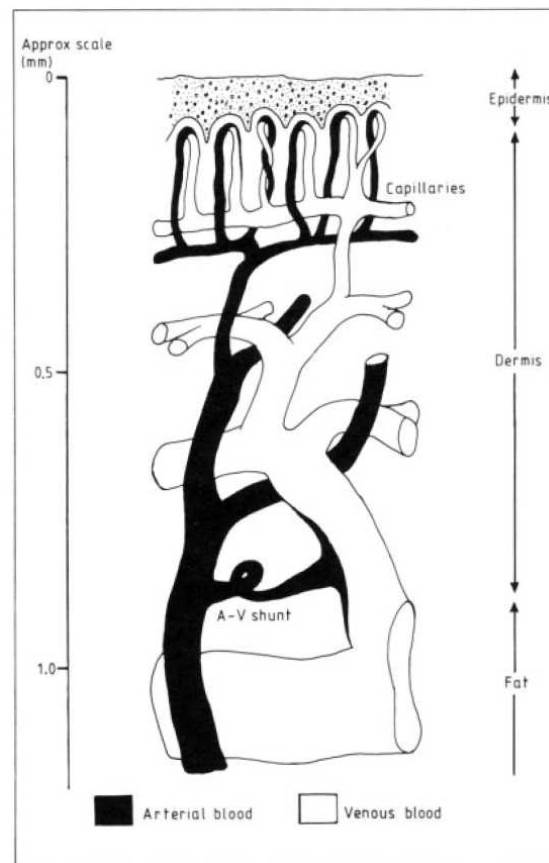


Figure 2-1. The structure of the skin showing the blood vessels.

The interaction of light with biological tissue is complex and includes the optical processes of (multiple) scattering, absorption, reflection, transmission and fluorescence [34]. Beer-Lambert's law helps understanding of the absorbance of light as it passes through living tissue and why and how PPG works. Beer-Lambert's law describes the attenuation of light travelling through a uniform medium containing an absorbing substance. If monochromatic incident light of an intensity I_0 enters the medium, a part of this light is transmitted through the medium while another part is absorbed. The intensity I of light travelling through the medium decreases exponentially with the distance, as can be expressed as

$$I = I_0 e^{-\varepsilon(\lambda)cd}, \quad (1-1)$$

where $\varepsilon(\lambda)$ is the *extinction coefficient* or absorptive of the absorbing substance at a specific wavelength, c the concentration of the absorbing substance which is constant in the medium, and d the optical path length through the medium. The concentration c is measured in mmol L^{-1} and the extinction coefficient is expressed in $\text{L mmol}^{-1} \text{cm}^{-1}$.

Beer-Lambert's law is based on the property that the sum of transmitted and absorbed light equals the incident light. It does not account for physical processes which include reflection of the light at the surface of the medium or scattering of light in the medium. However, incident light passing through human tissue is not only split into absorbed light and transmitted light as proposed Beer-Lambert's law. Some parts of the light are reflected and others are scattered. Several approaches have been made to create models which describe the real process within certain limits of accuracy [35-37].

The amount of light transmitted from the skin and received by the photodetector can be affected by many factors, such as blood volume, blood vessel wall movement, the orientation of red blood cells (RBC) and the wavelength of optical radiation. The signal detected by PPG consists of a steady component and a pulsatile component, which are related to the relative vascularisation of the tissue and the changing blood pulse volume, respectively [38]. In a study of fundamental aspects of the optical properties of blood in motion, Roberts [39] outlined a review of mathematical analyses of light scattering and diffusion processes taking place in blood; he proposed that light diffusion through blood, from a source outside a blood vessel, can diffuse preferentially in the direction of motion of blood which is added to the static diffusion process. Studies from D'Agrosa, Hertzman and Challoner [40, 41] have suggested that the orientation effect of RBC may play a role in the origin of the PPG signal as it could contribute to arterial opacity and would hence, affect the measurement of the PPG signal.

The wavelength of optical radiation is especially important in light-tissue interactions for three main reasons: (1) optical window, (2) isobestic wavelength, and (3) tissue penetration depth.

Optical window

The optical window is defined as the part of the wavelength spectrum which provides a relatively transparent illumination of the biological tissues. Human tissue is mainly composed of water, haemoglobin and melanin. As shown in Figure 2-2, light is increasingly absorbed by melanin towards the ultra-violet band and greatly absorbed by water in the microwave band. The optical window exists over the 600 to 1300 nm region [42], owing mainly to lack of strong absorption by blood and secondarily to lower optical scattering within the dermis, as thereby facilitates the measurement of blood flow or volume. Thus, the red or NIR wavelengths are often chosen for the PPG light source [33]. Although melanin absorption coefficients are, on average, greater than those of haemoglobin, the overall influence of melanin on light propagation in thick tissues is generally less substantial. This is due to the fact that melanin is typically confined to a thin, superficial skin layer, while haemoglobin is widely distributed throughout most tissue.

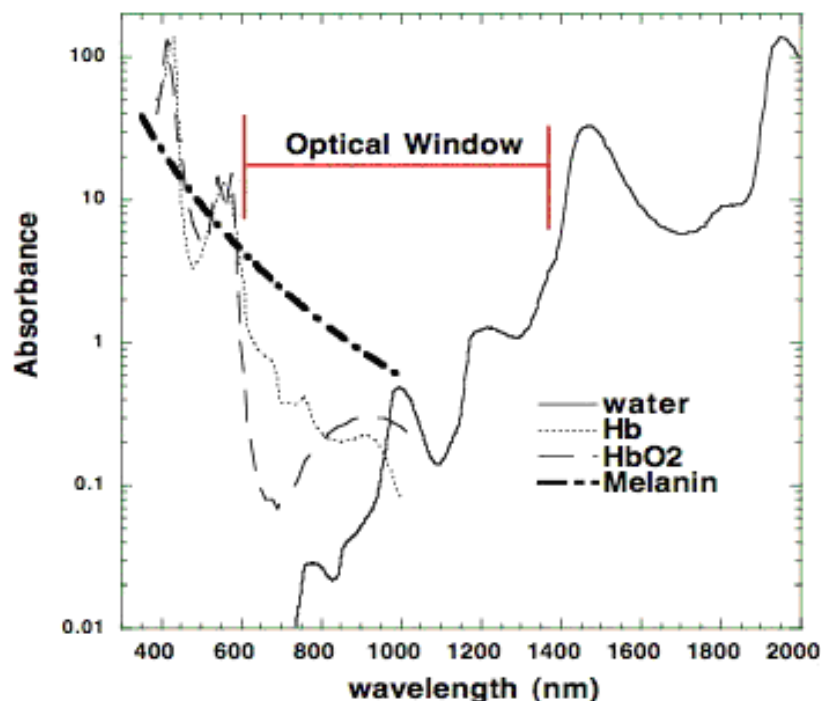


Figure 2-2. A tissue optical window exists between 600 and 1300 nm, owing mainly to lack of strong absorption by blood and secondarily to lower optical scattering within the dermis.

Isobestic wavelength

Within the optical window of transparency the most dominant absorption of red or NIR light is by haemoglobin in its various forms. Haemoglobin is carried in RBC, and constitutes approximately 40–45% of whole blood. It is responsible for delivering oxygen from the lungs to the body tissues. In the oxygenated state haemoglobin is known as oxyhaemoglobin (HbO_2). The de-oxygenated form, with no oxygen molecules attached, is known as deoxyhaemoglobin (Hb). The specific absorption spectra of HbO_2 and Hb, shown in Figure 2-3, differ significantly, particularly in the red region of the visible and the NIR except at the isobestic wavelengths. For measurements performed at an isobestic wavelength (i.e. close to 800 nm, for NIR range) the signal should be largely unaffected by changes in blood oxygen saturation. Using two wavelengths near the cross-over point, absorption data can be used to estimate oxygenation levels.

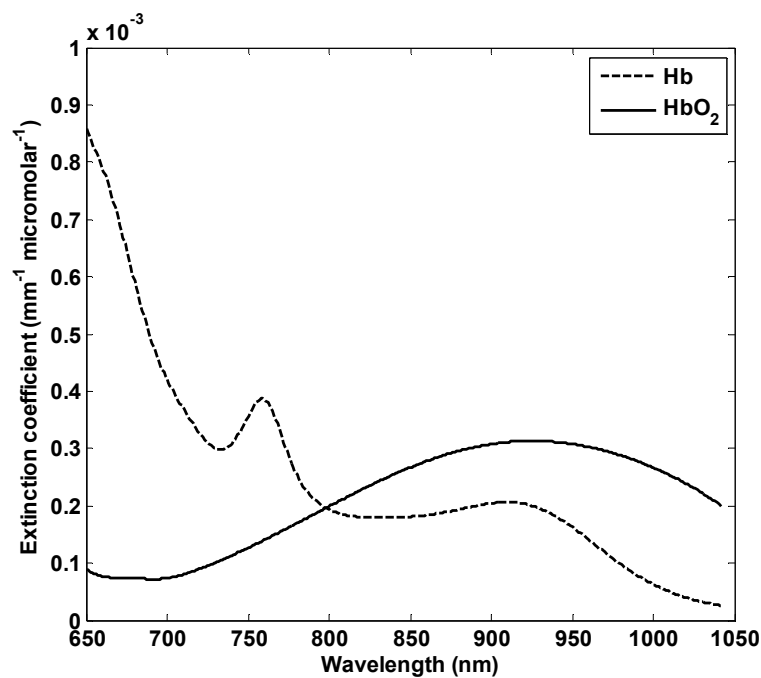


Figure 2-3. Absorption spectra of Hb and HbO_2 from 650-1050 nm. The isobestic point (near 800 nm) is the wavelength at which the absorption by the two forms of the molecule is the same. (data courtesy of <http://www.medphys.ucl.ac.uk/research/borl/index.htm>)

Tissue penetration depth

The penetration of optical radiation in the tissue is wavelength-dependent. For red light the penetration into the living skin is estimated to be between about 0.5 and 1.5 mm while for blue light this figure may be reduced by as much as a factor of four due to increased scattering and absorption in the dermis [33]. Table 2-1 gives estimated depths for which radiation is attenuated to $1/e$ of the incident radiation density, for fair Caucasian skin *in vitro*.

Table 2-1. Approximate depth for penetration of optical radiation in fair Caucasian skin to a value of $1/e$ (37%) of the incident energy density [34].

<i>Wavelength (nm)</i>	<i>Depth (μm)</i>
250	2
280	1.5
300	6
350	60
400	90
450	150
500	230
600	550
700	750
800	1200
1000	1600
1200	2200

2.2.2 PPG signal

In PPG, the emitted light is reflected, absorbed or scattered by different substances, including skin pigmentation, arterial and venous blood and bones. The resultant emerging modulated light is measured and the variations are amplified, filtered and recorded as a voltage signal—photoplethysmogram, i.e. the PPG signal. By convention, the photoplethysmogram is inverted so that it correlates positively with blood volume.

The PPG signals, as shown in Figure 2-4, are composed of two components: a DC component, which is a relatively constant voltage, but changes in magnitude depending on the nature of the tissue through which the light passes; and an AC or pulsatile component synchronous with HR and is superimposed onto a large quasi-DC

component that relates to the tissues and to the average blood volume. The AC pulse shapes are indicative of vessel compliance and cardiac performance and the amplitude is usually 1 to 2% of the DC value.

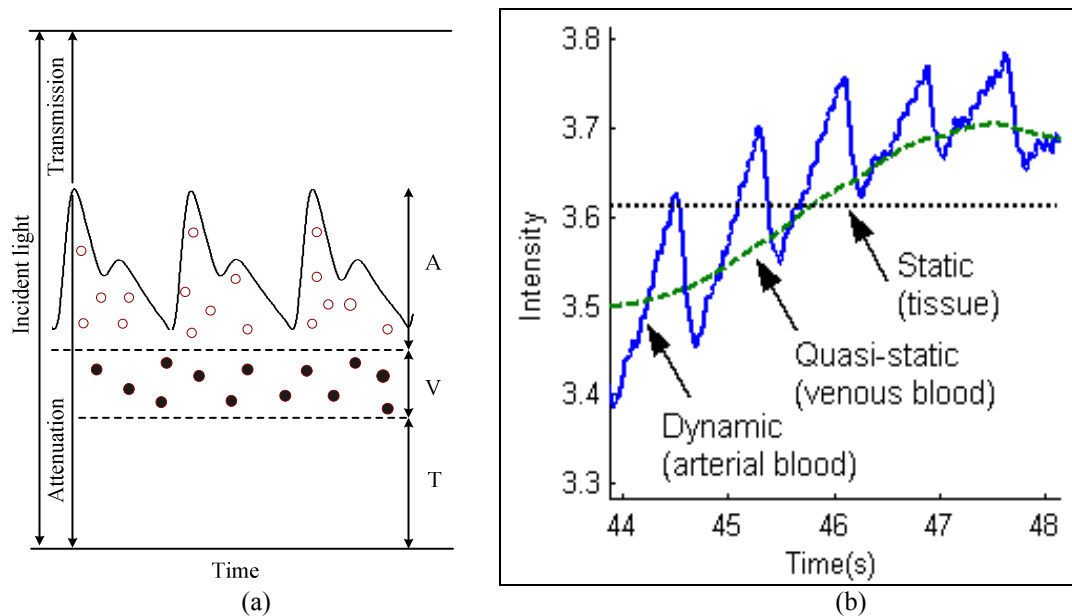


Figure 2-4. PPG signal. (a) Schematic of the pulsatile photoelectric output. The attenuation of the incident light is caused by A---arterial blood, V---venous blood, T---tissues. (b) Components of a raw PPG signal.

2.3 History of PPG

This section summarizes the early history of PPG and is taken from the excellent article by Challoner [40]. The first report of the application of PPG appeared in the mid 1930s. Molitor and Kniazuk [43] and Hanzlik *et al* [44] described similar instrument used to monitor blood volume changes in the rabbit ear following venous occlusion and with administration of vasoactive drugs. Molitor and Kniazuk also described the satisfactory recordings obtained from the skin of the human fingers using a reflection mode PPG system. A great pioneer, to whom this method owes much of its success, was A. B. Hertzman, who published his first paper on describing the use of a reflection mode system to measure blood volume changes in the fingers induced by exercise, cold and the Valsalva manoeuvre. His early work [45-48]

endeavoured to establish the validity of the method for measuring blood flow and blood volume changes. Hertzman and Dillon [49] split the AC and DC components with separate electronic amplifiers and monitored vasomotor activity. In 1940, Hertzman and Dillon [50] first used PPG for assessing the completeness of sympathectomy. The early workers in this field were limited by the size, reproducibility and sensitivity of their photodetectors. In the 1960s, with the advance of semiconductor technology these detectors have become much smaller and more sensitive and later authors have been able to investigate the technique further. Senay *et al* [51] and Hertzman and Flath [52] have used PPG to detect the onset of cutaneous vasodilatation in both forearm and digits. Many authors have applied PPG to tubed pedicles [53-55]. More recently, advances in opto-electronics and clinical instrumentation have significantly contributed to PPG's advancement. A major advance in the clinical use of a PPG-based technology came with the introduction of the pulse oximeter as a noninvasive method for monitoring patients' arterial oxygen saturation [56, 57]. PPG imaging is another emerging technology [58, 59].

2.4 PPG measurement system

2.4.1 PPG Instrumentation

Most PPG instruments consist of an optoelectronic sensor that is applied to the patient and a microprocessor-based system (MBS) that processes and displays the measurement. The optoelectronic sensor usually contains the low-voltage, high-intensity light-emitting diodes (LED) as light sources to shine light onto an area of tissue and one photodiode as a light receiver to convert an optical signal into an electrical signal. The light from the LED is transmitted through the tissue at the sensor site. A portion of light is absorbed by skin, tissue, bone, and blood. The photodiode, in response to the optical signal from the LED, measures the transmitted light. The electrical signal at the photodiode is amplified and then filtered to remove electrical and ambient noise, and then digitised by an analogue-to-digital converter (ADC). The digital signal is processed by the microprocessor to identify each pulse. Figure 2-5(a) shows a transimpedance amplifier design and Figure 2-5(b) shows the signal

conditioning stages surrounding this, including low pass filtering, high pass filtering and further amplification, signal inversion and signal interface.

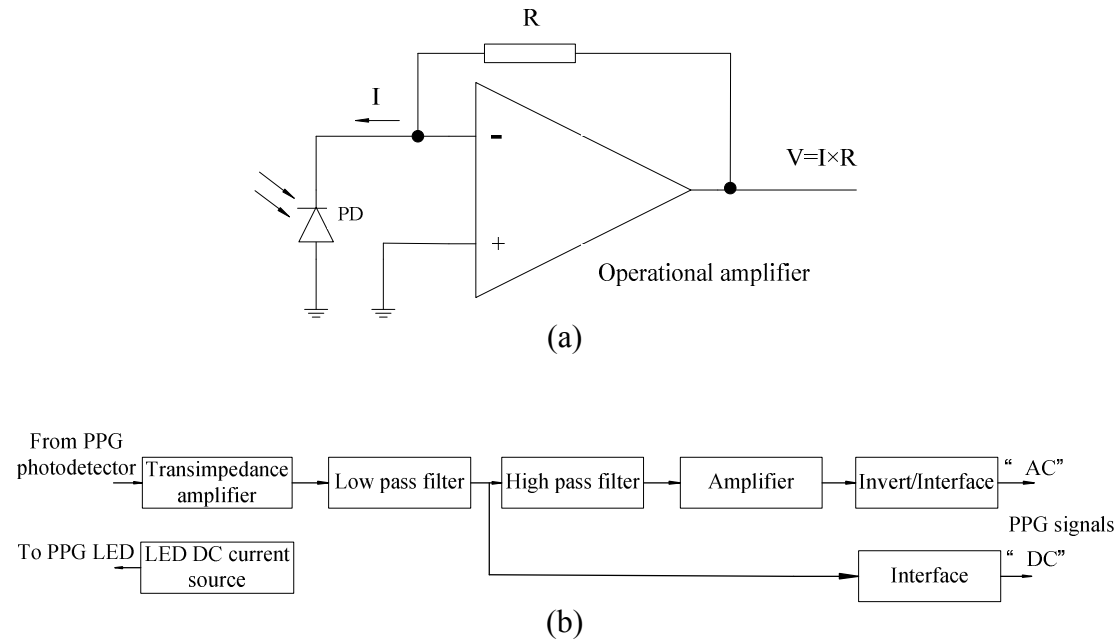


Figure 2-5. Electronic building blocks used in a typical PPG measurement system. (a) A transimpedance (current-to-voltage) amplifier stage that converts light intensity at the photodiode (PD) to an amplifier output voltage ($V = I \times R$, transimpedance gain proportional to feedback resistor value R). (b) The signal conditioning stages surrounding the transimpedance amplifier which include low pass filtering, high pass filtering and further amplification, inversion and signal interfaces. The AC component and a measure of the DC component are available for pulse wave analysis. A constant current driver stage for the PPG LED is also shown. [60]

2.4.2 Two modes of PPG operation

Two modes of measurement are generally used, namely the "transmission" and "reflection" modes, depending on the relative positions of the emitter and detector [61] as shown in Figure 2-6.

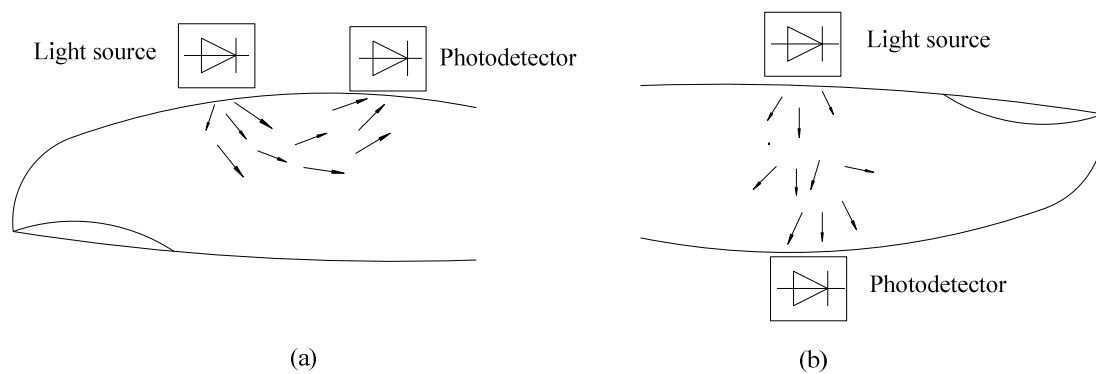


Figure 2-6. Two modes of PPG operation. (a) reflection mode and (b) transmission mode.

2.4.2.1 Transmission mode

Principles

In a transmission mode PPG, tissue is irradiated by a light source, and light intensity is measured by a photodetector on the other side of the tissue. A pulse of blood increases both the optical density and path length through the illuminated tissue (due to intravascular increases of RBC and the light-absorbing Hb they carry), which decreases the light intensity at the photodetector. Normally, transmission probes are placed on the subject's finger, toe, ear or nose.

Sensor placement

The sensor placement in transmission probes has been discussed in the literature [61]. The author indicated that the photodetector should be placed in line with the light source to obtain the detection of the maximum amount of the transmitted light, as the photodiode has to detect the light transmitted through the tissue. Also, the photodiode should be placed as close as possible to the skin without exerting force on the tissue. The author has asserted several factors that influence the contacting force. First, the amount of force applied by reusable probes is much larger than the amount of force applied by disposable probes. Second, the force applied also depends on the materials used to manufacture a particular probe and also on the company which produces the probes, e.g. Nellcor clip type probes exert less pressure than Ohmeda clip type probes. If the force exerted by the probe is significant, the blood under the tissue, where the probe is placed, may clot caused by external pressure applied. And if the distance between the light source and the photodiode increases, the amount of detected light will decrease as a result of the increased optical path length as seen from Beer-Lambert's law (section 2.2.1).

2.4.2.2 Reflection mode

Principles

In a reflection mode PPG, the light source and the photodetector are positioned adjacently in close proximity on the skin surface. The illumination received by the

photodetector is a result of the backscattered light that is returning from a range of depths within the highly scattering tissue. An opaque shield is usually positioned between the optoelectronics to prevent any direct illumination from the light source to the photodetector without first passing through the tissue. This configuration enables measurement from multiple locations on the body that is not accessible using transmission mode PPG. For an accurate measurement, the probe needs to be attached firmly on the skin, and thus the measurement sites need to have a flat and wide surface area, e.g. the chest, forehead and limbs.

Sensor placement

One of the requirements in designing a reflectance PPG sensor is to determine the optimum separation distance between the light source and the photodetector. Obviously, this distance should be such that plethysmograms with both maximum and minimum pulsatile components can be detected. These pulsatile components depend not only on the systolic blood pulse in the peripheral vascular bed, but also on the amount of arterial blood in the illuminated tissue.

There are two techniques that can enhance the quality of the plethysmogram [61]. One way is to use a large light source driving current, which determines the effective penetration depth of incident light and increase light intensity. For a given light source/photodetector separation, a larger pulsatile vascular bed will be illuminated by using higher levels of incident light. As a result the reflected plethysmograms will contain a larger AC component. Practical considerations, however, limit the light source driving current to the manufacturer specified maximum power dissipation. The other way is to place the photodetector close to the light source. This alternative means will cause the photodetector to become saturated, which is mainly due to the large DC component obtained by the multiple scattering of the incident photons from the blood-free stratum corneum and epidermal layers in the skin. Thus, the selection of a particular separation distance involves a trade-off. In summary, larger plethysmogram can be achieved by placing the photodiode farther apart from the light source, while a higher light source driving current is needed to overcome absorption due to increased optical path length.

2.5 Practical applications of PPG

2.5.1 Measurement protocols

The PPG technique can be used to give accurate comparative data, although it cannot give quantifiable measurement in absolute units. In practice, the normal healthy skin is capable of large and rapid changes in blood flow, and consequently any measurement taken in terms of ml s^{-1} may have no useful meaning as this same skin site may be very different a few minutes later, for no apparent external reason. Factors which are known to effect skin flow are the thermoregulatory process, emotional state, etc. All tests should be performed at a constant temperature and humidity and at such a temperature which is appropriate to the experiment, i.e. a temperature which will be suitable for those particular skin blood flow changes. It is also very useful to make sure that the subject is relaxed and accustomed to the measurement procedure so as to reduce the flow changes induced by emotional stress.

Reproducibility of PPG measurements is discussed by Allen [60], who indicated that many factors affect reproducibility, such as the method of probe attachment to tissue, probe–tissue interface pressure, pulse amplifier bandwidth, minimisation of movement artefact, subject posture and relaxation, breathing, wakefulness, room temperature and acclimatisation. As yet, however, there are no internationally recognised standards for clinical PPG measurement. Published research tends to be based on studies using quite differing measurement technology and protocols, thereby limiting the ease with which PPG physiological measurements can be replicated between research centres.

2.5.2 Limitations of current contact PPG

The limitations of current PPG include: (1) site of measurement: the use of the transmission PPG probe is limited to areas of the body such as the peripheries and earlobes in adults, and the palm and the foot in neonates. Owing to the high vascular content, the measurements are mostly performed in the fingers and the toes. In cases where a finger probe is utilised, the measurements can only be obtained on the

peripheries that have a good anatomical fit to the probe; (2) contact force of the probe: the PPG signals may be affected by the contact force between the PPG sensor and the measurement sites as the arterial geometry can be deformed by compression; and (3) wounds or damaged tissue: a contact probe cannot be employed to obtain measurements on skin with open wounds or in cases where there is external tissue damage. Moreover, the contact probe cannot be used for the measurement when there is a need for mechanical isolation. As a result, there is a need for research into an alternative method to overcome these drawbacks. A noncontact probe could introduce new applications where attaching probe or electrode is either inconvenient or unfeasible.

2.5.3 Noncontact PPG

The concept of NPPG is described as monitoring the perfusion of an area of tissue from the classical PPG practice in a contactless way. There are several issues that need to be considered with noncontact PPG monitoring [62].

The first issue concerns the dynamic range of the detected signal. The detected pulsatile (AC) signal is very small compared to the non-pulsatile (DC) signal. To achieve a greater amplification for the AC signal, a logarithmic amplifier is used. This can be implemented electronically using a nonlinear optical preamplifier which acts as an automatic gain control (AGC). Linear PPG systems with a separate AGC could also be used, but stand a risk of saturation at the detector.

The second issue is ambient light artefact. The photodetector receives increased ambient light due to the probe separation from the tissue bed. In current PPG applications, the artefacts that arise from ambient light interference can be reduced in several ways: by suitable probe attachment to the skin (e.g. using a dark Velcro wrap-around cuff), by further shading of the study site area and performing measurements in subdued lighting, and by electronic filtering (e.g. light modulation filtering) [61]. However, ambient artefact could pose a bigger problem in noncontact PPG settings because of the separation distance between the probe and the tissue.

The third issue is the effects of motion artefact, which could be induced by any voluntary and involuntary movements of the interface between the probe and tissue bed. This effect is minimised by increasing the field of view of the source and photodetector. These effects could be more significant in noncontact PPG system because the probe is more sensitive to tissue movements, especially to movements on the skin surface.

The last issue to be considered is the effect of direct coupling, which refers to direct illumination of the photodetector by the light source without any light/tissue interaction. The direct-coupled light can cause variations in the measured PPG signal.

2.6 Clinical applications of PPG

PPG has been applied in many different clinical settings, including clinical physiological monitoring, vascular assessment, and autonomic function.

2.6.1 Clinical physiological monitoring

Pulse oximetry has been one of the most significant technological advances in clinical patient monitoring over the last few decades [63-65]. It utilises PPG measurements to obtain information about the arterial blood oxygen saturation (SpO₂) and heart rate [61]. Some of the main areas in which they are used include anaesthesia [66], patient transport [67], fetal monitoring [68], neonatal and paediatric care [69], dentistry and oral surgery [70], and sleep studies [71]. In the early 1990s pulse oximetry became a mandated international standard for monitoring during anaesthesia. A recent and exciting development in pulse oximetry is the noninvasive measurement of venous oxygen saturation using external artificial perturbations applied close to the PPG probe (VENOX Technology, Chan *et al* [72], Echiadis *et al* [73]).

Arterial blood pressure is a very important clinical variable to measure. The measurement of the arterial pressure waveform at the finger with FinapresTM (for FINGER Arterial PRESSure) on a continuous beat-by-beat basis was introduced in the early 1980s. The method is based on the dynamic (pulsatile) vascular unloading of the

finger arterial walls using an inflatable finger cuff with built-in PPG sensor [74]. Blood pressure was also estimated using an algorithm based on the pulse arrival time and was compared with conventional arm blood pressure measurements [75-77]. Their approach showed promise as a method for home monitoring of blood pressure. Using empirically determined transfer functions, it is possible to derive the arterial blood pressure pulse from PPG measurements [78]. An example of a commercial device for automatic PPG-based limb pressure measurement is the Vascular AssistTM vascular assessment system (Huntleigh Healthcare, UK).

Respiration causes variation in the peripheral circulation, making it possible to monitor breathing using a PPG sensor attached to the skin. The low frequency respiratory induced intensity variations (RIIV) in the PPG signal are well documented [79-81]. The RIIV is not fully understood, but is believed to be caused by skin blood volume fluctuations induced by the respiratory variations in intra-thoracic pressure transmitted to the measurement site by the venous system [82, 83].

The stroke volume (the amount of blood pumped out of a ventricle during one ventricular contraction) can be estimated from PPG-derived pulse contour analysis on a beat-by-beat basis. However, there is ongoing discussion in the literature regard to the accuracy of PPG-based cardiac output assessments [84] (where cardiac output = stroke volume \times heart rate).

2.6.2 Vascular assessment

PPG occupies a unique position among noninvasive techniques in assessing patients with peripheral arterial disease. Indeed, much of vascular physiology and pathophysiology has been established based on PPG studies [85]. Disease detection with PPG is possible because the peripheral pulse usually becomes damped, delayed and diminished with increasing severity of vascular disease [86-88]. Multi-body site PPG measurements have been proposed for peripheral vascular disease detection [89-92]. The photoplethysmographic method proposed by Chowienczyk *et al* [93] could be a suitable alternative of noninvasive assessment of endothelial function. Gopaul *et al* [94] also detected endothelial dysfunction in diabetic patients using the

PPG-derived reflection index. Cooke *et al* [95] characterised the PPG pulse shape in healthy subjects and Raynaud's patients and found that both the pulse amplitude and the slope of the rising edge were good markers for the condition. The DC component of the PPG waveform can be used for the noninvasive assessment of lower limb chronic venous insufficiency [96] .

2.6.3 Autonomic function

The PPG signal is composite in nature and has low frequency components relating to respiration, blood pressure control and thermoregulation, as well as the high frequency components relating to the heart synchronous pulse waveform [97]. Rauh *et al* [98] showed that PPG was useful for detecting the gasp response and that there was a significant correlation between PPG and laser Doppler flowmetry techniques. Kistler *et al* [99] showed that vasoconstrictor waves at the finger are more easily demonstrable when the fingertip temperature is above 32°C.

Assessment of orthostasis is a growing research area in autonomic function testing. Nasimi *et al* [100] investigated sympathetic neuropathy in patients with diabetes mellitus by monitoring PPG frequency characteristics throughout a supine-to-standing posture challenge. Nasimi *et al* [101] also investigated periodic posture stimulation on local vasomotor reflexes. Linder *et al* [102] have investigated beat-to-beat changes in the ear and finger pulses on standing and have related these to heart rate dynamics.

Meanwhile, PPG shows considerable potential for neurological assessment, with the capability to give new insights into the physiology and pathophysiology of the central and peripheral nervous systems [103-105].

2.7 Summary

Chapter 2 details the fundamental aspects of PPG, including its principles, measurement system and applications. PPG can be simply defined as the continuous recording of the light intensity transmitted or scattered from a given source by the tissue and collected by a suitable photodetector. The PPG waveform comprises a

pulsatile ('AC') physiological waveform, and is superimposed on a slowly varying ('DC') baseline. There are two different modes of detection: a transmission mode and a reflection mode. Transmission mode, where the light source is on one side of the tissue and the detector on the other, is limited to areas such as the finger, toe, ear or nose. However, reflection mode, where the light source and photodetector are placed in parallel, allows measurement of backscattered light on virtually any skin area. Additionally, NPPG is introduced as an alternative to overcome the limitation of current CPPG. Researchers have become aware of various practical considerations which may lead to more meaningful data being obtained. The specific design of a system may be decided upon by individual experimenters to suit their particular requirements.

CHAPTER 3

NONINVASIVE CARDIOVASCULAR ASSESSMENT

Palpation of the pulse has been used since ancient times to assess physical health. The contour of a digital volume pulse (DVP) is determined mainly by characteristics of the systemic circulation. Thus, contour analysis of the optically derived DVP, e.g. the PPG pulse wave, provides a simple, reproducible, noninvasive approach to derive information about cardiovascular properties.

HR is one of the most important physiological variables, and HR variability (HRV) reflects the dynamic interplay between ongoing perturbations to circulatory function and the compensatory response of short-term cardiovascular control systems. A pulsatile PPG signal reveals the HR and hence could be used to monitor HRV. Linear and nonlinear methods are used for quantification of HRV.

3.1 Contour analysis of PPG pulse wave

3.1.1 Interpretation of pulse wave changes

The peripheral pulse wave is generated by blood ejected from the heart during the opening of the aortic valve. Some important characteristics of the PPG AC pulse waveform were described by Hertzman and Speelman [6]; the appearance of the pulse was defined as two phases: the anacrotic phase being the rising edge of the pulse, and the catacrotic phase being the falling edge of the pulse. The first phase is primarily concerned with systole, and the second phase with diastole and wave reflections from the periphery. A dicrotic notch is usually seen in the catacrotic phase of subjects with healthy compliant arteries. Pulse wave pattern changes during the cardiac cycle may provide valuable information about the peripheral circulation [97].

3.1.1.1 Respiratory interaction

The photoplethysmographic signal contains respiratory induced intensity variations (RIIV) that shapes the envelope of the cardiac pulsations. It is considered that RIIV includes contributions from the venous return to the heart caused by alterations in intra-thoracic pressure. A part of the respiratory-related fluctuations in perfusion also originates from the autonomous control of the peripheral vessels, synchronous with respiration [80, 106]. The physiological mechanisms relating to the RIIV are, however, not fully understood.

3.1.1.2 Amplitude

Marked beat-to-beat variations in amplitude result from changes in stroke volume. A large amplitude wave in the underlying bed indicates local vasodilation by a direct vascular action such as histamine release or decreased vasomotor tone as might result from deep anaesthesia, ganglion block, or increased body temperature. Compression of the artery supplying the sensor site could reduce pulse volume amplitude because of hypovolemia which causes blood flow to be redirected to essential organs.

3.1.1.3 Area under the curve and the dicrotic notch

In each peripheral pulse wave, the area under the curve is an indicator of the volume of blood in the tissue scanned by the transducer. The area under the curve could be influenced by the stroke volume, modified by changes in local vasomotor tone. An ideal waveform would show a broad peripheral flow wave with a large area under the curve.

The position of the dicrotic notch on the descending section of the pressure or pulse trace can be used as an indicator of vasomotor tone. With optimal systolic filling, the catacrotic phase of the waveform will be prolonged as perfusion pressure drops more slowly. The dicrotic notch normally remains midway in the catacrotic phase. The waveform is broad-based and rounded. With suboptimal systolic filling, the broad-based rounded waveform may either be preserved or become peaked, and the dicrotic notch moves towards the baseline. Additionally, hypovolaemia and subsequent vasoconstriction could produce a narrow-based, low-amplitude, peaked waveform with a rising dicrotic notch: filling of the arterial bed is incomplete, and thus decrease is faster. The double dicrotic notch may arise from the fact that strong pressure waves are reflected back via short (brachial) and long (femoral) artery pathways to reach a finger transducer at different times.

3.1.1.4 Baseline width

Comparing the width of the baseline with the width between the two flow peaks on either side gives an indication of the filling of the vascular bed for the prevailing vasomotor status. A rapid diastolic runoff with a relatively long baseline may indicate inadequate stroke volume.

3.1.2 Measurement and contour analysis of photoplethysmographic pulse

Analysis of the contour of the peripheral pulse to assess arterial properties was first described in the nineteenth century. Contour analysis of the PPG pulse wave measured at the finger is described by Millasseau *et al* [107], who gave a succinct history of the topic, highlighted the resurgence of interest in PPG-based pulse wave

analysis, and described the influence of ageing on the contour. There have been many developments since the 1940s in this pulse shape analysis. It appears that contour analysis of the DVP was initiated by Dillon and Hertzman [108], who described the shape of the DVP in terms of the crest time and dirotic notch height. They observed a tendency of the notch to rise with systemic vasoconstriction and to decrease after inhalation of the vasodilator amyl nitrite. Characteristic changes in crest time and triangulation of the DVP were noted in patients with hypertension and arteriosclerosis.

The work from Dawber *et al* [16], where they obtained the DVP in 1778 individuals, proposed that the DVP be classified into one of the following classes (see Figure 3-1): class 1, a distinct notch is seen on the catacrotic phase of the pulse wave; class 2, no notch develops but the line of descent becomes horizontal; class 3, no notch develops but there is a well-defined change in the angle of the descent; or class 4, no notch develops or no change in angle of descent occurs. They found class 1 to be prevalent in younger individuals and class 4 present in older participants.

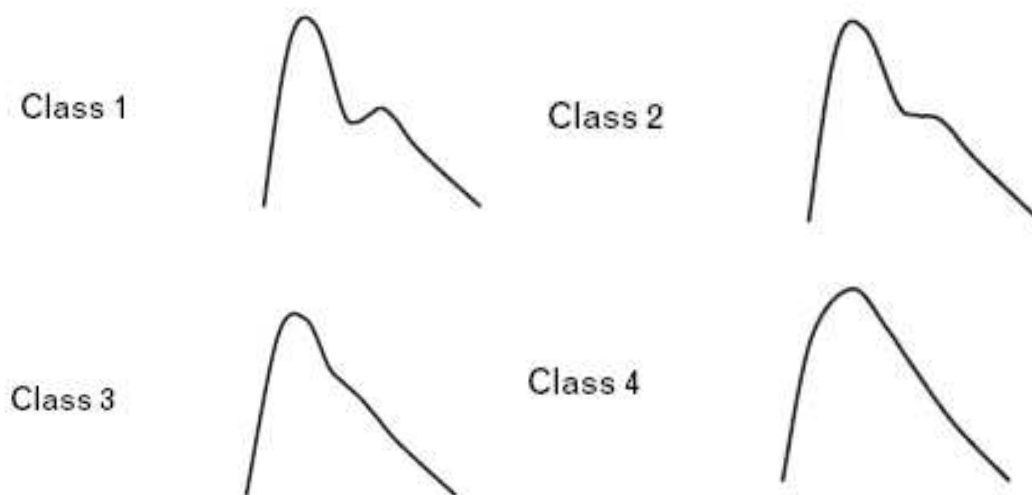


Figure 3-1. Classification of the digital volume pulse (DVP) waveform according to Dawber *et al* [16]. With increasing age and/or presence of vascular disease, the waveform changes from class 1 to class 4.

A sophisticated approach to contour analysis of the DVP has been developed by Japanese investigators [8, 10]. Their approach uses the second derivative of the finger PPG waveform to stabilise the baseline and enable the individual waves to be

visualised. Features from the second derivative of the photoplethysmogram have been correlated with vascular compliance [109-111], arterial stiffness [110], age [8, 10, 11], arterial blood pressure [8, 11], and effects of vasoactive drugs [112]. Other mathematical approaches to analysis of the DVP include artificial neural networks [12, 113, 114], the extraction of periodic components using frequency analysis [13] or nonlinear dynamical analysis [14]. The physiological and clinical characteristics relating to the derived mathematical parameters, however, have not been clearly identified.

3.2 Heart rate variability and pulse rate variability

HRV, derived from an electrocardiogram (ECG), is known to be a noninvasive indicator reflecting the dynamic interplay between perturbations to cardiovascular function and the dynamic response of the cardiovascular regulatory system. The fact that HRV analysis is able to assess overall cardiac health and the state of the ANS underlies its promise as a major tool in physiological monitoring. As the rise and fall of the PPG signal reflects the fluctuations of the heartbeats, it is possible that pulse rate variability (PRV) derived from the PPG signal does reflect the heart activity and the dynamics of the ANS.

3.2.1 HRV from ECG

3.2.1.1 ECG recording

ECG is the recording from the body surface of the electrical activity generated by the heart. ECG has provided an important noninvasive means of recording and detecting each cardiac cycle. The electrical signals within the heart are of relatively small amplitude, in the range of 100 mV. Since the inside of the human body consists of electrically conductive tissues, a part of the cardiac contraction signals is carried to the skin, where it can be detected by an ECG. At the skin, the signals are much lower in amplitude than at the heart, approximately 1 mV. However, these signals at the skin surface can be amplified and filtered sufficiently to provide a clear representation of original signals from the heart.

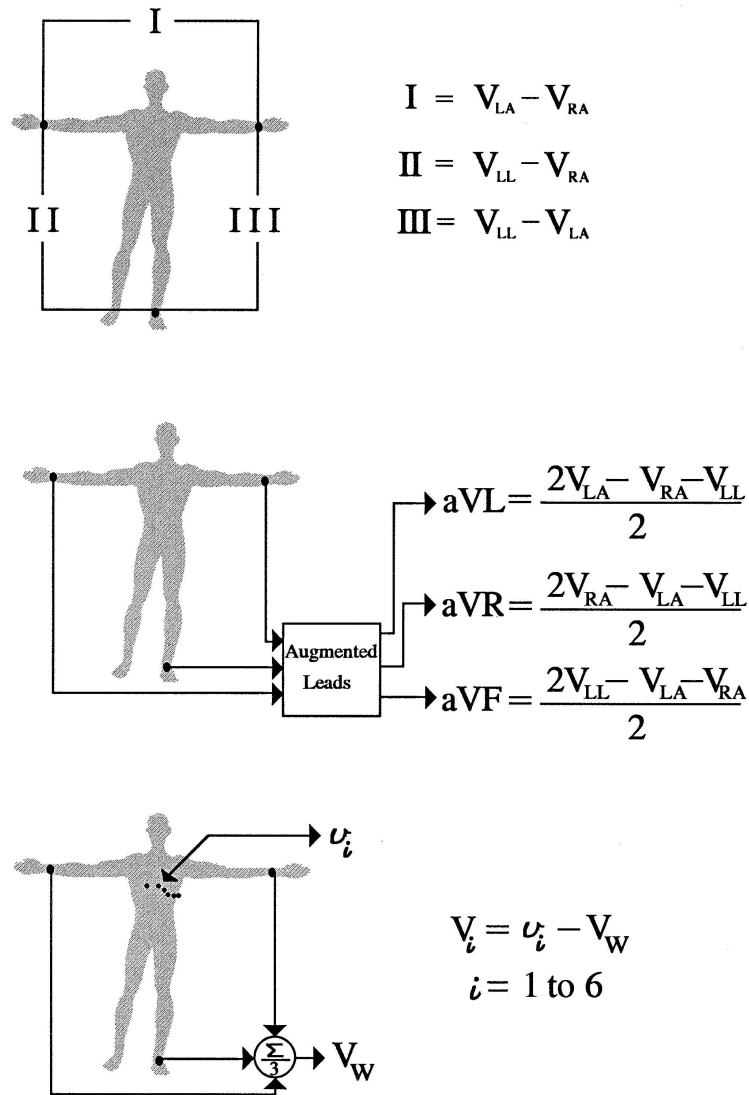


Figure 3-2. The 12-lead ECG is formed by the 3 bipolar surface leads: I, II, and III; the augmented Wilson terminal referenced limb leads: aVR , aVL , and aVF ; and the Wilson terminal referenced chest leads: V1 , V2 , V3 , V4, V5 , and V6.

In order to record an ECG waveform, a differential recording between two points on the body is made. Traditionally, each differential recording is referred to as a *lead*. The original Lead I, II and III ECG electrode placements were defined by Einthoven in 1912. The electrode placement, called Einthoven's triangle, is still used today for routine ECG measurement. Electrodes are placed on the left leg (on the shin above the foot), on the right arm (about one quarter of the way from the wrist on the medial surface) and on the left arm in the same location. The potentials at these body locations is denoted: v_{LL} , v_{RA} and v_{LA} , respectively. ECG lead I is the potential between the left arm (+) and the right arm (-), i.e. $V_I = v_{LA} - v_{RA}$. Lead II is taken

between the left leg (+) and the right arm (-), i.e. $V_{II} = v_{LL} - v_{RA}$, and Lead III is between the left leg (+) and the left arm (-), i.e. $V_{III} = v_{LL} - v_{LA}$. Because the body is assumed to be purely resistive at ECG frequencies, the four limbs can be thought of as wires attached to the torso. Hence, lead I could be recorded from the respective shoulders without a loss of cardiac information. Today, 12-lead ECG (using 10 electrodes) provides discriminatory information for diagnosing abnormalities in the pacing and conduction system of the heart. Figure 3-2 illustrates the 12-lead set. These sites are historically based, have a built-in redundancy, and are not optimal for all cardiac events. Figure 3-3 is a typical or stylised ECG recording from lead II. Einthoven chose the letters of the alphabet from P to U to label the waves and to avoid conflict with other physiologic waves being studied at the turn of the century.

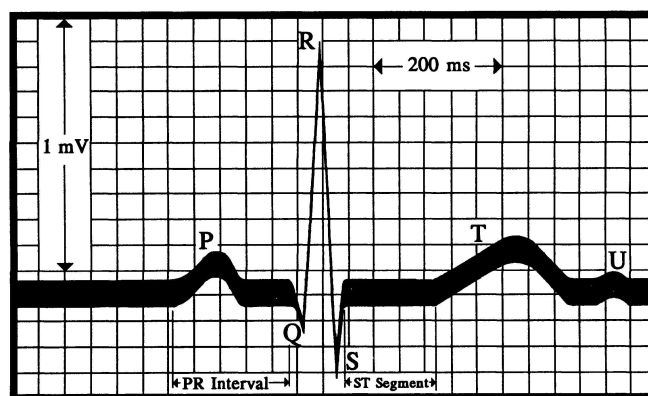


Figure 3-3. A stylised version of a normal lead II recording showing the P wave, QRS complex, and the T and U waves. The PR interval and the ST segment are significant time windows. The peak amplitude of the QRS is about 1 mV. The vertical scale is usually 1 mV/cm. The time scale is usually based on millimetres per second scales, with 25 mm/s being the standard form. The small boxes of the ECG are 1×1 mm.

The P wave is caused by atrial depolarisation. The QRS complex is a general term representing activation in the ventricles and is a result of the depolarisation of the ventricles. The T wave results from ventricular repolarisation. The U wave, which is not always recorded on the ECG, follows the T wave and usually has the same polarity as the T wave.

ECG monitoring electrodes must make very good electrical contact with the patient in order that adequate ECG waveforms can be obtained. However, this very characteristic poses potential problems in that the electrical contact could provide a

pathway for harmful external electrical currents to enter the body and then the heart, causing severe reactions or even death. These electrical currents might originate from a faulty nonmedical electrical device such as a television, a computer, or an electric shaver, or from a fault in one of the many line-powered medical devices in hospitals, or from the normal function of some medical devices such as electrosurgery machines. Although such fault currents are rare, especially with equipment of modern design that has been properly maintained, their consequences are so severe that safeguards must be taken.

3.2.1.2 Mechanisms of HRV

Healthy cardiac function is characterised by irregular time intervals between consecutive heartbeats. This variability, namely HRV, is a result of rhythmic oscillation of the regulatory components of cardiac activity that function to maintain cardiovascular homeostasis within a defined range and to orchestrate responses to challenges. It is a valuable tool to investigate the sympathetic and parasympathetic function of the ANS. Because of continuous changes in the sympathetic-parasympathetic balance, the sinus rhythm exhibits fluctuations around the mean heart rate. Frequent small adjustments in HR are made by cardiovascular control mechanisms (Figure 3-4). This results in periodic fluctuations in HR. HRV primarily emerges through the non-additive activity originating from the individual branches of the ANS [115-117], which in turn is influenced by neuronal, humoral and other physiological control and feedback mechanisms [17]. The central nervous system (CNS), in particular the formatio reticularis of the medulla oblongata (medullar circulation centre), the hypothalamus, and neocortical and paleocortical areas also participate in all levels of cardiovascular regulation.

In a normal heart with an integer ANS, there will be continuous physiological variations of the sinus cycles reflecting a balanced symphtho-vagal state and normal HRV [17]. In a damaged heart which suffered from myocardial necrosis, the changes in activity in the afferent and efferent fibres of the ANS and in the local neural regulation will contribute to the resulting symphtho-vagal imbalance reflected by a diminished HRV.

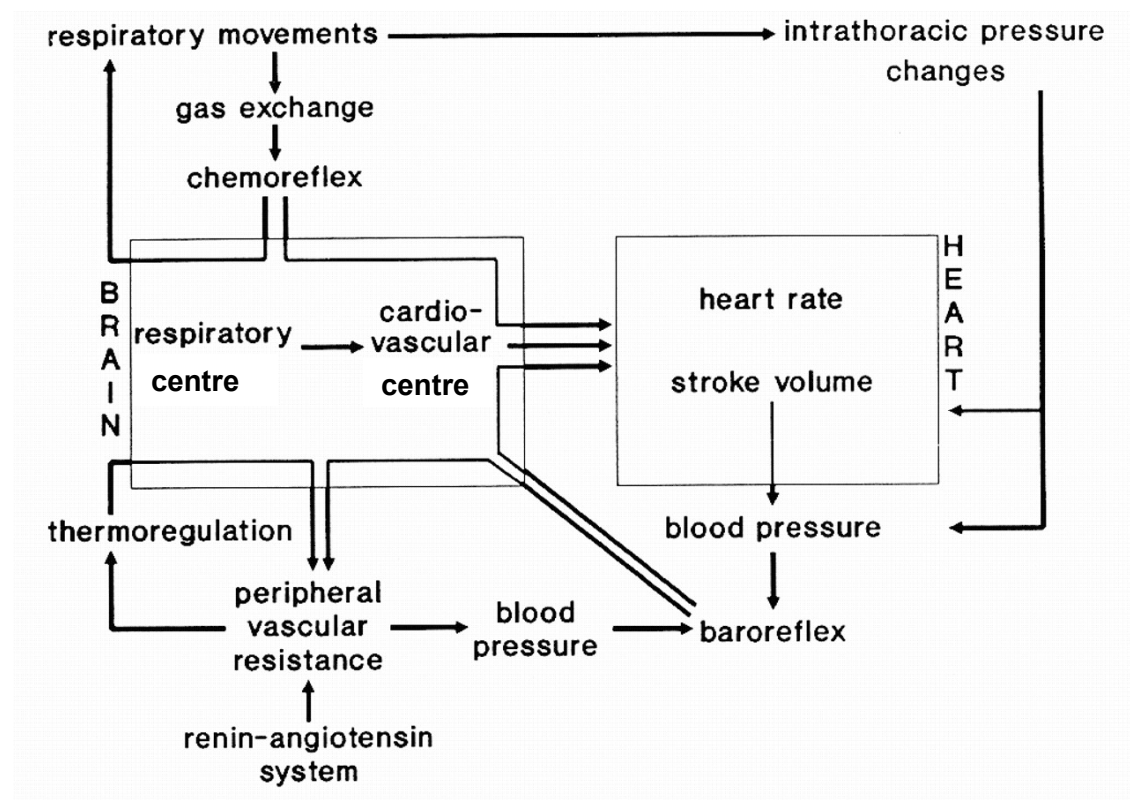


Figure 3-4. Scheme of the cardiovascular control mechanisms responsible for the main periodic fluctuations in heart rate [17]. The exact pathways through the brainstem are not visualised.

3.2.2 PRV from PPG

3.2.2.1 Mechanisms of PRV

PPG provides a qualitative measure of the tissue blood volume during cardiac cycle by measuring the light transmission through the tissue as a function of time. The AC component of the PPG pulse is synchronous with the beating heart and therefore can be a source of HR information. Pulse rate can be estimated from the time between two systolic peaks of pulse wave. Pulse rate variability (PRV) is the pulse-to-pulse alteration in pulse rate.

3.2.2.2 Comparability of PRV and HRV

Statistical operations on RRI (time domain analysis) or by spectral analysis (frequency domain) of an array of RRI via noninvasive techniques based on the ECG are being widely employed as markers of autonomic modulation of the heart. HRV

has been recognised as a simple and useful method to assess the regulation of heart behaviour. The measurement of typical multiple-lead ECG, however, requires several sticky electrodes to be carefully placed on the body. The clinical users must either confirm that the leads are correctly placed or optimise the leads' positioning before the recording. Such procedures could preclude frequent assessments of HRV in general populations. By contrast, PPG is simple and only requires a small optical probe to be applied to the skin, and can help reduce possible 'white coat' effects on subjects.

HR can be extracted from the AC component of the PPG signal via two different methods. The first method identifies individual heartbeat peaks and determines the time interval between them, and thus the time it takes to complete one cardiac cycle. The second method relies on the identification of the frequency of cardiac pulsations. The energy distribution in the frequency domain of the PPG waveform can be described by transforms such as the Fourier transform. This helps to identify the frequency of the power spike, which can be correlated to HR. The PPG pulse wave, owing to its easy applicability, is expected as a surrogate of ECG for the analysis of HRV. This needs further confirmation.

3.2.3 Measurement of HRV

Heart rate variability measurements were introduced into clinical practice in the 1960s by obstetricians who found decreased variability indicated fetal stress and compromised viability [118]. Since then, computers capable of easily and quickly solving complicated mathematical equations greatly expanded this area of inquiry. Like many other physiological parameters, HRV is influenced by a variety of factors like gender [119], age [120], race [121], circadian rhythm [122], respiration [123], fitness levels [124], posture [125] and physical activity [126]. In 1996, Task Force of the European Society of Cardiology (ESC) and the North American Society of Pacing and Electrophysiology (NASPE) defined and established standards of measurement for clinical application and physiological research [18]. Linear measures, including time domain indices, geometric methods and frequency domain indices, constitute the standard clinical parameters used nowadays. Nonlinear methods are applied to

measure nonlinear properties of HRV and to reveal the nonlinear dynamic behaviour of the cardiovascular system.

3.2.3.1 Time domain methods

The time domain measures of HRV are based on statistical or geometric analysis of the lengths of intervals between successive normal complexes [18].

Statistical measures

The statistical measures using the length of RRI include the mean normal-to-normal (NN) intervals, the standard deviation of all NN intervals (SDNN), standard deviation of the averages of NN intervals in all 5-minute segments of the entire recording (SDANN), and the mean of the standard deviations of all NN intervals for all 5-minute segments of the entire recording (SDNN index). SDNN reflects all cyclic components in the analysed period and thus depends on the length of the period. It is inappropriate to compare SDNN measures obtained from recordings of different durations.

The most commonly used measures derived from interval differences include the square root of the mean of the sum of the squares of differences between adjacent NN intervals (RMSSD), the number of interval differences of successive NN intervals greater than 50 ms (NN50), and the proportion derived by dividing NN50 by the total number of NN intervals (pNN50). All these measurements of short-term variation estimate high frequency variations in HR and thus are highly correlated.

The methods for expressing overall HRV and its long- and short-term components are not interchangeable. The use of SDNN (an estimate of overall HRV), SDANN (an estimate of the long-term components of HRV) and RMSSD (an estimate of the short-term components of HRV) as time domain measures of HRV are recommended [18].

Geometric measures

Geometrical measures present RRI in geometric patterns, and various approaches have been used to derive measures of HRV from them. The triangular index is a measure, where the length of RRI serves as the x -axis of the plot and the number of

each RRI length serves as the y -axis. The length of the base of the triangle is used and approximated by the main peak of the RRI frequency distribution diagram. The triangular interpolation of NN interval histogram (TINN) is the baseline width of the distribution measured as a base of a triangle, approximating the NN interval distribution (the minimum of HRV). Triangular interpolation approximates the RRI distribution by a linear function and the baseline width of this approximation triangle is used as a measure of the HRV index [127, 128]. This triangular index had a high correlation with the standard deviation of all RRI. But it is highly insensitive to artefacts and ectopic beats, because they are left outside the triangle. This reduces the need for pre-processing of the recorded data [128]. The major advantage of the geometric methods lies in their relative insensitivity to the analytical quality of the series of NN intervals [129], while the major disadvantage is the need for a reasonable number of RRI and a longer ECG recording. The statistical and geometric measures of HRV are shown in Table 3-1.

Table 3-1. Time domain measures of HRV [18].

Variable	Units	Description
Statistical measures		
SDNN	ms	Standard deviation of all NN intervals.
SDANN	ms	Standard deviation of the averages of NN intervals in all 5-minute segments of the entire recording.
RMSSD	ms	The square root of the mean of the sum of the squares of differences between adjacent NN intervals.
SDNN index	ms	Mean of the standard deviations of all NN intervals for all 5-minute segments of the entire recording.
SDSD	ms	Standard deviation of differences between adjacent NN intervals.
NN50 count		Number of pairs of adjacent NN interval differing by more than 50 ms in the entire recording.
pNN50	%	NN50 count divided by the total number of all NN intervals.
Geometric measures		
HRV triangular index		Total number of all NN intervals divided by the height of the histogram of all NN intervals measured on a discrete scale with bins of 7.8125 ms (1/128 s).
TINN	ms	Baseline width of the minimum square difference triangular interpolation of the highest peak of the histogram of all NN intervals.

3.2.3.2 Frequency domain methods

The time domain methods are computationally simple, but lack the ability to discriminate between sympathetic and parasympathetic contributions of HRV. These studies of HRV employed a power spectral density (PSD) analysis providing the basic information of how power (i.e. variance) distributes as a function of frequency. The HR signal is decomposed into its frequency components and quantified in terms of their relative intensity (power) [130]

Methods for the calculation of PSD may be generally classified as *non-parametric* and *parametric*. In most instances, both methods provide comparable results. The advantages of the *non-parametric* methods are: (a) the simplicity of the algorithm employed (fast Fourier transform—FFT—in most of the cases) and (b) the high processing speed. But these methods, i.e. FFT, suffer from spectral leakage effects due to windowing. The spectral leakage leads to masking of weak signal that are present in the data. The *parametric* (model based) power spectrum estimation methods avoid the problem of leakage and provide better frequency resolution than nonparametric or classical methods. The advantages of *parametric* methods are: (a) smoother spectral components which can be distinguished independently of preselected frequency bands, (b) easy post-processing of the spectrum with an automatic calculation of low and high frequency power components and easy identification of the central frequency of each component, and (c) an accurate estimation of PSD even on a small number of samples on which the signal is supposed to maintain stationarity. The basic disadvantage of parametric methods is the need to verify the suitability of the chosen model and its complexity (i.e. the order of the model).

The power spectrum of healthy subjects consists of four major frequency bands. They do not have fixed periods and the central frequencies may vary considerably. The limits for the spectral components usually used [18] are: high frequency (HF) component 0.15-0.4 Hz, low frequency (LF) component 0.04-0.15 Hz, very low frequency (VLF) component 0.003-0.04 Hz, and ultra low frequency (ULF) component <0.003 Hz. To account for inter-individual differences, LF and HF power may also be expressed in normalised units where the absolute value of each power

component is expressed as a proportion of either total power (e.g. LF/total power) or total power minus the VLF component (e.g. LF/ (total power – VLF power)) [18, 131]. The ratio between LF and HF components (LF/HF ratio) is also used [131, 132]. The normalisation tends to minimise the effect of the changes in total power on the values of the HF and LF components. Nevertheless, normalised units should always be quoted with absolute values in order to completely describe the distribution of power in the spectral components. The frequency domain measures of HRV are listed in Table 3-2.

Table 3-2. Frequency domain measures of HRV [18].

Variable	Units	Description	Frequency range
Analysis of short-term recordings (5 min)			
5 min total power	ms ²	The variance of NN intervals over the temporal segment	approximately ≤ 0.4 Hz
VLF	ms ²	Power in very low frequency range	≤ 0.04 Hz
LF	ms ²	Power in low frequency range	0.04-0.15 Hz
LF norm	n.u.	LF power in normalised units LF/(Total Power-VLF) \times 100	
HF	ms ²	Power in high frequency range	0.15-0.4 Hz
HF norm	n.u.	HF power in normalised units HF/(Total Power-VLF) \times 100	
LF/HF		Ratio LF [ms ²]/HF [ms ²]	
Analysis of entire 24 h			
Total power		Variance of all NN intervals	approximately ≤ 0.4 Hz
ULF	ms ²	Power in the ultra low frequency range	≤ 0.003 Hz
VLF	ms ²	Power in the very low frequency range	0.003-0.04 Hz
LF	ms ²	Power in the low frequency range	0.04-0.15 Hz
HF	ms ²	Power in the high frequency range	0.15-0.4 Hz
α		Slope of the linear interpolation of the spectrum in a log-log scale	approximately ≤ 0.04 Hz

Frequency domain methods should be preferred to the time domain methods when investigating short-term recordings. It is recommended that the duration of the recording should be at least 10 times the wavelength of the lowest frequency bound of the spectral component investigated [18], and, in order to ensure the stability of the

signal, should not be substantially extended. Thus, a recording of approximately 1 min is needed to assess the HF components of HRV while approximately 2 minutes are needed to address the LF component. In order to standardise different studies investigating short-term HRV, 5 min recordings of a stationary system are preferred unless the nature of the study dictates another design.

3.2.3.3 Nonlinear analysis methods

Nonlinear phenomena are certainly involved in the genesis of HRV. They are determined by complex interactions of haemodynamic, electrophysiological and humoral variables, as well as by autonomic and central nervous regulations. It has been speculated that analysis of HRV based on the methods of nonlinear dynamics might elicit valuable information for the physiological interpretation of HRV.

Poincaré plot

The Poincaré plot is a simple yet powerful graphical tool to describe the dynamics of a system. In principle, one state of the system (at discrete time n) is plotted versus its state at time step $n+1$. In the language of nonlinear dynamics this represents a two-dimensional embedding. In a seemingly random signal the Poincaré plot can easily demonstrate whether there is an underlying determinism in the signal. Even in RRI time series which appear extremely erratic, consistent patterns can be extracted by a simple two-dimensional Poincaré plot. There is a fundamental asymmetry in the Poincaré plot from RRI time series. This asymmetry is probably related to strong vagal inputs to the sinus node. Initial attempts to characterise the Poincaré plot qualitatively comprised descriptions of shapes in the embedded time series [133]. This approach, so called gestalt analysis, is, however, subject to different views of the operators. A quantitative approach was used by many researchers [134-137], where the standard deviation of the distance of points to the line of identity was measured.

The technique of fitting an ellipse to the plot is adopted to characterise the shape of the Poincaré plot mathematically, as Figure 3-5 details. A set of axes oriented with the line-of-identity is defined. The axes of the Poincaré plot are related to the new set of axes by a rotation of $\theta = \pi/4$ rad:

$$\begin{bmatrix} x_1 \\ x_2 \end{bmatrix} = \begin{bmatrix} \cos \theta & -\sin \theta \\ \sin \theta & \cos \theta \end{bmatrix} \begin{bmatrix} RR_n \\ RR_{n+1} \end{bmatrix}. \quad (3-1)$$

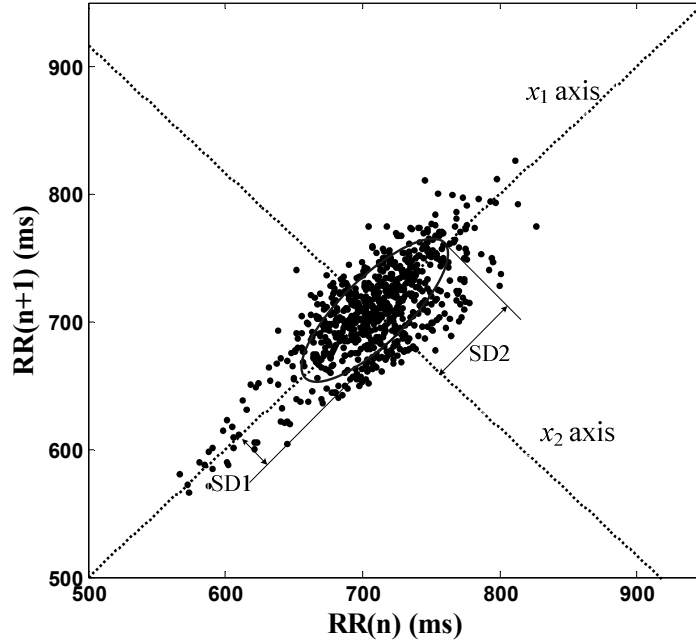


Figure 3-5. A typical Poincaré plot. An ellipse is fitted to the data points and the Poincaré plot indices are calculated by estimating the short diameter (SD1), the long diameter (SD2) and the ratio of the short and long diameters (SD1/SD2 ratio) of the fitted ellipse. SD1 is the standard deviation of the distances of points from x_1 axis, SD2 is the standard deviation of the distances of points from x_2 axis.

In the reference system of the new axis, the dispersion of the points around the x_1 axis is measured by the standard deviation denoted by SD1. This quantity measures the width of the Poincaré cloud and, therefore, indicates the level of short-term HRV. The length of the cloud along the line-of-identity measures the long-term HRV and is measured by SD2 which is the standard deviation around the x_2 axis. These measures are related to the standard HRV measures in the following manner:

$$SD1^2 = \text{Var}(x_1) = \text{Var}\left(\frac{1}{\sqrt{2}} RR_n - \frac{1}{\sqrt{2}} RR_{n+1}\right) = \frac{1}{2} \text{Var}(RR_n - RR_{n+1}) = \frac{1}{2} SDSD^2. \quad (3-2)$$

Thus, the SD1 measure of Poincaré width is equivalent to the standard deviation of the successive intervals, except that it is scaled by $1/\sqrt{2}$. This means that we can

relate SD1 to the autocovariance function (The autocovariance function related to the variance of the RRI is given in Appendix A)

$$SD1^2 = \phi_{RR}(0) - \phi_{RR}(1). \quad (3-3)$$

With a similar argument, it may be shown that the length of the Poincaré cloud is related to the autocovariance function

$$SD1^2 = \phi_{RR}(0) + \phi_{RR}(1). \quad (3-4)$$

By adding (3-3) and (3-4) together, we obtain the result

$$SD1^2 + SD2^2 = 2SDRR^2. \quad (3-5)$$

Finally

$$SD2^2 = 2SDRR^2 - \frac{1}{2}SDSD^2. \quad (3-6)$$

Recurrence plot

Recurrence plots (RP) are used to reveal nonstationarity of the series. These plots were first proposed by Eckmann *et al* [138] to visualise the time dependent behaviour of the dynamics of systems, which can be pictured as a trajectory $\vec{x}_i \in \mathfrak{R}^n$ ($i=1, \dots, N$) in the n -dimensional phase space. The main step of this visualisation is the calculation of the $N \times N$ matrix,

$$R_{i,j} = \Theta(\varepsilon_i - \|\vec{x}_i - \vec{x}_j\|) \quad i, j = 1, \dots, N, \quad (3-7)$$

where ε_i is a threshold distance, $\|\cdot\|$ is a norm (e.g. Euclidean norm), and $\Theta(\cdot)$ the Heaviside step function. The phase space vectors for one-dimensional time series μ_i from observations can be reconstructed by using the Taken's time delay method

$$\vec{x}_i = (\mu_i, \mu_{i+\tau}, \dots, \mu_{i+(m-1)\tau}), \quad (3-8)$$

where m is the embedding dimension and τ is the time delay.

One of the major reasons that RP is popular lies in the fact that the structures of RP are visually appealing. The binary values in $R_{i,j}$ can be simply visualized by a black and white matrix plot. Interpretation of RP is given in Appendix B.

3.3 Summary

PPG enables the noninvasive measurement of the peripheral pulse wave. Interpretation of the PPG pulse wave is based on pattern changes rather than on absolute measurements. Characteristics of the waveform reveal valuable information for circulatory dynamics. The PPG signal, reflecting the fluctuations of the heartbeats, has the potential to noninvasively provide valuable information for cardiovascular monitoring. ‘Heart Rate Variability’ has become the conventionally accepted term to describe variations of both instantaneous heart rate and RR intervals. HRV analysis, including time domain method, geometric method, frequency domain method and nonlinear methods, has been widely used to investigate ANS regulation of cardiovascular function.

CHAPTER 4

CARDIOVASCULAR MONITORING SETUPS, PROTOCOLS AND APPROACHES

The PPG technique for noninvasive cardiovascular assessment has been conducted in five different ways:

- Contour analysis of PPG pulse wave to assess artery stiffness.
- Quantifying PRV to investigate the reliability of acquiring dynamics pertaining to the autonomic nervous system (ANS) from PPG signal.
- Practical examples of PRV for cardiac function assessment.
- Development of noncontact reflection PPG (NRPPG) system.
- Examining the effectiveness of NRPPG for biomedical monitoring.

The experimental setup, protocols and approach are detailed in this chapter.

Five studies, pertaining to noninvasive cardiovascular assessment using the PPG technique, can be briefly described as below:

Study I: the contour analysis of the PPG pulse in a group of young adults;

Study II: the compatibility of PRV derived from PPG and HRV derived from ECG;

Study III: PRV analysis in smokers and non-smokers;

Study IV: the possibility of noncontact PPG instead of contact PPG;

Study V: a practical case utilising noncontact PPG for biomedical monitoring.

4.1 Engineering setups

4.1.1 Contact measurement

The lead II ECG signal (Study II) was collected with three electrodes on the right wrist, the left wrist and the right leg of the subjects. Ear PPG signal (Studies II and III) and finger PPG signal (Studies I and II) were recorded from the left ear lobe with an ear clip (MLT1020EC, ADInstruments, Australia) and the index finger with a finger spring clip (MTL1020FC, ADInstruments, Australia). The finger clip, consisting of a reflected infrared light (wavelength: 950 nm), works best where the light can reflect from the bone beneath the tissue. The ear clip uses infrared light (wavelength: 950 nm) transmitted through the tissue. The amplitude of the PPG signal depends primarily on the volume of blood in the capillary bed directly beneath the sensor, so it may be necessary to move the sensor around to find the best signal. The ECG signals were amplified by a low-noise, high-gain differential amplifier (BIO Amp ML135, ADInstruments, Castle Hill, Australia). The PPG signal and amplified ECG signals were fed continuously into a 16-channel input ADC (PowerLab/16SP, ADInstruments Corporation, Castle Hill, Australia) and recorded in its associated software (Chart 5.2) for further analysis. Figure 4-1 presents the setup for the contact measurement.

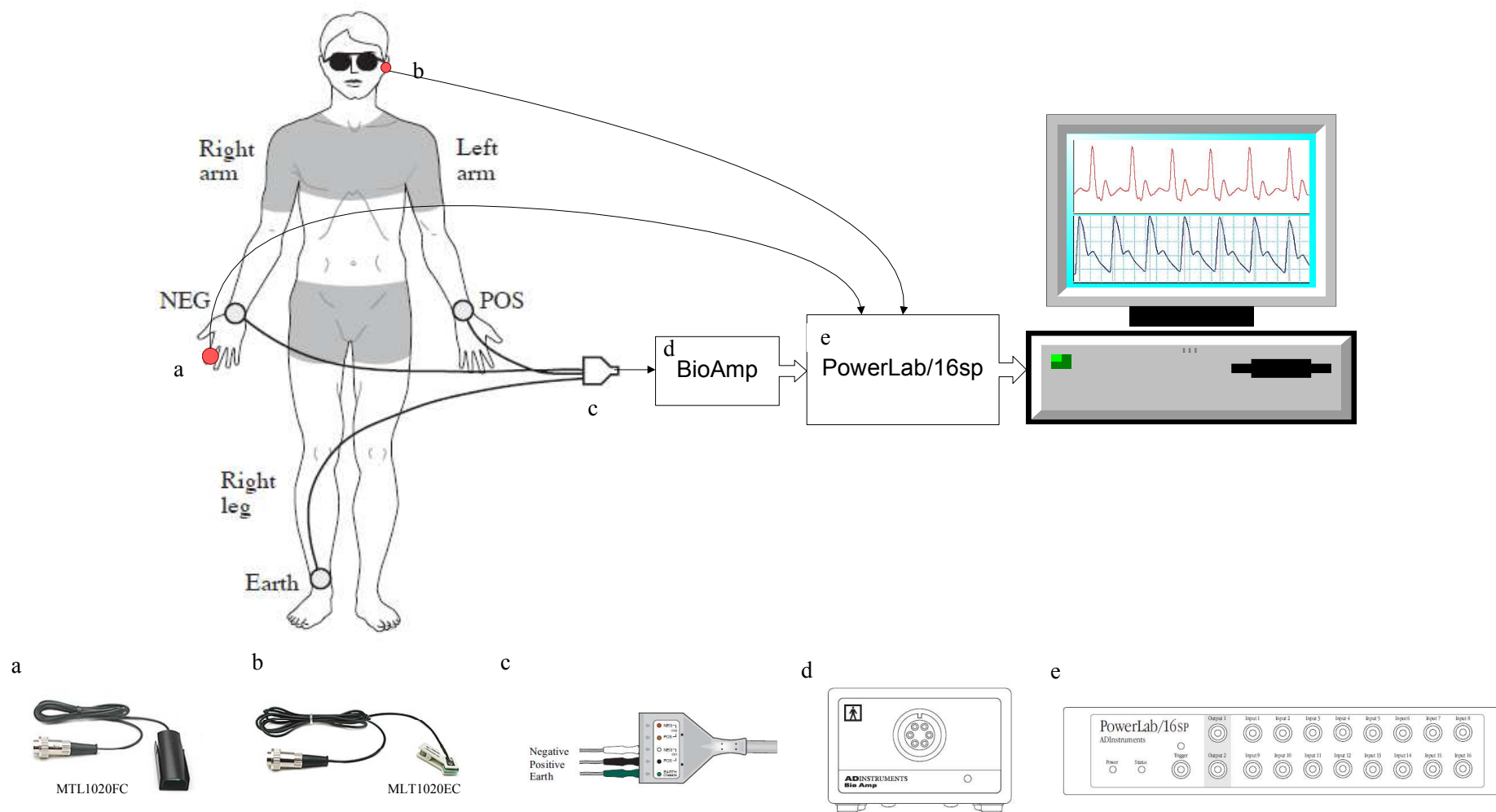


Figure 4-1. Contact measurement setup.

4.1.2 Noncontact measurement

4.1.2.1 Noncontact reflection PPG model

A NRPPG model based upon the Beer-Lambert's law [139] was taken into account to describe the relationship between the light incident on the biological tissue and the light received after transmission through it. This measurement method relies on the varying light absorption due to arterial blood volume change during a cardiac cycle.

Figure 4-2 shows a simplified diagram of the light distribution of the NRPPG model. I_i is the light incident on the skin surface; I_o is the intensity of light penetrating the skin; I_r is the reflected light intensity; and I is the intensity of light emerging from the tissue following a banana-shaped primary light path [140].

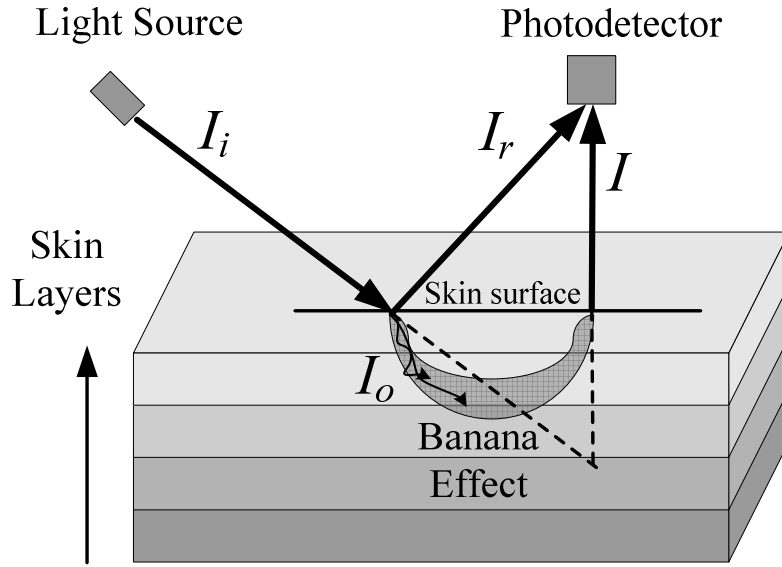


Figure 4-2. Simplified representation of light distribution.

The light reaching the photodetector can be separated into *non-dynamic* (DC) and *dynamic* (AC) terms. DC consists of the reflected component (I_r) and the static component (from non-variable absorbers, i.e. tissue, bone, static blood etc.), while AC represents the variation of light absorption due to arterial blood volume change. I , thus, can be expressed as:

$$I = I_o \exp(-\mu_{eff} r) = I_o \exp[-\mu_{dynamic} d(t) - \mu_{static} m], \quad (4-1)$$

where $\mu_{dynamic}$ is the extinction coefficient of the dynamic component, and μ_{static} is the extinction coefficient of static components. The light path length through the dynamic and static components are $d(t)$ and m , respectively.

The primary target of this study is to calculate pulse rate variability (PRV) derived from PPG signals, in which the accuracy of PRV depends upon the quality of the AC term. Therefore the *dynamic* (AC) term should be maximised during the measurement period. This can be achieved by maximising the light intensity that travels through the tissue I , while minimising the reflection component of the static signal I_r in order to avoid saturation of the photodetector. The light intensities at the illuminated surface and the detector are given by $I_i = I_o + I_r$ and $I_t = I_r + I$, respectively. The normalised AC term is directly proportional to I/I_r , and is maximised when I_r is minimised.

The light intensity at the detector can be expanded by applying the Taylor series first order approximation to the dynamic term for the exponential function ($e^{-x} = 1 - x, x \cong 0$):

$$I_t = I_r + I_o \exp[-\mu_{dynamic}d(t) - \mu_{static}m] = I_r + I_o \exp(-\mu_{static}m)[1 - \mu_{dynamic}d(t)]. \quad (4-2)$$

From equation (4-2), the *static* term $I_r + I_o \exp(-\mu_{static}m)$ is the DC component of the detected signal obtained by low-passing the signal, e.g. 10th order Butterworth [141] (see Appendix C for details), $f_{cut-off}$: 0.3Hz; and the AC component is $I_o \exp(-\mu_{static}m)\mu_{dynamic}d(t)$, which is obtained by band-passing the signal, e.g. 10th order Butterworth, f_1 : 0.5Hz, f_2 : 5Hz. The AC term becomes independent of the light source intensity by normalising the AC with respect to the DC :

$$\frac{AC}{DC} = \frac{I_o \exp(-\mu_{static}m)\mu_{dynamic}d(t)}{I_o \exp(-\mu_{static}m)} = \mu_{dynamic}d(t). \quad (4-3)$$

Hence the amplitude of the normalised AC is proportional to the time-variant arterial light path length, which in turn depends on the characteristics of the banana-shaped light path. In practice, the reflected light is significant, resulting in an additive term in the denominator of equation (4-3), the minimisation of which results in a maximised

dynamic term.

4.1.2.2 Noncontact reflection PPG photonics engineering setup

For the hardware setup, a vertical cavity surface emitting laser (VCSEL, Mode: PH85-F1P1S2, 10mw, 850nm, Roithner LaserTechnik Ltd, Austria) with an inherently narrow beam divergence of 30° and a high coherence was employed as a light source and was positioned to the illuminated tissue area at a changeable incident angle θ_{PL} . A high-speed silicon PiN photodiode (Mode: S5821-03, Hamamatsu Photonics UK Limited) with a high sensitivity over the spectral range of 500-1000 nm and the viewing angle of 10° was employed as a photodetector. The signals from the NRPPG engineering setup and a commercial CPPG probe (P861RA, 664 nm and 890 nm, Viamed Ltd. UK) were simultaneously captured by a 4-channel PPG board (DISCO4, Dialog Devices Ltd, UK). The analogue-to-digital conversion for these captured PPG signals was implemented by a data acquisition board (USB-6009, National Instruments Co., USA), and the control software of the PPG board was performed by LabView 7.1 (National Instruments Co., USA) running on a Pentium IV computer.

The NRPPG photonics engineering setup was used to find an appropriate geometrical relationship between the positions of the light source and the photodetector. Directly coupled (reflected) light is dependent on the incident angle (θ_{PL}). Assuming a point source illumination and a fixed probing area in an empirical noncontact reflection measurement setup, the separation between the point of illumination and the probed area (l), which is determined by the incident angle (θ_{PL}) as well as the distance between the photodetector and the tissue (d_{PH}), determine the characteristics of the banana-shape effect. The light source beam has a finite width in practice; therefore, it is necessary to introduce an additional parameter for the separation between the light source and the photodetector (d_{PL}) which determines the characteristics of the illuminated surface. The focus plane of the illuminated tissue varied with the distance of the palm to the photodiode (d_{PH}). Figure 4-3 illustrates the relationship between these parameters.

This process of optimisation for the geometrical characteristics of the NRPPG system aimed to minimise the direct coupling by adjusting incident angle θ_{PL} while determining separation d_{PL} for optimum dynamic signal detection. The angle of the photodiode was fixed perpendicular to the tissue. The VCSEL was positioned at an incident angle (θ_{PL}) of 35° , 25° and 15° as well as a distance of the sensor placement against the photodiode (d_{PL}) at 15 mm, 25 mm and 35 mm, respectively. The experimental results for the optimisation of sensor placement are presented in Chapter 5.

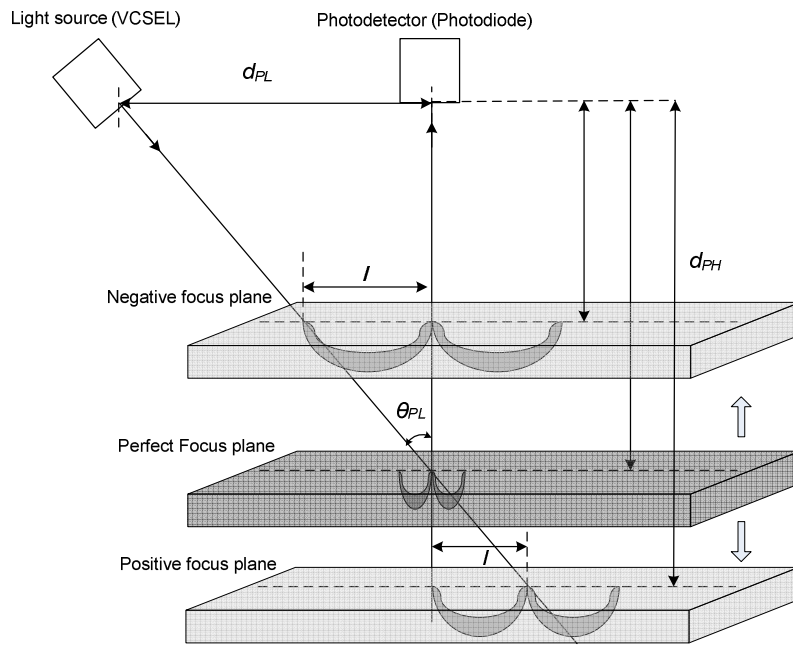


Figure 4-3. Instrumental hardware setup for NRPPG system illustrating the fundamental parameters. θ_{PL} and d_{PL} are the parameters that determine the position of VCSEL and photodiode. By moving the palm close to or further from the photodiode, the focus plane will change position accordingly.

4.2 Protocols

All experiment protocols were approved by both the Ethics Committees of Shanghai Jiao Tong University and Loughborough University. Measurements were conducted in a quiet room, at comfortable light and temperature levels. All subjects had no history of cardiovascular abnormality and none were taking medication. All subjects were requested to avoid strenuous exercise, refrain from consuming hot drinks or those containing caffeine, or eating a substantial meal for one hour prior to the studies. The PPG signals were recorded in the supine position (Studies I, II and III) or sitting

position (Studies IV and V) during spontaneous breathing. Subjects were asked to remove any fingerings or earrings prior to the recording session. The subjects' height and weight were recorded. In study III, smoker subjects were not allowed to smoke one hour before the measurement, as acute smoking may be associated with haemodynamic changes in the cardiovascular system [142]. All gave their informed consent to participate in the study which was approved by the local ethical advisory committee.

In study I, fifteen volunteers (Male/Female [M/F]: 9/6, age: 25.5 ± 4.1 years) participated in the measurement. The subjects are formed into gender and age groups: nine males (age: 26.4 ± 5.1 years), six females (age: 24.0 ± 1.3 years), eight subjects under 25-year-old (age: 22.8 ± 1.4 years), and seven subjects over 25-year-old (age: 28.6 ± 4.0 years).

In study II, fourteen volunteers (M/F: 7/7, age: 25.8 ± 4.2 years) participated in the measurement.

In study III, eight healthy habitual smokers (M/F: 7/1, age: 38.6 ± 17.6 years) having more than 10 cigarettes daily and with over 5 years smoking history, and eight healthy non-smokers (M/F: 7/1, age: 31.6 ± 12.6 years) within the same age range ($p=0.51$) participated in the measurement.

In study IV, twenty-two healthy subjects (M/F: 12/10, age: 29.0 ± 9.0 years) participated in the measurement. The PPG signals from NRPPG and CPPG system were recorded simultaneously from the right index fingertip and the right palm.

In Study V, the physiological monitoring for one subjects (female, 27 years) was investigated. The PPG signals from the NRPPG setup were collected in the morning and in the afternoon each day during a period of fourteen working days. The PPG signals were recorded for 3 minutes during each recording at the same location of the left palm, where the peripheral arteries are close to the skin surface.

The basic information of the subjects and experimental protocols are presented in Tables 4-1 and 4-2 respectively.

Table 4-1. Descriptive information of the subjects in Studies I-V.

Item	Study I	Study II	Study III		Study IV	Study V
			Habitual smokers	non-smokers		
Size (n)	15	14	8	8	22	1
<i>Male</i>	9	7	7	7	12	0
<i>Female</i>	6	7	1	1	10	1
Age(years) for Group/Subgroup:	All(15):25.5±4.1 Male(9):26.4±5.1 Female(6):24.0±1.3 Younger(8):22.8±1.4 Older(7):28.6±4.0	25.8±4.2	38.6±17.6	31.6±12.6	29.0±9.0	27
Height(m)	167.5±7.8	167.5±7.9	n/a	n/a	1.70±0.10	1.56
Weight(kg)	59.1±11.3	56.1±7.8	n/a	n/a	69.0±19.5	54
BMI(kg/m ²)	20.9±2.9	19.9±1.5	n/a	n/a	23.1±4.6	22.2
Cardiovascular assessment	Arterial stiffness in the young adults by the mean of PPG pulse wave analysis	PRV can serve as an alternative approach to obtain HRV Information	Practical study of PRV analysis for distinguishing the heart activity between smokers and non-smokers		NRPPG can serve as alternative technique for CPPG	NRPPG used for physiological monitoring

The values are means ± SD or the numbers of subjects in each group when appropriate.

Table 4-2. Overview of the protocols in Studies I-V.

Item	Study I	Study II	Study III	Study IV	Study V
Position	Supine	Supine	Supine	Sitting	Sitting
Site	Finger tip	Arm and leg, Finger tip, Ear lobe	Ear lobe	Finger tip, Palm	Palm
Signal	PPG	Lead II ECG, PPG	PPG	PPG	PPG
Data acquisition system	Powerlab	Powerlab	Powerlab	Costumed system	Costumed system
Requirements	<ol style="list-style-type: none"> 1. avoid strenuous exercise, refrain from consuming hot drinks or those containing caffeine, or eating a substantial meal for one hour prior to the studies; 2. remove any fingerings or earrings during the signal recordings; 3. keep still and breathe spontaneously; 4. temperature-controlled room ($25\pm 1^{\circ}\text{C}$); 5. smoker subjects were asked not to smoke one hour before the measurement in study III. 				
Design	Between groups, Within subjects	Within subjects	Between groups, Within subjects	Within subjects	n/a
Time to perform	10 minutes	12 minutes	10 minutes	3 minutes	3 minutes
Approval	<ol style="list-style-type: none"> 1. approved by the both Ethics Committees of Shanghai Jiao Tong University and Loughborough University. 2. all gave their informed consent to participate in the study which was approved by the local ethical advisory committee. 				

4.3 Physiological parameter measurements

4.3.1 Contour analysis of PPG waveform

In Study I, the PPG pulses for the young adults clearly exhibit first and second peaks as shown in Figure 4-4. The first peak corresponds to a direct forward-travelling pressure wave from the heart to the finger where it produces a change in arterial diameter and hence volume, and the second peak corresponds to the backward-travelling ‘reflected’ pressure wave [107]. A simple and robust algorithm is required to effectively detect and characterise the dicrotic wave since the distinct notches were found to be prevalent in younger individuals [16]. The well-defined dicrotic notch searching algorithm (WDNSA) seeking the “well-defined dicrotic notch (WDN)” between the maximum (a, y_a) and the following minimum at (b, y_b) , *i.e.* *local minimum* (Figure 4-4) can be principally outlined as follows:

1. For each sample i between a and b , define j_i to be the location of the lowest pressure between a and i .
2. Define m to be the sample for which $y_m - y_{jm}$ is the greatest (or least negative). Then take (j_m, y_{jm}) to be the dicrotic notch.
3. Mark the dicrotic notch position as successfully found only if $y_m - y_{jm}$ is 5% or more of the cycle height.

Not all pulse waveforms with second peak are WDN pulses. Only the waveform with the distinct notch defined by the above algorithm is accounted for WDN pulse. Relevant parameters, *i.e.* H_{pulse} , T_{peak} , T_{pulse} , H_{notch} and T_{notch} , were extracted from the PPG pulses, as shown in Figure 4-4. The absolute and relative vertical and horizontal PPG notch positions were measured. These parameters are given in Table 4-3.

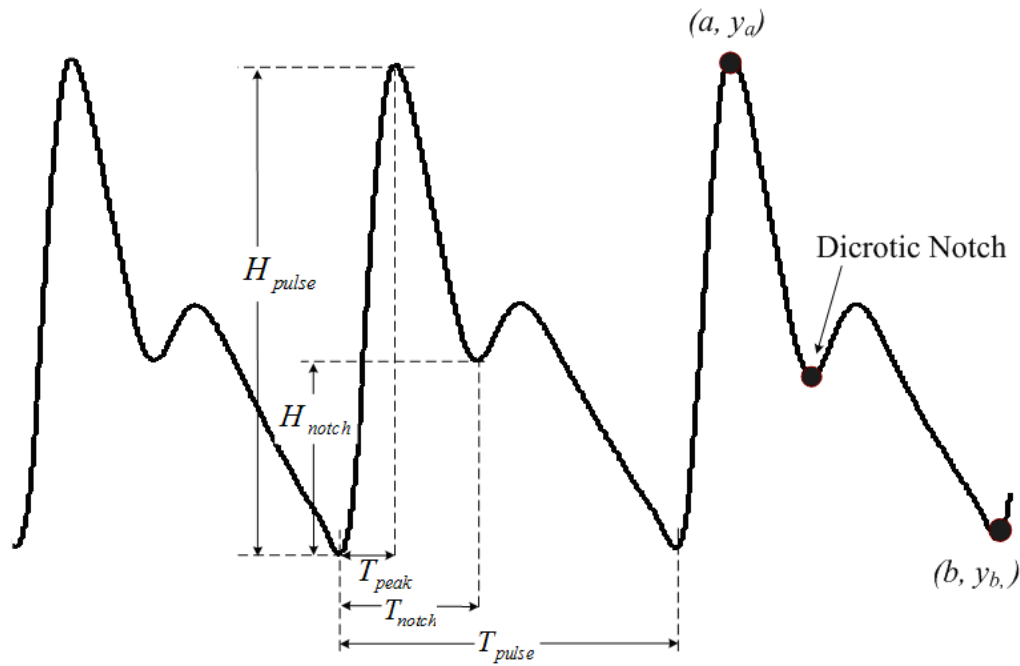


Figure 4-4. The schematic dicotic notch and the associated parameters.

Table 4-3. Descriptions of the PPG features.

Features	Measurement	Parameters	Abbreviation
PPG amplitude	Distance from the pulse baseline to the pulse maximum during the cycle	H_{pulse}	
peak duration	Elapsed time between the start of the cycle and the time of the pulse maximum	T_{peak}	
pulse duration	Total pulse duration	T_{pulse}	
PPG notch amplitude	Distance from the baseline to the notch minimum	H_{notch}	
notch duration	Elapsed time between the start of the cycle and the time of the notch minimum	T_{notch}	
PPG peak latency	Percentage of the time-to-peak to the total pulse duration	$\frac{T_{peak}}{T_{pulse}}$	PPL
notch relative amplitude	Percentage of the notch amplitude to the total pulse amplitude	$\frac{H_{notch}}{H_{pulse}}$	PNRA
PPG notch latency	Percentage of the time-to-notch to the pulse time	$\frac{T_{notch}}{T_{pulse}}$	PNL
Peak-to-notch latency		$\frac{T_{notch} - T_{peak}}{T_{pulse}}$	PTNL
Notch index		$\frac{T_{notch}}{T_{pulse} - T_{notch}}$	NI

4.3.2 Measurement of HRV and PRV

4.3.2.1 Time Domain measures

The cardiac time intervals were extracted from ECG signal and PPG signal (Studies II and IV). Simple time domain variables include the average HR, the mean HR, the range of NN interval (the difference between the longest and shortest NN interval), and the mean NN interval. The most commonly used measures derived from interval differences comprise SDNN, SDSD, RMSSD, NN50, and pNN50.

4.3.2.2 Frequency domain measures

For HR series or pulse rate series (Studies II and III), Welch's method [143] (named periodogram method) for estimating power spectra was carried out by dividing the time signal into successive blocks, and averaging squared-magnitude discrete Fourier transform of the signal blocks. In Welch's method, principally, the data are divided into eight segments with 50% overlap between them. The overlap between segments tends to introduce redundant information; this effect is diminished by the use of a nonrectangular window, which reduces the importance or weight given to the end samples of segments. The averaging of modified periodograms tends to decrease the variance of the estimate relative to a single periodogram estimate of the entire data record. Low frequency (LF: 0.04–0.15 Hz) and high frequency (HF: 0.15–0.4 Hz) power components were taken into account. LF and HF were also expressed in normalised units (n.u.) $[(\text{absolute power}) \times 100 / (\text{total power} - \text{VLF power})]$, where LF(n.u.) and HF(n.u.) represent the relative power component to the total power minus the VLF component [18, 131].

The power spectrum of PPG signal for healthy subjects consists of three major frequency bands (Study IV). They do not have fixed periods and the central frequencies may vary considerably. The limits for the spectral components, according to the heart rate of normal subjects, usually used are: very low frequency component

for PPG signal (pVLF) 0.01-0.5 Hz, low frequency component for PPG signal (pLF) 0.5-1.5 Hz and high frequency component for PPG signal (pHF) 1.5-6 Hz [1].

4.3.2.3 Nonlinear measures

Poincaré plot and Lagged Poincaré plot

The Poincaré plot is an intuitive and commonly used method to assess complex physiological signals in a nonlinear manner. The Poincaré plot was used to outline the PRV measurements and to provide the detailed pulse-to-pulse dynamics (Studies II, IV and V). The dispersion of the points perpendicular to line-of-identity measures the width of the Poincaré plot and reflects the level of short-term PRV (SD1). The dispersion of the points along the line-of-identity measures the length of the plot and is thought to indicate the level of long-term PRV (SD2).

The conventional two-dimensional Poincaré plot, i.e. 1-lagged Poincaré plot, is generated by plotting each RRI as a function of its previous RRI ($[RR_i, RR_{i+1}]$). The clue that the next RRI is determined by the previous ones leads itself to further generalisation with different intervals, i.e. m-lagged Poincaré plots ($[RR_i, RR_{i+m}]$, $m \geq 1$). In Study III, instead of the plotting RR_n , against RR_{n+1} , in conventional two-dimensional Poincaré plots, the plotting of successive pulse-to-pulse intervals was investigated, i.e. PP_n against PP_{n+m} , where m is allowed to vary from 1 to 10. In nonlinear dynamics, the 2-D phase space with the time series is embedded with lag m , and the plot is generally still clustered around the line-of-identity. However, the length and the width of the plot are altered as the lag is increased. SD1 and SD2 generalised for lag m are given by [144].

$$SD1(m)^2 = \phi_{PP}(0) - \phi_{PP}(m), \quad (4-4)$$

$$SD2(m)^2 = \phi_{PP}(0) + \phi_{PP}(m), \quad (4-5)$$

where $\phi_{PP}(m)$ is the autocovariance function, and is expressed as

$$\phi_{PP}(m) = E\left[\left(PP_n - \overline{PP}\right)\left(PP_{n+m} - \overline{PP}\right)\right]. \quad (4-6)$$

Considering the facts that m -lagged Poincaré plots can be described as the autocovariance function, and the autocovariance function monotonically decreases with the increasing lag for values of lag less than 10, lags between 1 and 10 for each subject were applied in Study III. $SD1_m$ and $SD2_m$ were introduced to express the width and the length in m -lagged Poincaré plots, respectively.

Recurrence plot

In Study IV, RP was used to reveal the differences between signals detected from CPPG and NRPPG; and a fixed ε_i and the Euclidean norm are used, resulting in a symmetric RP.

4.4 Statistical analysis

Continuous variables were expressed as mean \pm SD (Studies I-V) or median and interquartile range* (Studies II, III and IV). p -values <0.05 were considered statistically significant.

Kurtosis and Skewness coefficients were used to assess the probability distributions of the signal series (Study II).

The Kurtosis is defined as:

$$\text{Kurtosis} = \frac{E[(X - \mu)^4]}{\sigma^4}, \quad (4-7)$$

where X is the data set, i.e. the RRI or PPI series, μ is the mean value of the data set, and σ represents the SD of the data set, and $E(t)$ represents the expected value of the quantity t . The Kurtosis measures how sharply peaked a distribution is, relative to its width. A Kurtosis greater than 3 indicates a leptokurtic data set and a value less than 3 indicates a platykurtic data set.

* interquartile range: the distance from the 25th percentile to the 75th percentile

The Skewness is defined as:

$$\text{Skewness} = \frac{E[(X - \mu)^3]}{\sigma^3}, \quad (4-8)$$

where X is the data set, i.e. the RRI or PPI series, μ is the mean value of the data set, σ represents the standard deviation of the data set, and $E(t)$ represents the expected value of the quantity t . The Skewness measures the asymmetry of the tails of a distribution. A positive Skewness indicates that most of the data are located to the left of the mean and a negative value shows that most of the data are on the right side of the mean.

The agreement analysis between two measurements (HRV and PRV in Study II) or techniques (CPPG and NRPPG in Study IV) was performed using Bland-Altman statistic method. The Bland-Altman ratio is expressed as the half range of limits of agreement (LA) to the mean of the pairwise means (MPM),

$$\text{Bland - Altman ratio} = \frac{0.5 \times [\max(LA) - \min(LA)]}{MPM}. \quad (4-9)$$

A Bland-Altman ratio up to 0.1 is considered as good agreement [145]. A ratio between 0.1 and 0.2 is considered as moderate agreement. Insufficient agreement for clinical purposes is defined as a Bland-Altman ratio higher than 0.2. The Bland-Altman ratio provides a numerical assessment of agreement between two methods as an alternative to that provided visually by the Bland-Altman plot.

The Bland-Altman plot [146, 147] is based on the mean and standard deviation of the differences between the measurements by the two methods. The x axis of the plot shows the mean of the results of the two methods ($[A + B]/2$), whereas the y axis represents the absolute difference between the two methods ($[B - A]$). The standard deviation of the differences between measurements made by the two methods provides a good index of the comparability of the methods. If we can estimate the mean and standard deviation reliably, with small standard errors, we can then say that the difference between methods will be at most two standard deviations on either side of the mean for 95% of observations. These $\text{mean} \pm 1.96\text{SD}$ limits for the difference are called the 95% limits of agreement.

Correlation is a technique for investigating the relationship between two quantitative, continuous variables. Pearson's correlation coefficient (r) was calculated as a measure of the strength of the association between two variables (Study I, II and IV). The formula for Pearson's correlation takes on many forms. The formula applied in this work is shown as follows,

$$r = \frac{\sum XY - \frac{\sum X \sum Y}{N}}{\sqrt{\left(\sum X^2 - \frac{(\sum X)^2}{N}\right) \left(\sum Y^2 - \frac{(\sum Y)^2}{N}\right)}} \quad (4-10)$$

where N is the number of the data, and X and Y are the variables, respectively.

Table 4-4 lists the measures applied in Studies I-V.

4.5 Summary

Chapter 4 describes the protocol designs of different studies to examine the photoplethysmographic assessment of cardiovascular function. Also this chapter describes the physiological parameter measurements and statistics in the five studies.

Table 4-4. The measures in Studies I-V.

Item	Study I	Study II	Study III	Study IV	Study V
Processing	PPG waveform	HRV and PRV series	e-PRV series	PPG signal and PRV series	PRV series
Time domain measures		average heart rate, Range NN, Mean NN, SDNN, SDSD, RMSSD, NN50, pNN50,		Range of PPI, Mean of PPI, NN50, pNN50, RMSSD, SDSD, SDNN, SD1, SD2, SD1/SD2,	
Frequency domain measures		TP, LF, LF(n.u.), HF, HF(n.u.), LF/HF	TP, LF, LF(n.u.), HF, HF(n.u.), LF/HF	pVLF, pLF, pHF,	
Nonlinear measures		Poincaré plot: SD1, SD2, SD1/SD2	Lagged Poincaré plot: SD1 _m , SD2 _m , SD1 _m /SD2 _m	Poincaré plot: SD1 _m , SD2 _m , Recurrence plot	Poincaré plot: SD1, SD2, SD1/SD2
Statistical analysis	Pearson correlation coefficient	Kurtosis, Skewness, Bland-Altman ratio, Pearson correlation coefficient		Bland-Altman plot, Pearson correlation coefficient	Comparison plot
Other	Contour analysis				

CHAPTER 5

PHYSIOLOGICAL CHARACTERISTICS

DERIVED FROM

PHOTOPLETHYSMOGRAPHY SIGNALS

Significant results from the experimental studies are based on contour analysis of photoplethysmographic pulse, measurement and analysis of HRV and PRV, and analysis of heart rate information from NRPPPG. These results are presented in detail in this chapter.

5.1 Dicrotic notch in PPG waveform from young adults

In Study I, the arterial stiffness of the young adults was noninvasively investigated by means of contour analysis of PPG waveform. The waveform information from these young adults is exhibited in Table 5-1, which presents the number of total waveforms, the number of WDN pulses, and their *Ratio* (Number of WDN pulse/Number of whole waveform) to measure the percentage of the WDN pulse in the whole pulse number.

The characteristics of PPG waveforms are summarised in Table 5-2. The *t*-tests were performed to express the significance between genders or between different age groups. Three parameters, i.e. NI, PNL and PTNL, were found significantly bigger in the female group than those in the male group (all $p < 0.02$). No significant difference was found for PNRA between genders. The parameter, PNRA, was found significantly bigger in the older group compared to the younger group ($p = 0.016$). No significant difference was found for NI, PNL and PTNL between groups of different age.

The relationships between NI and PNL, NI and PTNL or PNL and PTNL, as shown in Figures 5-1(a), 5-1(c) and 5-1(e), present a highly significant linear correlation with r from 0.8 to 1.0 (all $p < 0.001$). PNRA and PTNL present negative correlation with $r = -0.48$, as shown in Figure 2(f).

Figure 5-2 shows the correlation between age and parameters. A good correlation ($r = 0.77$, $p < 0.001$) between the parameters of PNRA and age were found, as shown in Figure 5-2(c).

Table 5-1. Waveform information in the young adults. The values are given as median and interquartile range.

Group(n)/Clinical parameter	Number of total waveforms	Number of WDN pulses	Ratio(Number of WDN pulses/ Number of total waveforms)(%)
Whole(15)	928(810-1079)	86(18-307)	10.3(1.9-40.3)
Female(6)	996.5(917-1076)	22.5(17-89)	2.4(1.7-9.6)
Male(9)	867 (713-1078)	224 (84-576)	25.8 (7.9-88.3)
under 25-year-old(8)	1079(976-1108)	137(68.5-521)	12.9(6.3-64.1)
over 25-year-old(7)	814(745-890)	25(13.5-154)	2.5(1.7-18.0)

Table 5-2. Waveform characteristics. The values are given as mean \pm SD.

Group(n)/Clinical parameter	NI	PNL	PNRA	PPL	PTNL
Whole(15)	0.72 \pm 0.17	0.40 \pm 0.05	0.58 \pm 0.08	0.17 \pm 0.02	0.24 \pm 0.04
Female(6)	0.84 \pm 0.13	0.44 \pm 0.03	0.58 \pm 0.09	0.18 \pm 0.02	0.26 \pm 0.04
Male(9)	0.64 \pm 0.14 ^a	0.38 \pm 0.05 ^b	0.58 \pm 0.08	0.16 \pm 0.03	0.22 \pm 0.03 ^c
under 25-year-old(8)	0.69 \pm 0.11	0.40 \pm 0.03	0.54 \pm 0.05	0.16 \pm 0.01	0.24 \pm 0.03
over 25-year-old(7)	0.75 \pm 0.22	0.41 \pm 0.07	0.63 \pm 0.08 ^d	0.17 \pm 0.03	0.23 \pm 0.05

^a $p=0.012$; ^b $p=0.014$; ^c $p=0.019$; ^d $p=0.016$. The t -tests are performed between genders or between different age groups. n is the number of the subjects in the group..

Correlation coefficients between relevant parameters

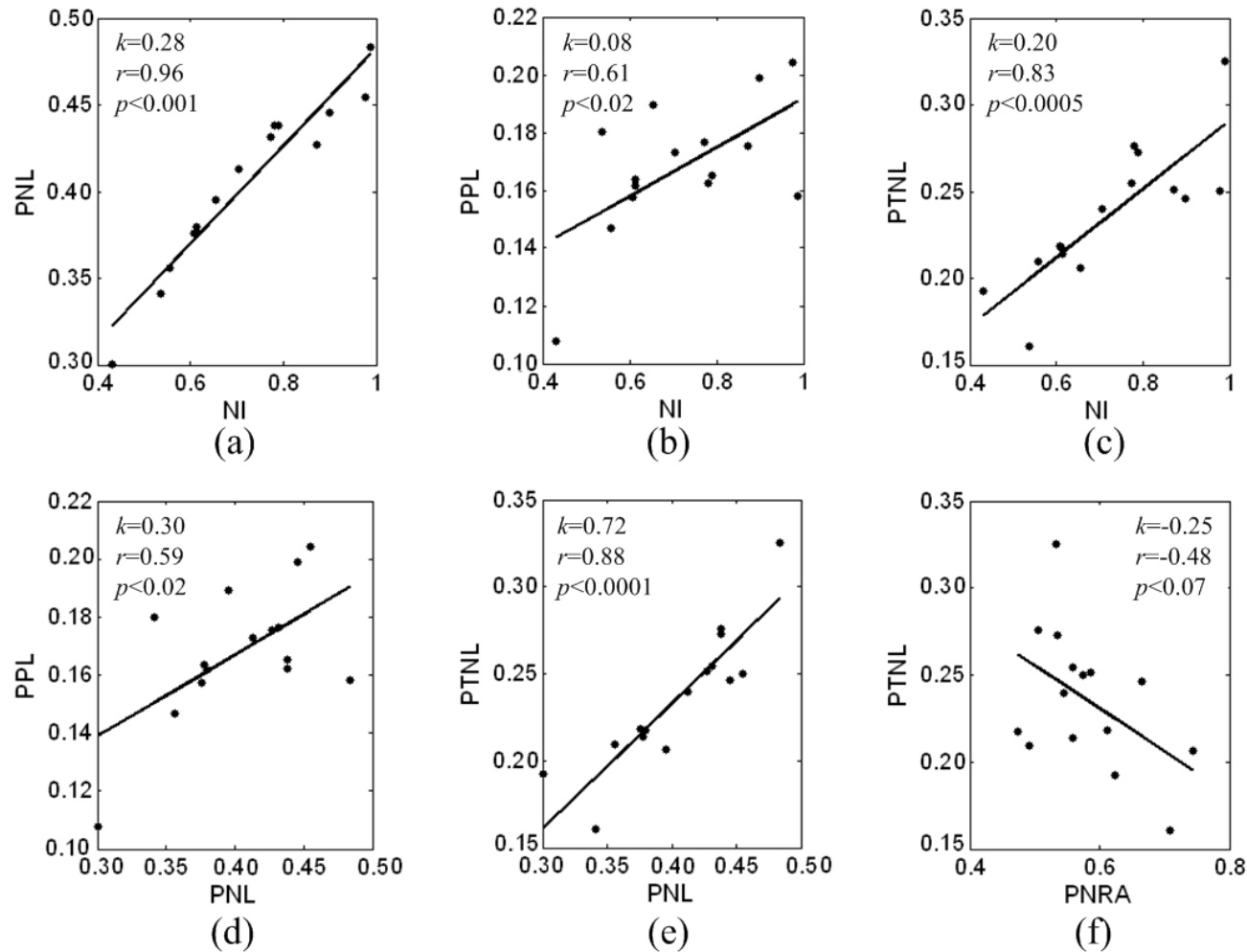


Figure 5-1. Linear correlation analysis between relevant parameters. Dots represent the values of these parameters. k , r and p represent the line slope, the correlation coefficients and the significance, respectively. The relationships are between (a) NI and PNL, (b) NI and PPL, (c) NI and PTNL, (d) PNL and PPL, (e) PNL and PTNL and (f) PNR and PPL. NI and PNL display a strong linear correlation ($r=0.96$, $p<0.001$). Both NI and PNL show a good linear correlation with PTNL ($r=0.83$, $p<0.0005$ and $r=0.88$, $p<0.0001$, respectively).

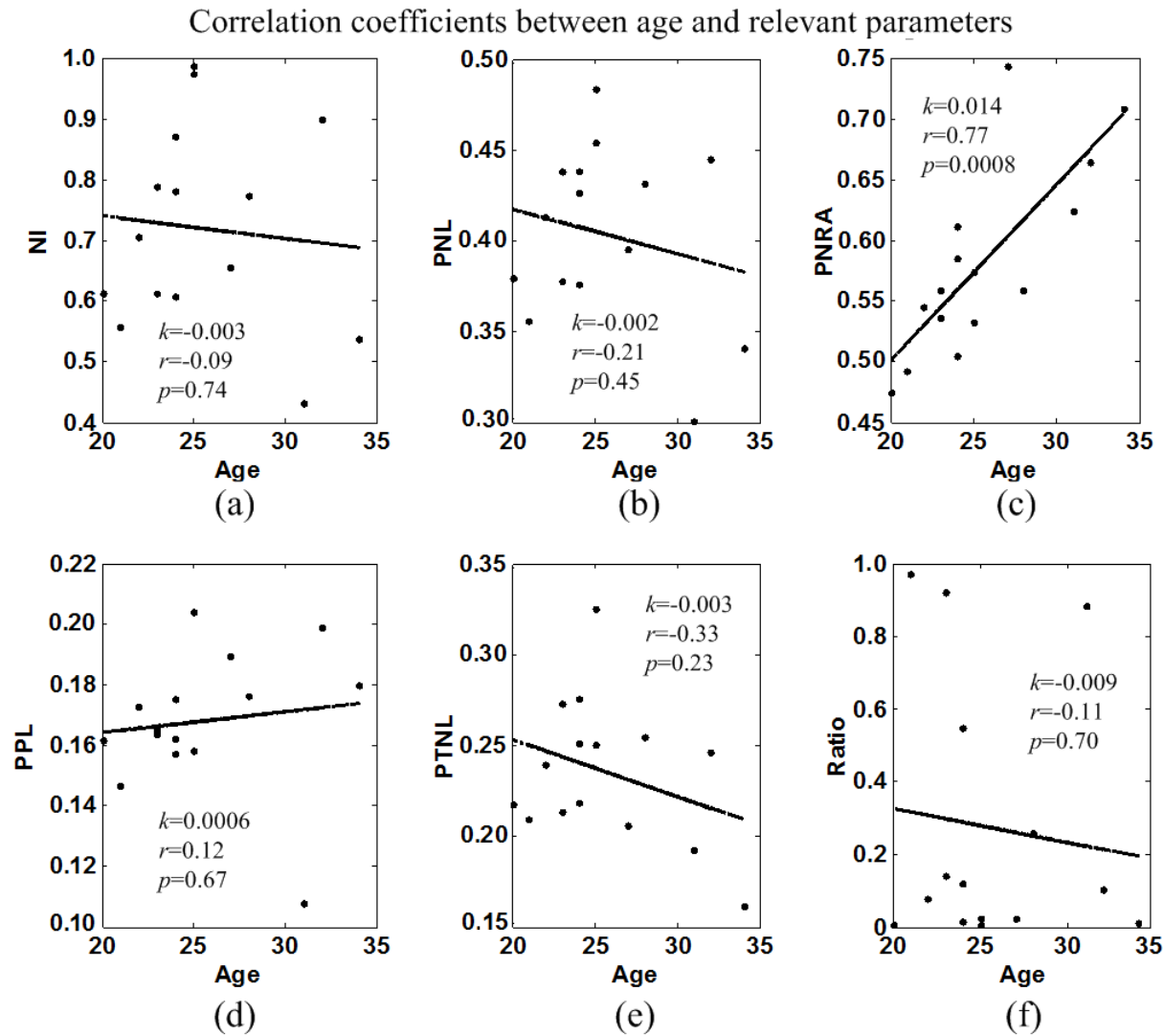


Figure 5-2. Linear correlation analysis between age and relevant parameters. Dots represent the values of these parameters. k , r and p represent the line slope, the correlation coefficients and the significance, respectively. The relationships are between age and (a) NI, (b) PNL, (c) PNRA, (d) PPL, (e) PTNL and (f) ratio. A good correlation ($r=0.77$, $p<0.001$) is found between age and PNRA.

5.2 PPG technique for physiological monitoring

5.2.1 PPG PRV as a surrogate to ECG HRV

In Study II, the HRV derived from ECG and the PRV derived from PPG were compared by computing time and frequency domain parameters. The RRI series derived from ECG signal were used as reference data and compared to the PPI time series derived from PPG signal on the finger tip and the ear lobe. The finger-PRV (fPRV) and ear-PRV (ePRV) features were very similar to those of the HRV. This similarity can be clearly observed in Figure 5-3, where the parameters of the time domain and the frequency domain were used to compare HRV and PRV. The larger DI (ratio of IQR to median value) in this measurement revealed a more dispersed distribution of the parameters. The frequency domain parameters from these fourteen subjects suggested a decentralised distribution.

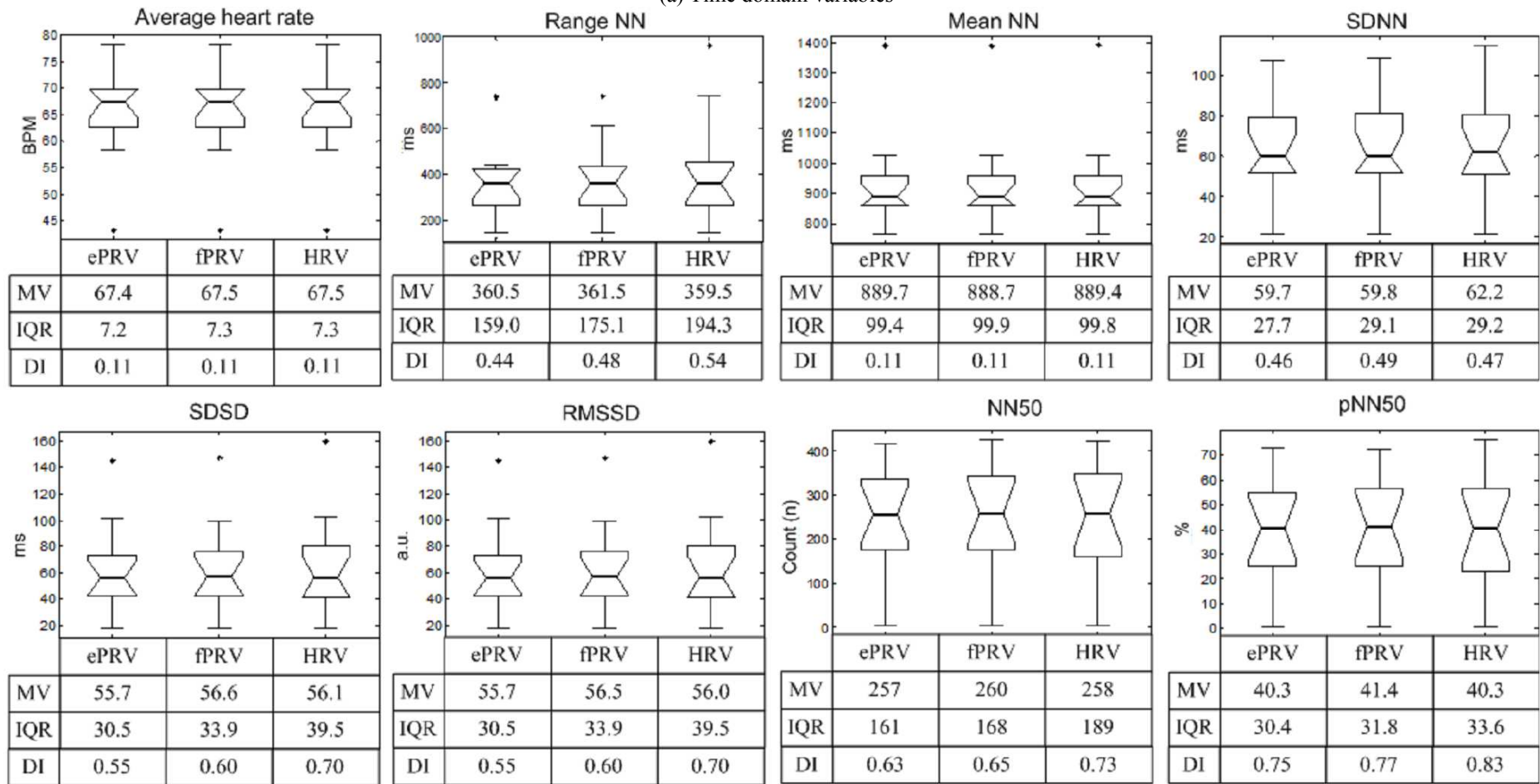
Bland-Altman ratios were calculated to present the agreements between HRV and PRV. All ratios, indicated in Table 5-3, were below 0.1 except the NN range, where the Bland-Altman ratios were 0.181 for ePRV and 0.157 for fPRV, respectively. The correlation coefficients, presented in Table 5-4, were used to compare ePRV and fPRV with corresponding HRV. Except the range NN, where the correlation coefficients were 0.92 and 0.85 respectively, coefficients deviated only 2% or 1%.

Based on Kurtosis and Skewness coefficients in Table 5-5, the distributions of RRI series and PPI series were similar between each other in all fourteen subjects except for the subjects S7 and S12. The Kurtosis coefficients for PPI from subjects S7 and S12 were both less than 3, indicating that PPI distribution was platykurtic; yet the Kurtosis coefficients for RRI from were both more than 3, showing their leptokurtic distributions. Moreover, the Skewness coefficients for all subjects except subject S2 were positive, indicating the distribution of PPI or RRI was trended on the left side of the mean values of the PPI or RRI data series.

Tables 5-6 and 5-7 present the results of ePRV, fPRV and HRV with the time and the frequency domain for two representative subjects.

The geometrical methods present the shape characteristic of the HRV or PRV, which can visually inspect the ECG or PPG signals, such as disease diagnosis [148], assessment of nonlinear characteristics in HRV [144, 149] and evaluation of paced breathing [150]. Figures 5-4 and 5-5 present the likeness of the characteristics of HRV and PRV in the geometrical shape in individuals.

(a) Time domain variables



(continued on next page)

(continued from previous page)

(b) Frequency domain variables

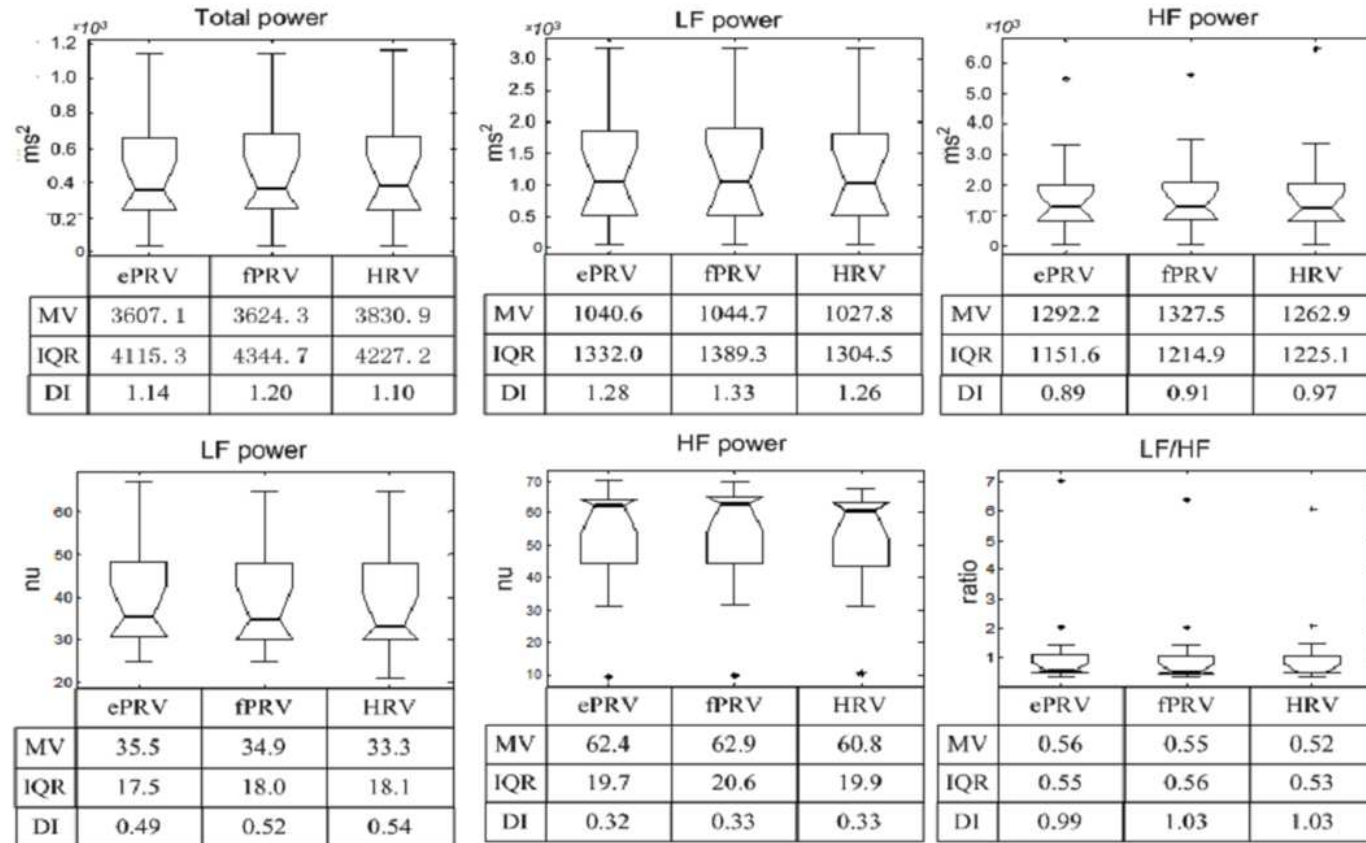


Figure 5-3. Box-and-whisker plots for (a) time domain variables and (b) frequency domain variables from ePRV, fPRV and HRV. The points beyond the whiskers are displayed with ‘*’. The means and deviations are presented under each figure. MV: median values, IQR: interquartile range of a sample, IQR presents the range of the majority data. DI: distribution index. DI is the ratio of IQR to MV, the larger the ratio, the more dispersed the distribution.

Table 5-3. Agreement analysis between ePRV or fPRV from PPG and HRV from ECG.

	<i>Average HR</i>		<i>Range NN</i>		<i>Mean NN</i>		<i>SDNN</i>		<i>SDSD</i>		<i>RMSSD</i>	
	ePRV	fPRV	ePRV	fPRV	ePRV	fPRV	ePRV	fPRV	ePRV	fPRV	ePRV	fPRV
Bland-Altman ratio	2.34×10^{-4}	3.71×10^{-4}	0.181	0.157	2.35×10^{-4}	3.61×10^{-4}	0.024	0.024	0.059	0.057	0.059	0.057

	<i>NN50</i>		<i>pNN50</i>		<i>Total power</i>		<i>NN50</i>		<i>pNN50</i>		<i>Total power</i>	
	ePRV	fPRV	ePRV	fPRV	ePRV	fPRV	ePRV	fPRV	ePRV	fPRV	ePRV	fPRV
Bland-Altman ratio	0.0284	0.0254	0.0260	0.0223	0.0437	0.0414	0.0284	0.0254	0.0260	0.0223	0.0437	0.0414

	$LF(ms^2)$		$HF(ms^2)$		$LF(nu)$		$HF(nu)$		LF/HF	
	ePRV	fPRV	ePRV	fPRV	ePRV	fPRV	ePRV	fPRV	ePRV	fPRV
Bland-Altman ratio	0.00964	0.0172	0.0939	0.0856	0.0261	0.0246	0.0295	0.0239	0.127	0.0476

Table 5-4. Correlation coefficient (r) between ePRV or fPRV from PPG and HRV from ECG ($p<0.001$).

[illegible]

Table 5-5. Kurtosis and Skewness coefficients of RRI and PPI distribution.

	Subject	S1	S2	S3	S4	S5	S6	S7	S8	S9	S10	S11	S12	S13	S14
Kurtosis	ePRV	2.98	2.31	2.65	1.65	1.95	2.25	2.46	2.09	2.38	2.20	2.32	1.93	1.85	1.58
	fPRV	2.49	2.30	2.96	1.65	2.02	2.35	2.51	1.95	2.38	2.13	2.15	2.23	1.72	1.58
	ECG	2.26	2.36	2.85	2.55	2.21	2.44	3.67	2.17	2.37	2.35	2.33	3.70	2.11	1.96
Skewness	ePRV	0.95	-0.13	1.04	0.34	0.53	0.79	0.88	0.75	0.76	0.85	0.80	0.53	0.47	0.18
	fPRV	0.68	-0.12	1.13	0.31	0.60	0.84	0.93	0.70	0.76	0.80	0.73	0.73	0.46	0.09
	ECG	0.69	-0.13	1.08	0.63	0.63	0.89	1.35	0.82	0.78	0.93	0.81	1.40	0.61	0.32

Table 5-6. Time domain and frequency domain analyses for the first selected subject.

	<i>Average HR (BPM)</i>	<i>Range NN (ms)</i>	<i>Mean NN (ms)</i>	<i>SDNN (ms)</i>	<i>SDSD (ms)</i>	<i>RMSSD</i>	<i>NN50</i>	<i>pNN50 (%)</i>	<i>Total power (ms²)</i>	<i>LF (ms²)</i>	<i>HF (ms²)</i>	<i>LF (nu)</i>	<i>HF (nu)</i>	<i>LF/HF</i>
ePRV	69.9	172.4	858.9	24.7	21.0	21.0	4	0.567	671	258	36.7	67.1	9.51	7.05
fPRV	69.8	177.7	859.1	25.3	22.4	22.4	4	0.574	699	263	41.2	64.0	10.02	6.39
HRV	69.9	178.8	858.9	25.2	22.1	22.1	6	0.861	691	255	42.2	63.4	10.48	6.05

Table 5-7. Time domain and frequency domain analyses for the second selected subject.

	<i>Average HR (BPM)</i>	<i>Range NN (ms)</i>	<i>Mean NN (ms)</i>	<i>SDNN (ms)</i>	<i>SDSD (ms)</i>	<i>RMSSD</i>	<i>NN50</i>	<i>pNN50 (%)</i>	<i>Total power (ms²)</i>	<i>LF (ms²)</i>	<i>HF (ms²)</i>	<i>LF (nu)</i>	<i>HF (nu)</i>	<i>LF/HF</i>
ePRV	78.4	423	766	81.3	72.7	72.6	335	42.8	6726	1861	1777	46.8	44.7	1.05
fPRV	78.4	437	766	82.7	75.5	75.4	342	43.9	6913	1918	1864	46.1	44.8	1.03
HRV	78.3	456	766	82.4	78.5	78.5	359	45.7	6851	1823	1796	44.4	43.7	1.01

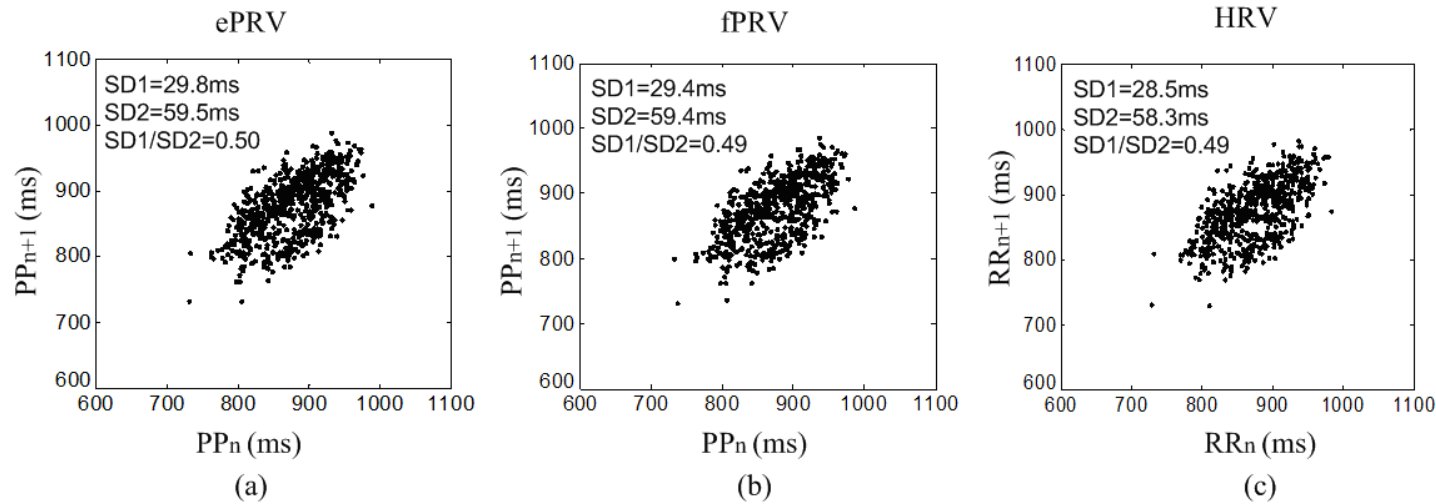


Figure 5-4. Poincaré plots of the PPI from (a) ePRV, (b) fPRV and RRI from (c) HRV. The current NN interval (x axis, PPI_n or RRI_n) is plotted against the next NN interval (y axis, PPI_{n+1} or RRI_{n+1}). Poincaré plot indices, i.e. SD1, SD2 and the ratio SD1/SD2, are measured for comparison between PRV and HRV.

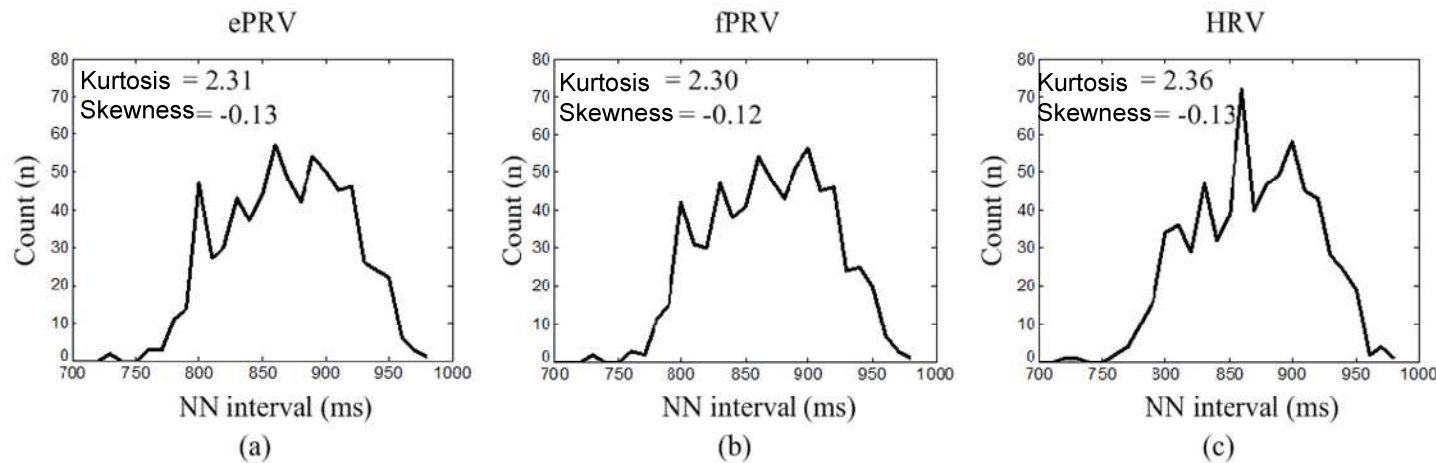


Figure 5-5. Density distribution of NN interval from one subject. The distribution reveals that the RRI from the HRV in (c), with a higher density compared to the PPI from fPRV and ePRV in (a) and (b). Kurtosis and Skewness are calculated for comparison between distributions of RRI and PPI.

5.3 Combination of lagged Poincaré plot and spectral characteristics to analyse pulse rate variability

In Study III, a combination of lagged Poincaré plots and spectral characteristics were used to investigate the effect of cigarette smoking on the ANS. Pulse rate variability (PRV), extracted from pulse-to-pulse intervals (PPI) of ear PPG waveforms, was used to obtain HRV information. Spectral power analysis of the PRV was performed to determine LF and HF components, and a lagged Poincaré plot was introduced to evaluate the nonlinear characteristics of PRV. The correlations between lagged Poincaré plot and spectral power indices were studied in the healthy habitual cigarette smokers and compared to non-smokers.

5.3.1 Frequency domain parameters

Spectral power indices of PRV are provided in Table 5-8. Significant reduction ($p=0.03$) of HF component was found in the smokers. There was no difference between the groups for LF ($p=0.16$), LF(n.u.) ($p=0.75$), HF(n.u.) ($p=0.63$) and the ratio LF/HF ($p=0.67$).

Table 5-8: Comparisons from frequency domain between habitual smokers and non-smokers. LF: low-frequency power; HF: high-frequency power; LF(n.u.): normalised PRV indices [LF/(LF + HF)]; HF(n.u.): normalised PRV indices [HF/(LF + HF)]; LF/HF: the power ratio of low-frequency to high-frequency.

	<i>Smokers</i>	<i>Non-smokers</i>	<i>p</i>
<i>LF(ms²)</i>	392.3(116.9-731.4)	823.3(716.4-1242.5)	0.16
<i>LF(n.u.)</i>	59.1(50.6-63.8)	50.6(38.7-68.9)	0.75
<i>HF(ms²)</i>	180.6(84.6-261.9)	752.9(589.2-1105.4)	0.03
<i>HF(n.u.)</i>	33.9(22.3-42.3)	44.6(22.0-48.2)	0.63
<i>LF/HF</i>	1.73(1.28-2.92)	1.13(0.81-3.17)	0.67

Values are given as median and interquartile range except for *p*.

5.3.2 Lagged Poincaré plots indices

Table 5-9 summarises the lagged Poincaré plot indices for the two groups. Compared to the healthy non-smoker group, the width ($SD1_m$) and the length ($SD2_m$) of lagged Poincaré plots in the smoker group significantly shrunk for all lags (all $p < 0.05$) except $SD1_4$ and $SD1_5$. In both groups, the relative maximum changes of $SD1_m$ and $SD2_m$ occurred at lag 6 or lag 7. The relative maximum changes of $SD1_m$ were 97.5% for the smoker group and 85.9% for the healthy non-smoker group, respectively, while the relative maximum changes of $SD2_m$ were 16.5% and 22.5%, respectively. The ratios of $SD1_m$ to $SD2_m$ became bigger with the increasing lags in both groups. Yet no significant differences were found for ratios between the two groups.

Table 5-9. Summary of the lagged Poincaré plot indices for the habitual smokers and the non-smokers.

<i>Lag</i>	$SD1_m$ (ms)		$SD2_m$ (ms)		$SD1_m/SD2_m$	
	<i>Smokers</i>	<i>Non-smokers</i>	<i>Smokers</i>	<i>Non-smokers</i>	<i>Smokers</i>	<i>Non-smokers</i>
1	16.2±6.0 ^c	31.3±9.6	50.3±17.3 ^a	80.6±23.8	0.33±0.13	0.39±0.06
2	23.1±10.1 ^c	45.5±16.3	47.5±15.5 ^a	73.4±20.2	0.49±0.14	0.61±0.09
3	27.1±13.3 ^a	49.8±20.0	45.1±13.5 ^b	70.4±17.2	0.59±0.18	0.69±0.12
4	29.4±15.2	51.0±24.4	43.5±11.9 ^c	68.8±15.2	0.65±0.22	0.73±0.24
5	31.1±15.4	54.9±26.9	42.5±11.2 ^c	65.2±12.9	0.70±0.21	0.84±0.34
6	32.0±14.7 ^{a,d}	58.1±27.0	42.0±11.4 ^{c,d}	62.5±11.9 ^d	0.74±0.18	0.93±0.36
7	31.8±13.8 ^a	58.2±25.6 ^d	42.2±12.2 ^b	62.7±13.5	0.73±0.16	0.93±0.32
8	31.3±12.8 ^a	57.0±23.9	42.6±12.9 ^b	64.1±15.0	0.72±0.13	0.89±0.26
9	31.3±11.9 ^a	56.0±21.6	42.6±13.6 ^b	65.4±15.9	0.73±0.12	0.85±0.17
10	31.5±11.3 ^a	54.5±18.4	42.5±14.1 ^b	67.1±18.1	0.74±0.12	0.81±0.10
<i>Max change</i>	97.5%	85.9%	16.5%	22.5%		

$SD1_m$: the width of m-lagged Poincaré plot, $SD2_m$: the length of m-lagged Poincaré plot.

The significant test is in $SD1_m$ or $SD2_m$ between smokers and non-smokers. ^d the relative maximum changes of $SD1_m$ and $SD2_m$ (taking 1-lag Poincaré plot indices as the references).

^a $p < 0.05$, ^b $p < 0.01$, ^c $p < 0.005$.

5.3.3 Correlation between lagged Poincaré plot indices and frequency domain parameters

Figure 5-6 presents the correlation coefficients between lagged Poincaré plot width ($SD1_m$) and spectral power indices (HF, LF, HF(n.u.) and LF(n.u.)) of PRV in the habitual smoker group and the non-smoker group. Moderate ($r > 0.5$) or highly ($r > 0.7$) positive correlations are found between $SD1_m$ and HF or LF components as shown in Figure 5-6(a) and 5-6(b). Yet the correlations between $SD1_m$ and HF(n.u.) or LF(n.u.) are moderate or poor ($|r| < 0.5$). Negative and positive coefficients are found in both groups with the increase of lags as presented in Figures 5-6(c) and 5-6(d). Particularly, the coefficients between $SD1_m$ and LF component in the non-smoker group in Figures 5-6(b) and 5-6(d)) are higher than these in the habitual smoker group except for $SD1_{10}$, whereas the similar results are not found in the relationship between $SD1_m$ and HF component as presented in Figures 5-6(a) and 5-6(c).

Figure 5-7 shows the correlation coefficients between lagged Poincaré plot length ($SD2_m$) and spectral power indices (HF, LF, HF(n.u.) and LF(n.u.)) of PRV in the two groups. The correlations between $SD2_m$ and HF component were all positive as shown in Figures 5-7(a) and 5-7(b). Highly positive correlations between $SD2_m$ and HF for all lags were found in the non-smoker group as presented in Figure 5-7(a). Conversely, the highly positive correlations for all lags between $SD2_m$ and LF were only found in the smoker group as shown in Figure 5-7 (b). Referring to the correlations between $SD2_m$ and HF(n.u.) and LF(n.u.) as presented in Figures 5-7 (c) and 5-7(d), either positive or negative coefficients were found in the non-smokers. For the smoker group, $SD2_m$ correlated positively with HF(n.u.) and negatively with LF(n.u.).

The correlation coefficients between two ratios, i.e. $SD1_m/SD2_m$ and LF/HF , are presented in Figure 5-8. The coefficients move from negative to positive with the increase of the lags for the smoker group. However, such similar changes were not found for the non-smoker group.

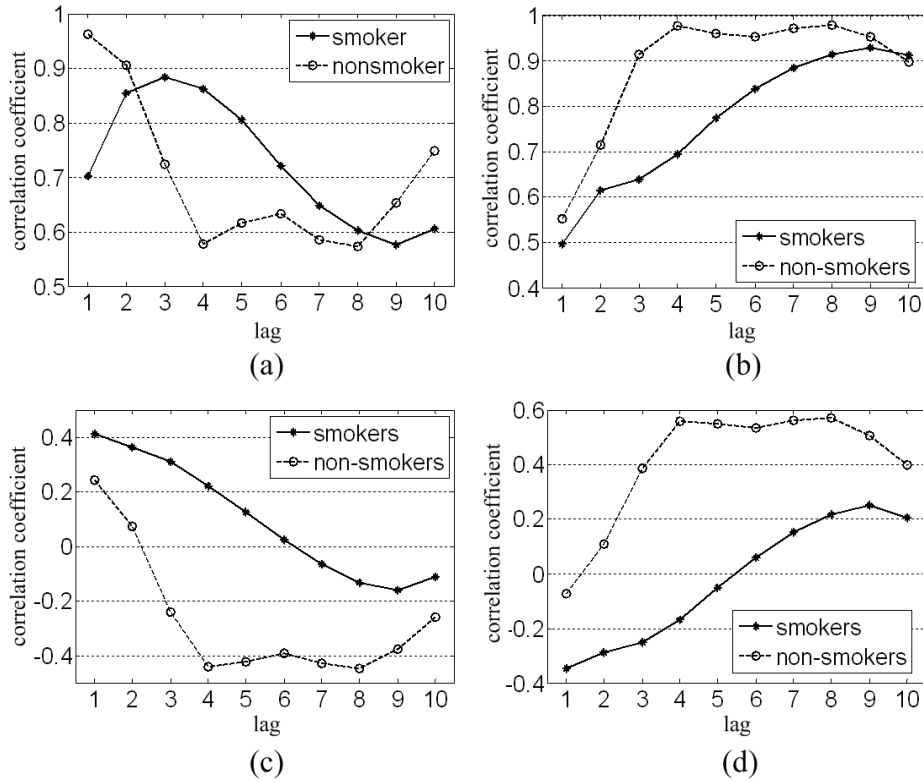


Figure 5-6. The correlations between $SD1_m$ and frequency domain indices: (a) HF, (b) LF, (c) HF(n.u.) and (d) LF(n.u.), respectively. The correlation coefficients (r) with respect to the lags for the two groups are presented.

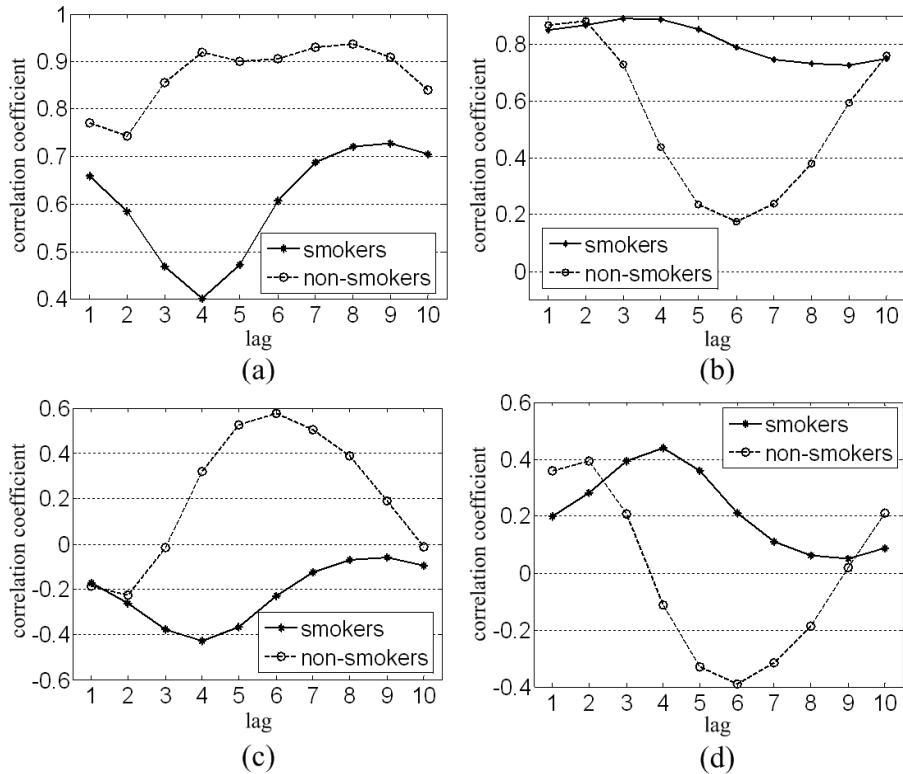


Figure 5-7. The correlations between $SD2_m$ and frequency domain indices: (a) HF, (b) LF, (c) HF(n.u.) and (d) LF(n.u.), respectively. The correlation coefficients (r) with respect to the lags for the two groups are presented.

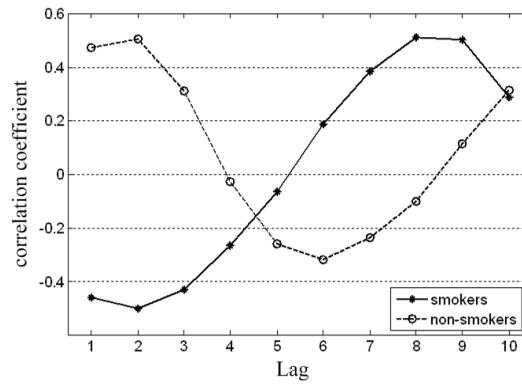


Figure 5-8. The correlation between $SD1_m/SD2_m$ and LF/HF.

5.4 Noncontact PPG as a substitute technique for contact PPG

5.4.1 Geometrical parameters for noncontact reflection PPG photonics engineering setup

In Study IV, depending on the quality of the opto-electronic signal, the detectable range of the distance between the photodetector and palm (d_{PH}) was divided into three ranges:

- (1) the saturation range: the opto-electronic signal was captured but the photodetector became saturated easily in some cases;
- (2) the optimal range: a cleaner PPG signal was detected without any saturation of photodetector, and also the amplitude of the PPG signal varied with the change of the light source (VCSEL) output; and
- (3) the low signal range: the PPG signal was clearly detected with a bigger power of light source, and the PPG signal was sensitive to the interference of ambient light.

As shown in Table 5-10, by increasing the separation distance between the VCSEL and the photodiode from 15 mm to 35 mm and decreasing the incident angle from 15° to 35° , the variations of the three defined ranges were given experimentally. The distance between entry and exit points (l) related to banana-shaped light path in the

three configurations was measured accordingly. Figure 5-9 presents the representative signals captured from the saturation range, the optimal range and the low signal range, respectively.

Table 5-10. Three ranges depending on the quality of opto-electronic signal.

Configuration No.	<i>I</i>		<i>II</i>		<i>III</i>	
θ_{PL} ($^{\circ}$); d_{PL} (mm)	35; 15		25; 25		15; 35	
	d_{PH} (mm)	l (mm)	d_{PH} (mm)	l (mm)	d_{PH} (mm)	l (mm)
Saturation range	<30	<6	<30	<11	<40	<-24*
Optimal range	30 to 50	6 to 20	30 to 110	11 to 26	40 to 90	-24 to 11
Low signal range	>50	>20	>110	>26	>90	>11

θ_{PL} : the angle of the VCSEL set against the photodiode.

d_{PL} : the distance between the VCSEL and the photodiode.

d_{PH} : the distance between the palm and the photodiode.

l : the banana shape distance between light entry and exit points.

*: the negative value referring to the position of palm at the negative focus plane.

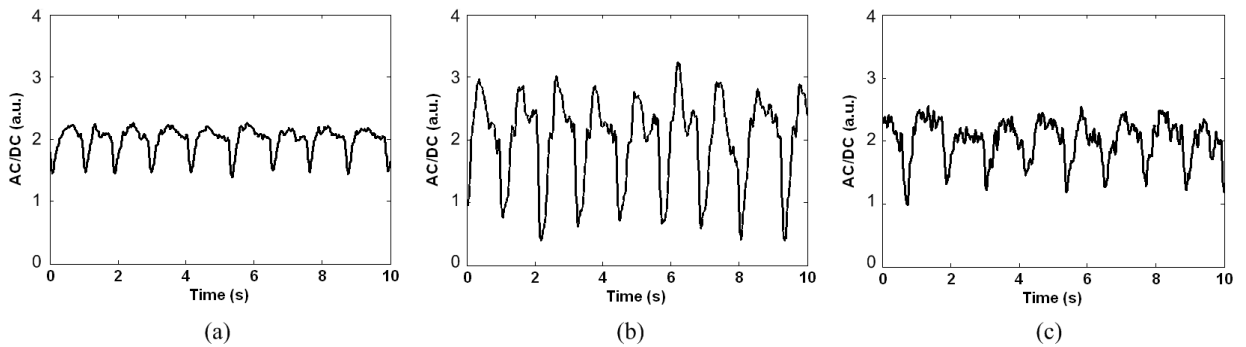


Figure 5-9. Representative PPG signals captured from NRPPG photonics engineering setup: (a) Saturation range, (b) Optimal range and (c) Low signal range.

5.4.2 The feature of synchronised PPG signals

Figure 5-10 presents a synchronising record of PPG signal detected by CPPG and NRPPG for 5 seconds from one subject. The feature of the PPG signals captured by NRPPG shows a similarity to that from CPPG.

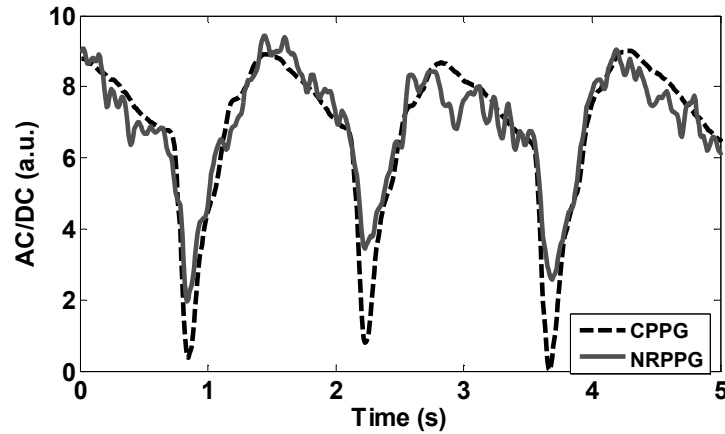


Figure 5-10. Comparison of CPPG and NRPPG signal.

5.4.3 The spectra of PPG signals

Figure 5-11 compares the distribution of spectral regions from CPPG signals with those from synchronised recorded NRPPG signals for 22 subjects. The pVLF component spectra for CPPG signal had a more concentrated distribution, and were found significantly lower than those detected from NRPPG, as shown in Figure 5-11(a). No significant differences were found in the components of pLF and pHF and the pTF.

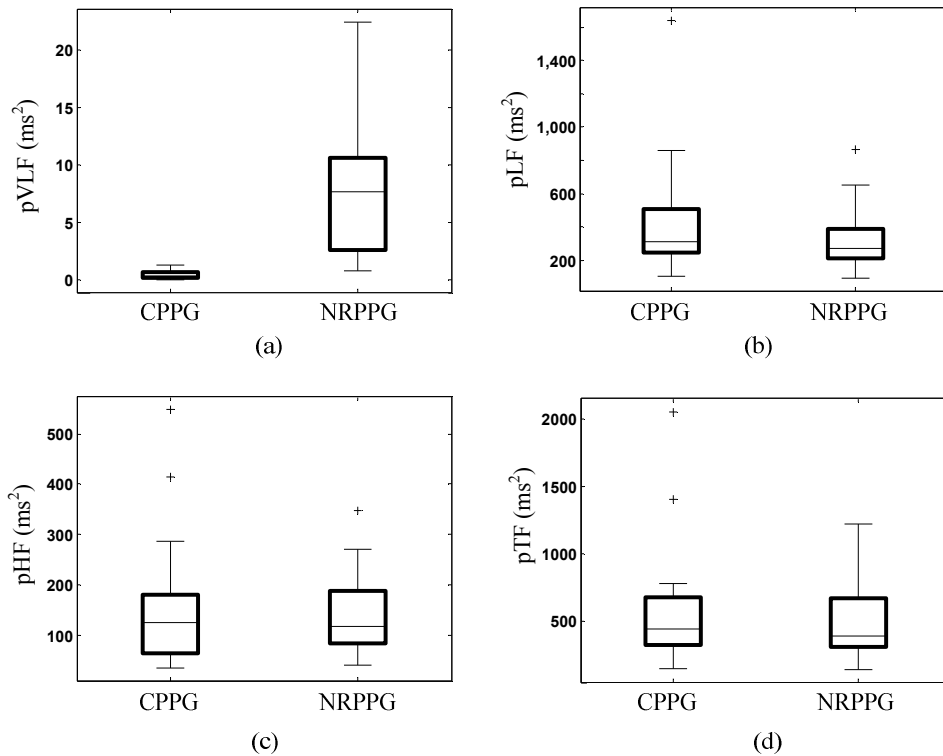


Figure 5-11. The spectra of PPG signals. (a) pVLF component 0.01-0.5 Hz, (b) pLF component 0.5-1.5 Hz, (c) pHF component 1.5-6 Hz and (d) total power (pTF).

The frequency spectra of the PPG signals from a representative person are presented in Figure 5-12. CPPG signal shows a higher major peak than NRPPG signals in the pLF band, which is related to the beating heart. In contrast, power in the pVLF band for the NRPPG signal is higher than that in the CPPG signal, and power in the pHF band for NRPPG is lower.

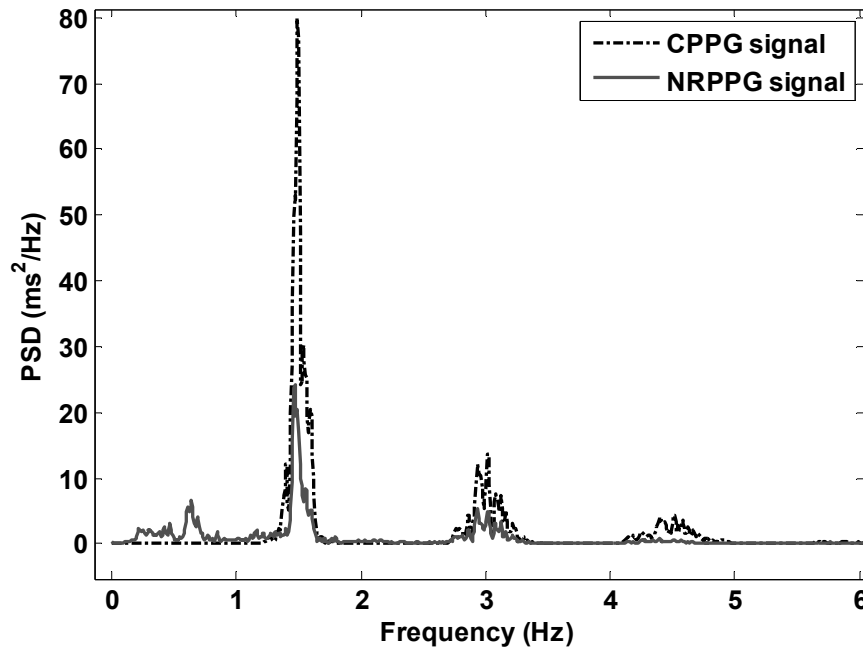
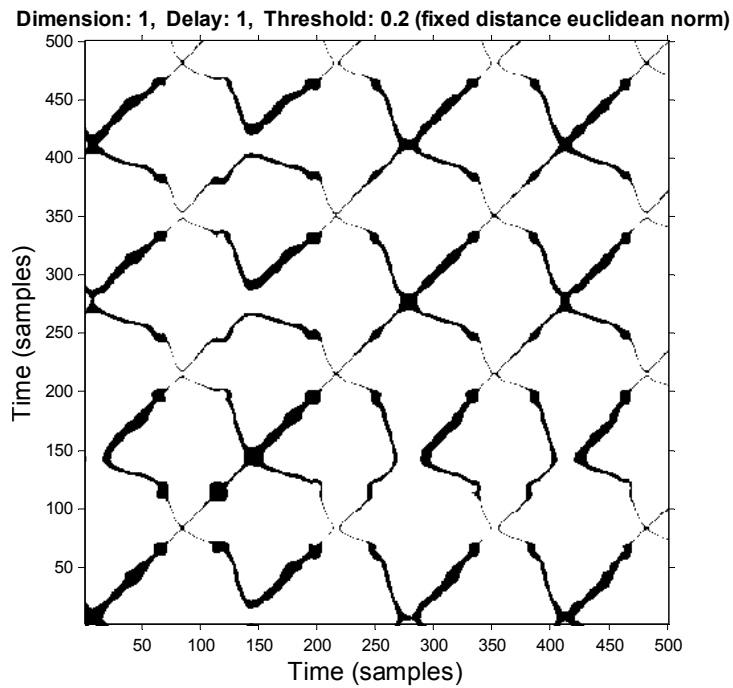
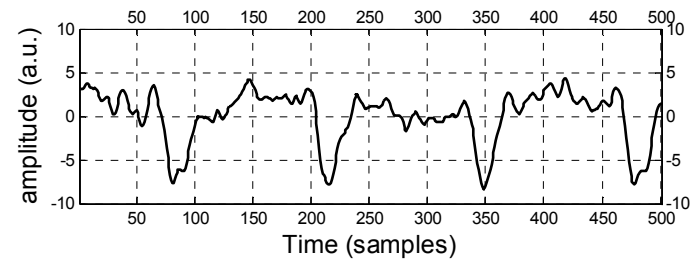
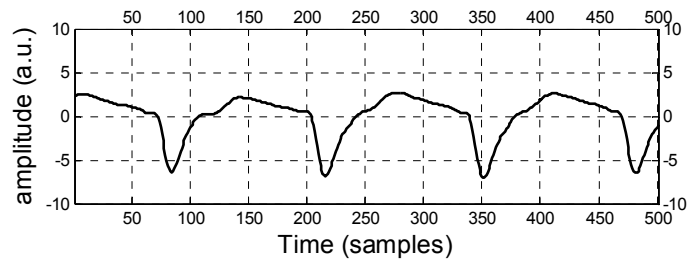


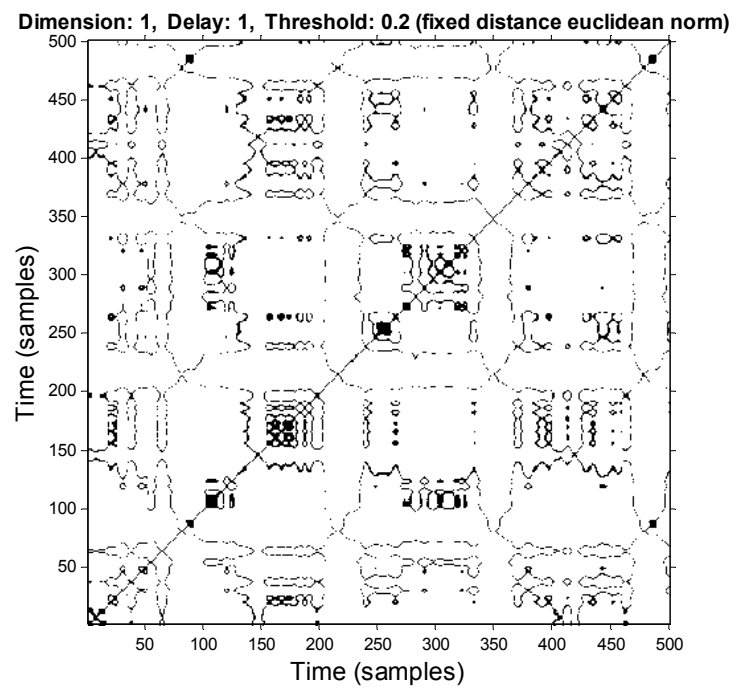
Figure 5-12. Frequency spectrum of the PPG signal from a representative person.

5.4.4 Results from recurrence plot

The different RP patterns derived from the CPPG signal and NRPPG signal are shown in Figure 5-13. The continuous diagonal line and the periodic pattern are presented for the CPPG signal. The horizontal and vertical lines and the irregular structure are presented for the NRPPG signal.



(a)



(b)

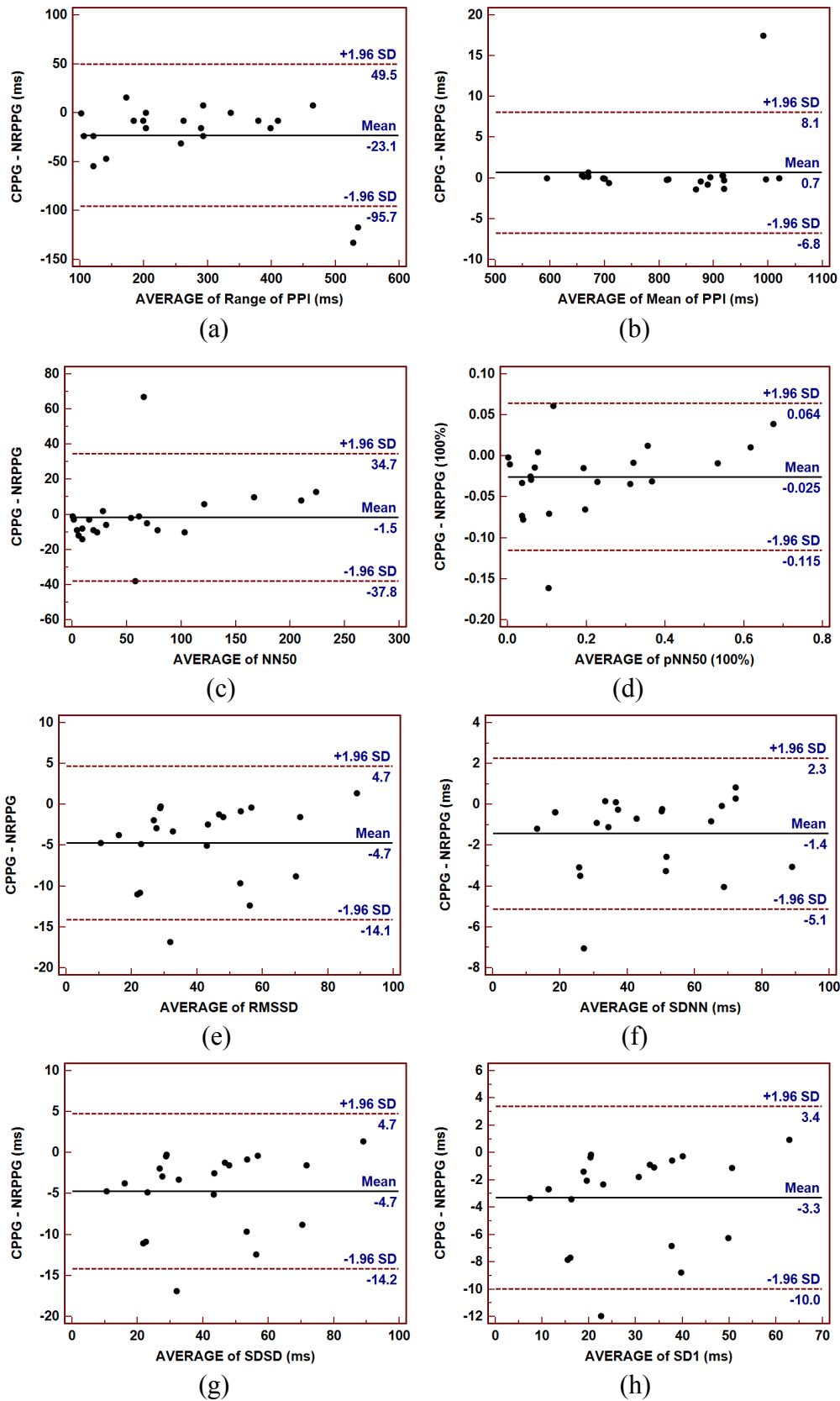
Figure 5-13. Recurrence plot is introduced as a graphical tool to tentatively study the (a) CPPG signal and (b) NRPPG signal.

5.4.5 The agreement analysis of PPG signal for physiological parameters

The pulse rate parameters from CPPG and NRPPG are presented in Table 5-11 to show the compatibility of the two techniques. Median values and the interquartile ranges are given for comparison. Strong linear associations ($r \geq 0.97$) were found between two measurements of each parameter. Figure 5-14 shows the results of Bland-Altman analysis between the paired values of pulse rate parameters from CPPG and NRPPG. The good agreements were presented for Range of PPI (-95.7 to 49.5 ms), Mean PPI (95% CI: -6.8 to 8.1 ms), NN50 (-37.8 to 34.3), pNN50 (0.115 to 0.064 %), RMSSD (-14.1 to 4.7), SDNN (95% CI: -5.1 to 2.3 ms), SDSD (14.2 to 4.7 ms), SD1 (95% CI: -10 to 3.4 ms), SD2 (95% CI: -3.2 to 1.9 ms), and SD1/SD2 (95% CI: -0.239 to 0.097).

Table 5-11. The comparison and correlation relationship between CPPG and NRPPG for PR variables parameters. Values are given as median and interquartile range except correlation coefficients and p .

<i>Parameters</i>	<i>CPPG</i>	<i>NRPPG</i>	<i>correlation coefficients</i>	<i>p</i>
<i>Range of PPI (ms)</i>	250.0(179.7~365.2)	269.5(169.9~371.1)	0.97	0.0081
<i>Mean of PPI (ms)</i>	842.3(677.6~916.7)	843.1(677.1~916.4)	0.99	0.42
<i>NN50</i>	34(7.25~92)	33(16.25~81.5)	0.96	0.70
<i>pNN50 (100%)</i>	0.11 (0.03~0.31)	0.16 (0.07~0.33)	0.98	0.016
<i>RMSSD</i>	35.7(24.0~49.5)	42.4(28.2~56.0)	0.97	<0.001
<i>SDSD (ms)</i>	35.8(24.1~49.6)	42.5 (28.2~56.1)	0.97	<0.001
<i>SDNN (ms)</i>	39.7(25.8~60.9)	40.2 (30.8~62.2)	0.99	0.002
<i>SD1 (ms)</i>	21.1 (15.0~35.1)	26.4(19.6~39.7)	0.97	0.0002
<i>SD2 (ms)</i>	52.5 (33.8~76.8)	52.5(35.2~77.0)	0.99	0.03
<i>SD1/SD2</i>	0.43(0.37~0.55)	0.53(0.43~0.61)	0.80	<0.001



(continued on next page)

(continued from previous page)

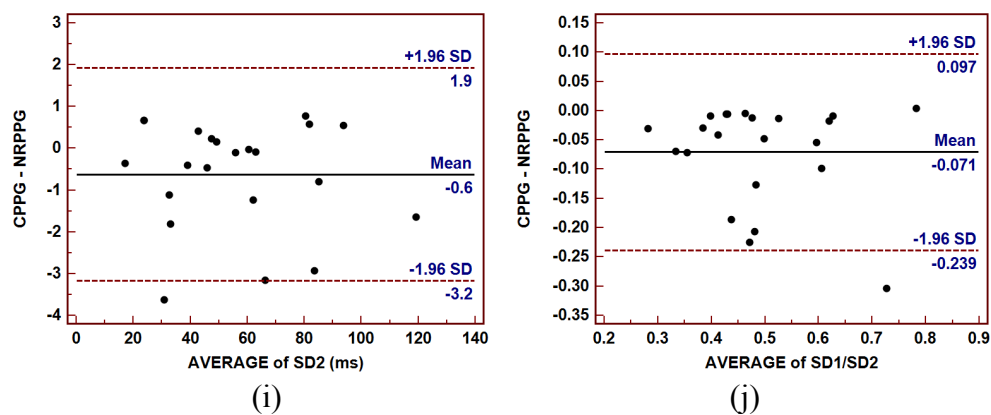


Figure 5-14. Bland-Altman plot was applied to the agreement analysis between CPPG and NRPPG for (a) Range of PPI, (b) Mean of PPI, (c) NN50, (d) pNN50, (e) RMSSD, (f) SDNN, (g) SDSD, (h) SD1, (i) SD2, (j) SD1/SD2, respectively, which reflect cardiovascular measurement. (solid lines: the mean value of differences, broken lines: the upper and lower limits of agreement, i.e. the mean value of differences $\pm 1.96SD$, SD: standard deviation).

5.5 The effectiveness of noncontact PPG for physiological monitoring

Figure 5-15 presents the results of changes in Poincaré plot indices for 14 days in Study V. Significant increases for SD1 ($p=0.0074$) and SD1/SD2 ($p=0.001$) were found in the afternoon compared to those in the morning. No significant change was found for SD2 ($p=0.1280$).

Figure 5-16 presents the representative Poincaré plots of the test in the morning and in the afternoon on the same day. The physiological difference could be interpreted from the shape of the cloud.

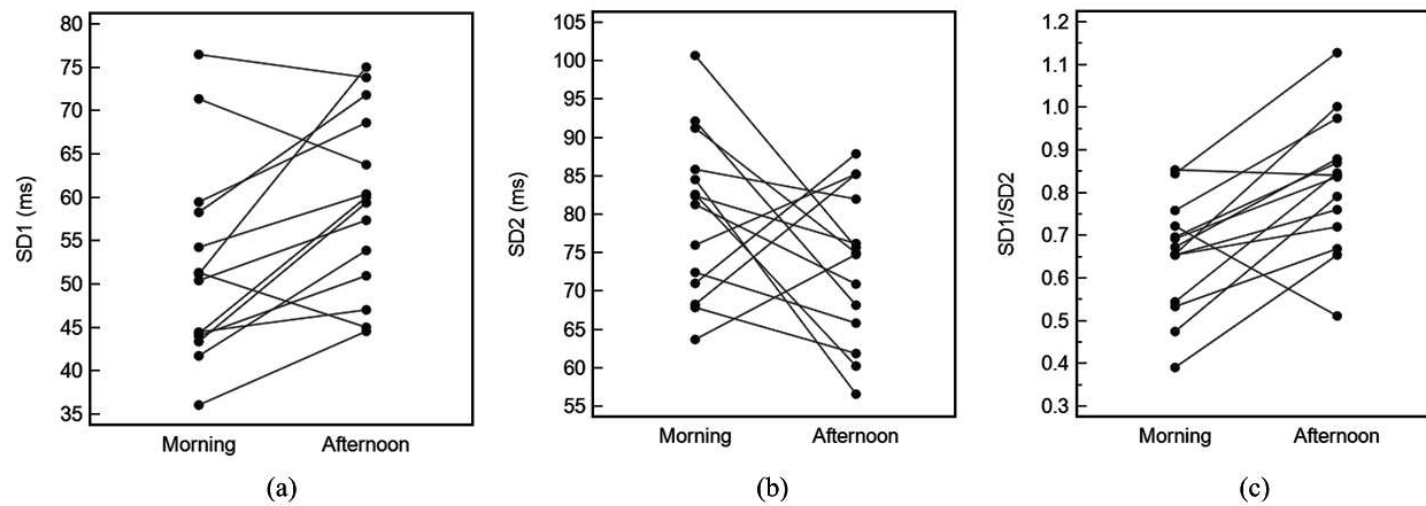


Figure 5-15. Illustrated individuals: (a) SD1, (b) SD2 and (c) their ratio SD1/SD2 from the physiological monitoring.

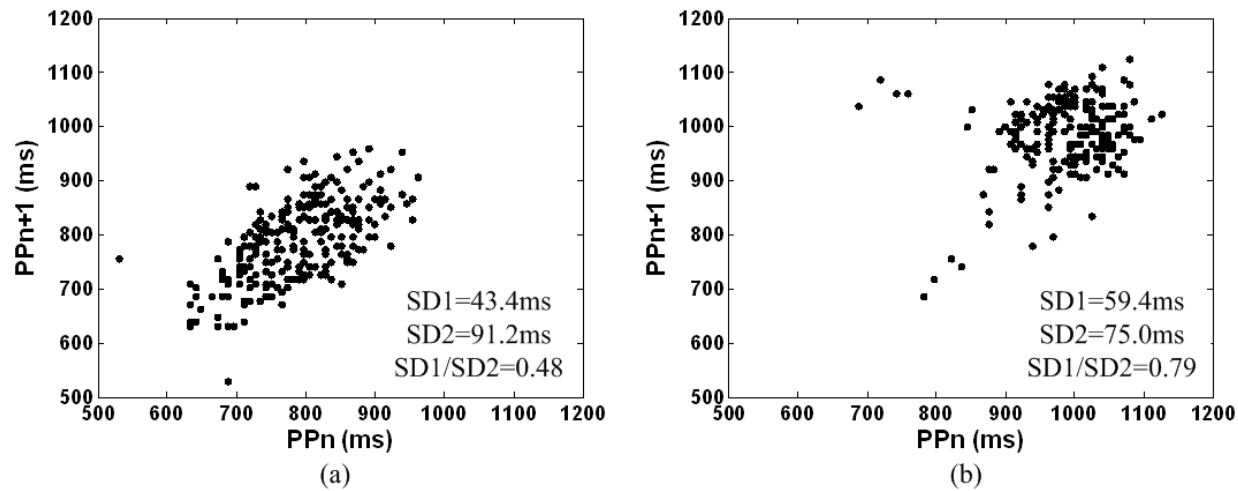


Figure 5-16. Representative Poincaré plots demonstrating cardiovascular variations in (a) morning and (b) afternoon in same day

5.6 Summary

This chapter presents the physiological characteristics derived from PPG signal in three aspects:

1. The arterial stiffness was investigated in a group of young adults by means of contour analysis of PPG waveform (Section 5.1).
2. The PRV derived from PPG can be used to assess the cardiovascular activity, and lagged Poincaré plot can be applied to effectively distinguish different groups (Sections 5.2 and 5.3).
3. NRPPG was introduced as an alternative for monitoring cardiovascular dynamics. The signal detected from NRPPG was similar with the synchronised recorded signal from CPPG. The agreements of the physiological parameters from these two techniques were within acceptable ranges. The application of NRPPG for a office worker was studied (Sections 5.4 and 5.5).

All the significant findings are discussed in Chapter 6.

CHAPTER 6

DISCUSSION

The PPG signals are analysed based on their signatures, and how those relate to known physiology and empirical observations. The significant findings are discussed from these aspects as follows.

- Arterial stiffness occurs in young adults, and arterial stiffness difference exists between young male and female. Measuring characteristic notch on the PPG pulse facilitates identifying subjects with different vascular activity.
 - PPG-derived PRV can be used as an alternative measurement of HRV. PRV can be applied to quantify and assess dynamic characteristics of the ANS.
 - The sensor placement in NRPPG system is essential for quality of signal. The NRPPG system is capable of obtaining HR information from skin tissue.
-

6.1 Waveform analysis for arterial stiffness

Study I investigated the arterial stiffness in young adults by determining the characteristics of the dicrotic notch in PPG pulses. The distinct dicrotic notch, prevalently seen in these young individuals, is ascribed to the reflected wave from the periphery. Millasseau *et al* [78] demonstrated that a single mathematical transfer function can be used to relate the digital volume pulse to the peripheral pressure pulse. This implies that the information in the PPG pulse is similar to that contained in the radial pressure pulse, and that the physiological determinants of the PPG pulse are similar to those of the radial pressure pulse. In principle, the systolic component of the PPG pulse mainly arises from a forward-going pressure wave transmitted along a direct path from the left ventricle to the finger. The diastolic component is mainly derived from the pressure waves transmitted along the aorta to the small arteries in the lower body, where they are then reflected back along the aorta as a reflected wave that then travels to the finger [107]. During systole, the increased pressure in the aorta is not transmitted instantaneously to the peripheral circulation but travels as a forward-going pressure wave travelling at a certain speed known as the PWV. It has been broadly accepted that the pressure waves travel faster through stiff vessels than through pliable ones, i.e. a PWV increase [151]. Hence, the PWV in the subjects with higher arterial stiffness is faster than those with lower arterial stiffness.

More WDN pulses in the younger and male groups detected by WDNSA (Table 5-1, see Section 5.1) are due to the larger amplitude of the reflected wave. Reflected waves arising mainly from the lower body are delayed relative to the direct wave, and therefore produce an inflection point or second peak in the PPG pulse. The amplitude of the reflected wave depends on the amount of reflection and hence on muscular tone in small arteries. While arterioles are the major source of wave reflection in humans, reflection can arise at any point of impedance mismatch [93, 152, 153].

Arterial stiffness is accompanied by the phenomenon of early wave reflection [154-156]. With increasing stiffness of the conduit arteries, the reflected wave arrives early and its contribution moves from the diastolic to the systolic component of the pulse. Therefore, the inflection point, i.e. notch height, on the contour of the pulse is

lower for the less stiff arteries compared to that in the stiffer arteries. The parameter PNRA, indicating the relative height of the notch in this study, is the marker of arterial aging. As presented in Table 5-2 (see Section 5.1), PNRA is significantly larger in the older subject group than in the younger group (0.63 ± 0.08 vs. 0.54 ± 0.05 , $p=0.016$), indicating lower arterial stiffness for the younger subjects. The change in PNRA could occur as a result of vasodilation of the arteries, which contributes most to wave reflection, thus reducing the reflected wave and hence PNRA. Meanwhile, PNRA, measuring the amplitude of the reflected wave, increases with age because the stiffer vessel generates a reflected wave with larger amplitude in the older subjects. Taken together, the findings above suggest that PNRA is a more sensible index than the other three parameters to distinguish different age groups.

The timing of the reflected wave relative to the first peak is determined by the PWV in the aorta and conduit arteries [93, 157]. The three parameters, i.e. NI, PNL and PTNL, mirror the relative time point at which the reflected wave generates a notch on the waveform. The smaller values of these three parameters indicate the shorter time that the reflected wave takes to generate a notch, suggesting a faster PWV and hence the stiffer arteries. These three parameters from the female group are significantly larger than those from the male group (NI: 0.84 ± 0.13 vs. 0.64 ± 0.14 , $p=0.012$; PNL: 0.44 ± 0.03 vs. 0.38 ± 0.05 , $p=0.014$; PTNL: 0.26 ± 0.04 vs. 0.22 ± 0.03 , $p=0.016$, see Table 5-2 in Section 5.1). Thus, the female subjects have a lower PWV than the male subjects, suggesting lower arterial stiffness for the female. One factor that could be of importance for the difference in arterial stiffness between male and female is sex steroids [158]. The lower arterial stiffness for the female could be related to the specific effects of oestrogens, which increase arterial distensibility [159].

The correlation analysis for relevant parameters shows that NI and PNL present a strong linear correlation ($r=0.96$, $p<0.001$, see Figure 5-1(a) in Section 5.1), and that NI and PNL present a good linear correlation with PTNL ($r=0.83$, $p<0.0005$, see Figure 5-1 (c) and $r=0.88$, $p<0.0001$, see Figure 5-1 (e) in Section 5.1). This indicates that changes for the timing of the reflected wave relative to the first peak generate the same direction changes of the four parameters. The notch points are a valuable characteristic of the PPG waveform. A good correlation ($r=0.77$, $p<0.001$) was found between age and PNRA (see Figure 5-2(c) in Section 5.1). However, there were poor

correlations between age and other parameters.

Some researchers [157, 160] quantified the PPG finger pulse shape using the Stiffness Index (SI) and Reflection Index (RI) representing arterial stiffness and vascular tone, respectively. The SI is calculated from the body height divided by the time delay between the pulse systolic peak and the inflection point of the reflection wave. RI is calculated as the ratio of the height of the diastolic notch to the peak pulse height. However, the same SI or RI could come from separate waveforms such as the phenomenon shown in Figure 6-1. The two pulses displayed by the solid line and the dashed line possess the same RI and SI caused by the same peak height and the same peak-to-peak time delay. The qualitative relationship between arterial stiffness and PWV or volume of the reflection wave can be obtained from PNL and PNRA as two pulses have different height of notch and different time point of notch. Hence, the two parameters, i.e. PNL and PNRA, could be complementary to RI and SI while describing the arterial stiffness.

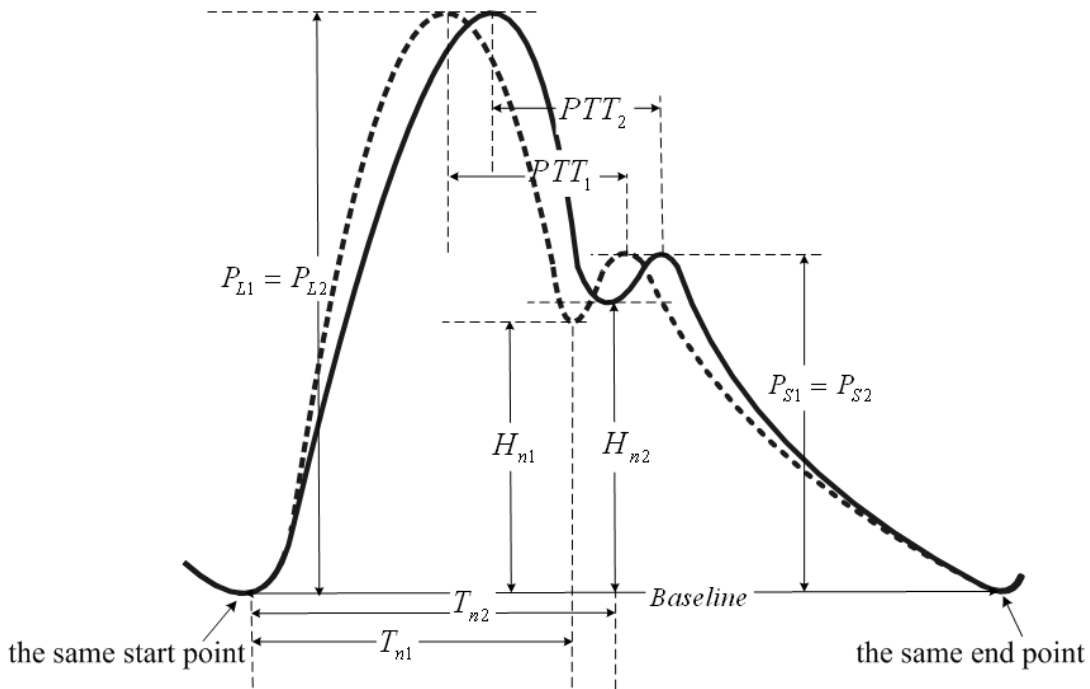


Figure 6-1. Separate waveforms with the same RI and SI yet different PNL and PNRA. The two pulses in the solid line and the dashed line possess the same RI and SI because of the same peak height ($P_{L1}=P_{L2}, P_{S1}=P_{S2}$) and the same peak-to-peak time delay ($PTT_1=PTT_2$). Their differences can be described by the PNRA and the PNL as two pulses have different notch height ($H_{notch1} \neq H_{notch2}$) and different notch duration ($T_{n1} \neq T_{n2}$).

6.2 PPG-derived PRV as a surrogate to ECG-derived HRV

In a clinic or a hospital, ECG is extensively used and accepted to provide information of diagnostic value. In home care and nursing, constrained measurement by this oscillometric method could make patients nervous. Also, long-term ECG monitoring cannot be easily and rapidly implemented at home. PPG, with its noninvasive nature and flexible measurement, could be a good alternative for clinicians and patients to easily and economically use. Study II attempted to demonstrate the reliability of PPG-derived pulse measurement for determining HRV parameters.

Constant *et al* [161] suggested that PRV derived from PPG signals is not a surrogate for HRV derived from ECG signals. In their work, the correlation between ECG and PPG assessed HRV parameters was only in a range about 0.8. In the physiological Study II, the correlation between HRV and PRV is very strong for all parameters. These differences might be due to the varying experimental settings. The study population in Constant *et al*'s work was children with implanted pacemaker triggering a 'constant' heart rate, which minimises beat-to-beat-variability. The setting in Study II is more comparable to the natural conditions of screening purposes, and hence the findings of high correlations between both physiological indicators of HRV and PRV can be considered valid. Also, the PPG signal obtained from the ear lobe is more stable than that from finger tip, as evidenced by a lower correlation of the NN Range between the HRV and fPRV.

The agreement analysis (see Table 5-3 in Section 5.2) indicates that the Bland-Altman ratios were small enough to be confident that PRV can be used instead of HRV. Time domain and frequency domain analyses provide the quantitative comparison between PRV and HRV. The reliability of the ePRV and fPRV is verified by comparing both time and frequency domain parameters of the HRV. Particularly, good agreement in time domain analysis could be demonstrated for heart rate, duration of NN intervals, SDNN, and RMSSD. Convincingly, a considerable number of subjects at risk for serious cardiovascular events could potentially benefit from the widespread use of PPG, the inexpensive heartbeat measuring device. In contrast, the results of frequency domain analysis are relatively less comparable. Hence, patients should always be measured with the same device during the course of HRV studies. While looking for

frequency domain variable reference values in the published literature, one should keep in mind the algorithm used for their calculation because different mathematical methods for the analysis of frequency domain variables lead to different results. Without expert knowledge and specific experience, however, the results of spectrum analysis should not be interpreted for medical purposes.

HRV is regarded as a noninvasive electrocardiographic method to measure the autonomic nervous system. LF/HF ratio has been exploited to mirror sympathy/vagal balance or to reflect sympathetic modulations [25, 131]. Although frequency domain parameters are sensitive for sympathetic and parasympathetic tones, they are unable to adequately assess transient changes in heart rate associating with rapid changes in physiological status [162]. Therefore, in screening studies performed by family doctors, only time domain variables should be used.

Geometric methods for RRI or PPI distributions and the Poincaré plot provide qualitative comparison between PRV and HRV. Figure 5-5 indicates that the PPI from ePRV and fPRV had a more decentralised distribution than the distribution of RRI intervals from HRV. The Poincaré plot portrays the nature of the fluctuations in the intervals between heartbeats [137], and visually inspects the shapes of the RRI and PPI (Figure 5-4). The compatibility of Poincaré plots for PRV and HRV can be explained by their reliance on the same principles of physiology and pathology.

With application of only one reusable probe, which can be fixed to the patient's finger or ear without undressing, PPG is easier to apply, more cost efficient and ecologically friendly than an ECG. On the other hand, HRV and PRV are comparable methods in screening studies while looking for "mean values in large groups". However, PRV is limited for decision making in medical diagnostics because the feature of a normal pulse may be less morphologically distinct than the QRS complex of an ECG.

6.3 Combination of lagged Poincaré plot and spectral characteristics to analyse pulse rate variability

Study III proffered an example that the combination of lagged Poincaré plots and spectral analysis of PRV could provide a detailed and visual method to distinguish the healthy habitual smokers from healthy non-smokers. PRV is offered as an alternative approach to obtain HRV information in Study III. Since HRV is a non-invasive indicator of cardiac sympathetic and parasympathetic tone, a method to measure the ‘instantaneous’ temporal changes in HRV could deliver physiological, diagnostic and prognostic information [163]. For the linear analysis alone, however, only HF (ms^2) was significantly different between the groups and was lower in the smokers compared to the non-smokers (see Table 5-8 in Section 5.3). The lower level of HF in the healthy habitual smokers is associated with parasympathetic withdrawal [18].

The intrinsic nonlinear nature of the autonomically regulated cardiac rhythm implies that the linear data processing techniques do not predict the pathophysiological ‘state’ of the ANS. The Poincaré plot is a simple yet powerful nonlinear tool to describe the physiological signal dynamics. An association between ANS and the Poincaré plot has been well established [148], where the smaller plot width and length indicate the larger sympathetic activity. The SD1_m and SD2_m were found to be significantly smaller in the smokers compared to the non-smokers, suggesting that habitual cigarette smoking augments sympathetic nerve activity. This finding is consistent with earlier studies [164]. Meanwhile, the concentrated plots often imply decreased HRV [133], which is associated with poor cardiovascular health [165, 166].

Brennan *et al* [144] suggested that when the simplified Poincaré plot was used solely as a tool to represent summary statistics it was ignoring some of its most potent abilities to display nonlinear aspects of the interval sequence. They expressed the view that the set of lagged Poincaré plots could be a complete and better description of the autocovariance function and the power spectrum of the intervals [144]. In Study III, lagged Poincaré plots provide information about the cardiac response for the habitual smoker that is less evident in the linear-based methods. It has been reported that a heartbeat influences not only the beat immediately, but also up to 6–10 beats downstream [167], which could be a consequence of respiratory sinus arrhythmia.

The $SD1_m$ increases to the maximum at lag 6 and 7 in the smoker group and the non-smoker group, respectively (see Table 5-9 in Section 5.3). $SD2_m$ decreases to the minimum at lag 6 in both groups, which is coincident with the respiratory sinus arrhythmia. After lag 6 or lag 7, $SD1_m$ and $SD2_m$ become relatively stable. The joint changes of $SD1_m$ and $SD2_m$, measured by their ratio $SD1_m/SD2_m$, reflect the different inter-beat correlation between m -lagged PPI series. The comet shapes with a lower ratio of $SD1_m/SD2_m$ hold a higher inter-beat correlation between the current series and the downstream series than the fan or round shape with a higher ratio of $SD1_m/SD2_m$ [168]. Although no statistical differences are found for the $SD1_m/SD2_m$, the ratios augment with the increasing lags in both groups, indicating the correlations between neighboring inter-beats become weaker.

A combination of linear and nonlinear HRV analysis techniques on an automated system would greatly facilitate the development of interventional measures [163]. In this study, the correlations between lagged Poincaré plot indices and spectral power indices separate the healthy habitual smokers and the healthy non-smokers. In the healthy non-smokers, all $SD1_m$ except $SD1_1$ correlates better with the LF component than those in the habitual smokers (see Figure 5-6(b) in Section 5.3). Similarly, $SD2_m$ in the healthy non-smokers correlates better with the HF component than those in the habitual smokers (see Figure 5-7(a) in Section 5.3). Although the similar results are not observed in the correlations between $SD1_m$ and $LF(n.u.)$ or between $SD2_m$ and $HF(n.u.)$, the high correlation coefficients values are evident in the non-smoker group (see Figures 5-6(d) and 5-6(c) in Section 5.3). Previous works [169] have expressed that the HF component contributes to the width of Poincaré plot in a larger amount, and that the LF component contribution is relatively minor. Moreover, they stated that the width of the Poincaré plot may be considered a measure of the total modulation. Such a physiological model in their studies was established on a conventional Poincaré plot (lag=1). As to the lagged Poincaré plot, with the augment of the lags, there is no consensus about how the width and the length of lagged Poincaré plot are contributed by LF or HF components. The results gained from Figure 5-6 and Figure 5-7 (in Section 5.3) could be attributed to the coincidental regulation in the non-smoker group whereas a breakable rule in the smoker group because of the influence of cigarette smoking on the ANS. As to the relationship between $SD1_m/SD2_m$ and LF/HF in both groups, the two curves cross at lag 5. The results

indicate that medium-term inter-beat correlation could be a valuable index which is probably related to the respiratory sinus arrhythmia.

As well as highlighting the utility of lagged Poincaré plot indices for the HRV assessment, Study III outlines an overall relationship of the frequency components and Poincaré plot with lags from 1 to 10. By exploiting a physiological model, Brennan *et al* [169] established that the length and width of a Poincaré plot are a weighted combination of LF and HF. Thus, establishing a physiological model for the lagged Poincaré plot could help for better understanding of its properties. Measurements made during paced breathing deserve further investigation to learn the mechanism of respiratory sinus arrhythmia in the lagged Poincaré plot. Moreover, the value of the method needs justification in cardiovascular disease groups.

6.4 Noncontact PPG as a substitute technique for contact PPG

6.4.1 Geometrical parameters in noncontact reflection PPG photonics engineering setup

Direct coupling is the phenomenon whereby the photodetector detects light directly from the light source without first interacting with the tissue. This occurs when light is illuminated directly onto the photodetector or when the photodetector is exposed directly to ambient light, which is usually a result of inappropriate probe selection or positioning [170]. Direct coupling should not be negligible in noncontact PPG as light could be illuminated directly from the light source to the photodetector, depending on the positions of the light source, the photodetector and the tissue. The minimisation of direct coupling has been considered in the engineering model for NRPPG (see Section 4.1.2.1) to obtain a clear PPG signal.

In the NRPPG photonics engineering setup (see Section 4.1.2.2), the geometrical parameters, i.e. θ_{PL} and d_{PL} , were consolidated in the physical experiment to achieve a better performance. In the engineering setup, the light source and the photodetector are placed on the same side of skin surface. The geometrical consideration in this

reflection PPG sensor is to determine the optimal distance between the light source and the photodetector. In the existing literature [61], there are two techniques that can enhance the quality of the plethysmogram: a large light source driving current utilisation and closer placement of photodetector to light source. The technique used in noncontact measurement not only considered the above principles but also the combination of the incident angle θ_{PL} and the distance d_{PL} , because these two geometrical parameters help to decide the optimal range which determines the quality of PPG signal captured in the setup. The present sensor configuration in this study allowed the examination of the banana shape effect on its length (l) as well as the distance d_{PL} between the VCSEL and the photodiode in the noncontact reflection measurement.

As detailed, the range of d_{PH} between 30-110 mm was spotted as the largest optimal range when θ_{PL} is at the angle of 25° and d_{PL} is 25 mm. In the optimal range, the quality of the PPG signals is determined by (1) the illumination area with banana-shape effect, and (2) the output power of light from the VCSEL to the illuminated tissue. The light from the VCSEL could generate a scattered light throughout the surrounding tissue. It has been identified theoretically and experimentally [140, 171] that the backscattered light on the tissue surface is most likely to travel along a curved banana-shaped path through the tissue, and the depth and the length of the curve is proportional to the distance between the light source and the detector. The experimental results suggest that the length of banana-shaped curve determines the quality of PPG signals. Also, the banana-shape effect on the optimal range is from 6 mm to 26 mm, which is consistent with the previous work [140, 171], where the light propagation in a model of the adult head was examined in a similar situation. Additionally, the light illuminating the tissue should be strong enough to be detected by the photodiode since the output power of the VCSEL decreases with increasing distance d_{PL} .

6.4.2 Comparison of PPG signals between NRPPG and CPPG

The PPG signal is composed of two components: a DC component, which is a relatively constant voltage but changes in magnitude depending on the nature of the

tissue through which the light passes (skin, cartilage, venous blood, etc), and an AC or pulsatile component synchronous with HR. Furthermore, the AC component can be divided into three parts [1]: (1) the frequency component in the range 0.01-0.5 Hz, which reflects the activity of the sympathetic nervous system; (2) the frequency component in the range 0.5-2 Hz, where the major peak depends on the individual heart rate; and (3) the frequency component above 2 Hz, which is due to the harmonics and has minimal clinical value. Attenuation of pressure and flow waves occurs as a function of distance travelled through the arterial system. In the aorta the harmonic components spread up to the 20th harmonic, while at the finger capillary bed it is difficult to detect at and above the third harmonic as shown in Figure 5-12. The higher harmonics are filtered out by the precapillary sphincter.

In Study IV, the PSD differences between CPPG and NRPPG signals could be attributed to: (1) the different probed skin location, i.e. finger for CPPG and palm for NRPPG. The pulse shape and amplitude can vary with change of the relative position between the detector and the skin surface; and that will further influence the signal PSD; (2) pressure exerted on the skin by the contact sensor can also influence the AC signal in CPPG [172]; and (3) the effects of motion artefact, which includes any voluntary and involuntary movements of the interface between the probe and tissue bed, and can be more significant in NRPPG system because the probe is more sensitive to tissue movements.

The knowledge of transitions between regular or chaotic behaviours is essential to understand the underlying mechanisms behind complex systems. While several linear approaches are often insufficient to describe such processes, and most nonlinear techniques, such as fractal dimensions and Lyapunov exponents, require rather long time observations. To overcome these difficulties, RP is used as a graphical tool for the diagnosis of drift and hidden periodicities in the time evolution. The RP based on the vertical structures exhibits characteristic large-scale and small-scale patterns that are caused by typical dynamic behaviour [138], e.g. continuous and periodic diagonal lines, which is caused by the periodic states or related to the similar local evolution of different parts of the trajectory, can be seen in both patterns for CPPG and NRPPG signal. Horizontal and vertical black lines, which indicate that the state does not change for some time, were only found in the NRPPG signal (see Figure 5-13(b) in

Section 5.4). The pattern of RPs can be used to discriminate differences between the two signals. However, the physiological meanings of the patterns in the signals require further understanding.

In order to achieve a practical utilisation, the NRPPG needs to perform comparably the main functions of the available photoplethysmographic device. In the reality of NRPPG application, measuring heart activity and displaying a plethysmogram were targeted as the priority in this study. The comparison between CPPG and NRPPG seems essential to recognise both performances of these two techniques in a good agreement with Bland-Altman plot regardless of the operation conditions. Study IV presented the comparison results between NRPPG and CPPG with respect to their primary functions of PPG by means of graphical and numerical analysis methods. The correlation coefficients were close to 1, and the errors between CPPG and NRPPG from Bland-Altman plots were distributed within the reasonable ranges. The good agreement for the heart rate indices indicates that NRPPG is compatible with CPPG.

6.5 The effectiveness of noncontact PPG for physiological monitoring

In Study V, the results from the physiological monitoring experiment demonstrate that the NRPPG has a prospect of applicability in physiological assessment. The quantitative Poincaré plot from the NRPPG signal reveals the short-term beat-to-beat variance of the PPI (SD1), the long-term beat-to-beat variance of the PPI (SD2) and their balance (SD1/SD2). The expending scatter due to the enhancement of sympathetic activity in the afternoon (see Figure 5-16 in Section 5.5) can be observed in the Poincaré plots, which is consistent with the explanations in the work from Tulppo *et al* [137]. The authors reported that SD2 decreased and SD1/SD2 ratio increased during exercise after a complete parasympathetic blockade. This experiment indicatess that sympathetic activation in the afternoon results in progressive reduction in the long-term oscillation of heart rate.

CHAPTER 7

CONCLUSIONS AND FURTHER WORK

The photoplethysmographic technique has been used to analyse the state of the human cardiovascular regulation. Challenges remain in this field, including the standardisation of measurements and establishing a comprehensive normative data range for comparison with patients. Future work is also required in analysis techniques, including fast diagnosis, multi-location utility and monitoring from a greater distance.

7.1 Conclusions

The main focus of this thesis is to investigate cardiovascular regulation by means of the PPG technique. The main contributions can be summarised as follows: (1) contour analysis of PPG waveform exploiting the arterial stiffness in young adults; (2) exploring the reliability of PPG-derived PRV serving as an alternative approach to obtain HRV information; (3) a novel approach for exploiting the PRV characteristics by means of combined indices of lagged Poincaré plots and frequency domain; and (4) development of a NRPPG system for biomedical monitoring.

7.1.1 Waveform analysis

The first contribution illustrates the differences of waveform between younger and older subjects and between male and female subjects. The PPG waveform exhibits a characteristic notch in its catacrotic phase for young adults. Study I has demonstrated that there exists a trend of arterial stiffness with ageing in young adults, and confirmed that the process of the arteries stiffening starts from around the early decades of life in healthy subjects. Meanwhile, male subjects have stiffer arteries than female subjects. The PNL and PNRA in Study I have provided a useful tool for evaluating arterial stiffness. In conclusion, photoplethysmographic assessment of the pulse waveform may provide a useful method for examining vascular activity.

7.1.2 Reliability of PPG in heart rate monitoring

The second contribution strongly suggests a good alternative to understanding dynamics pertaining to the ANS without the use of an ECG device. Due to the inconvenience of ECG measurement, frequent assessments of HRV and associated disease studies are not broadly applied in practical applications, i.e. mobile medical assistance and homecare. PPG enables the noninvasive measurement of the peripheral pulse wave enabling assessment of cardiac time interval. Estimation of HRV from peripheral pulse wave by means of PPG sensor has also demonstrated its superiority in terms of flexibility and convenience for HRV measurement.

7.1.3 Utility of PRV in heart activity assessment

In the third contribution, characteristics of PRV were investigated for the assessment of the function of the ANS in smokers and non-smokers. It has demonstrated that the combination of lagged Poincaré plots and spectral characteristics could show promise as a method for distinguishing between different cardiovascular groups. Convincingly, PRV has the potential to provide valuable interpretation of biomedical phenomena.

7.1.4 Feasibility of noncontact PPG

In the fourth contribution, a proof of concept for NRPPG with an engineering model was created to achieve sophisticated and dynamic measurement in Study IV and Study V. The NRPPG exhibits a good performance of the PPG signal detection in a proper geometrical arrangement. The compatibility of the techniques between NRPPG and CPPG for the evaluation of heart activity makes NRPPG an attractive technique in the biomedical and clinical community.

7.2 Future work

7.2.1 Standardisation of measurements

In this thesis, HR behaviour was studied in more controlled and stationary conditions, e.g. in supine or sitting positions. Thus, the effects of nonstationarities on the results were possibly better eliminated in these studies. However, the frequency and depth of breathing were not controlled, which means that the conditions were not completely standardised. The majority of the specific problems associated with PPG measurement can be largely eliminated by careful consideration at the strict control of experimental procedures. Meanwhile, the participants in current studies are limited to healthy persons. It is significant to establish comprehensive normative data ranges for comparison with patients.

7.2.2 Advanced signal processing

Further studies are warranted to determine whether the novel signal processing method in Study III for PRV assessment is applicable in cardiovascular disease groups. Future trends in the PPG application are being heavily influenced by the availability of increasingly powerful methods of digital signal processing. Physiological signals with their time-varying nature and characteristic morphologies and spectral signatures are particularly well suited for analysis and interpretation using time-frequency and time-scale analysis techniques, such as the short time Fourier transform (STFT) and wavelet transform (WT). Signal processing algorithms implemented both in hardware and software play a major role in transforming the optical signals and extracting useful information. In some cases, it could be possible to borrow from existing paradigms in statistics, engineering, computer science, and physics to design these methods. Indeed, use of existing methods should be the first step. The unique features of PPG signal itself, however, are leading rapidly to a need for signal processing and statistical methods developed specifically for these PPG studies.

7.2.3 Understanding of physiology-related PPG

A pulsatile photoplethysmogram reveals the HR and could be used to monitor HRV. But as an HR-monitoring modality, PPG is unable to distinguish between electrically narrow-complex and wide-complex beats, and electrical–mechanical disassociation could cause a discrepancy between a photoplethysmographic HR and electrocardiographic HR. There is insufficient evidence to warrant the use of PPG for primary HR monitoring and fast diagnosis because the shape of a normal pulse may be less morphologically distinct than the QRS complex of an electrocardiogram. Therefore, a better understanding and interpretation of the underlying physiology of the PPG can help the clinician provide better care for their patients.

7.2.4 Multi-location utility

The results from NRPPG concern measurement in the palm. Although clear signals have been measured at other anatomical locations, such as the forehead and wrist, the palm signal is typically stronger and an engineering setup for palm signal recording is relatively easy for the participants in a large group. A robust comparison of noncontact PPG signal strengths as a function of anatomical location is a subject for future investigation. Also, development of noncontact PPG for multi-location utility is another focus for future work.

7.2.5 Engineering improvements on noncontact PPG

Notably, a remote PPG probe could be very useful for front-line-clinicians to comfortably and confidently cope with a range of situations. Such an instrument may not compete with conventional devices for routine bedside monitoring or for ambulatory monitoring, but would most likely find applications in specialised areas such as sleep studies, intensive care, neonatal monitoring, and patients with burns or healing skin. Nevertheless, applications from bench to bedside need more engineering efforts, such as increasing dynamic measurement range, improvement of signal-to-noise ratio and reduction of motion artefact. Noncontact monitoring from a much greater distance will be another focus for future study. Though obstacles to developing a clinically useful device remain, the allure of a noncontact PPG and the ability to measure cardiovascular function by noncontact means are strong.

7.2.6 All-in-one monitoring

Reducing the occurrence of false alarms would be beneficial in all applications, but especially during long term monitoring when staff cannot always be in the room. In hospital environments for monitoring during surgery, recovery, and intensive care, all-in-one monitoring seems to be the goal. Furthermore, next generation PPG offers the prospect of transmission of information via radio waves to central stations.

APPENDIX A:

AUTOCORRELATION AND AUTOCOVARANCE

The autocorrelation function is an important measure of HRV simply because its Fourier transform is the power spectrum of intervals. The autocorrelation function of the RR intervals is defined as

$$\gamma_{RR}(m) = E[RR_n RR_{n+m}] \quad (\text{A-1})$$

Spectral analysis is normally performed on the mean-removed RR intervals and, therefore, the mean-removed autocorrelation function, called the autocovariance function, is often preferred

$$\phi_{RR}(m) = E[(RR_n - \overline{RR})(RR_{n+m} - \overline{RR})] \quad (\text{A-2})$$

For stationary RR intervals, the autocovariance function is related to the autocorrelation function

$$\phi_{RR}(m) = \gamma_{RR}(m) - \overline{RR}^2 \quad (\text{A-3})$$

The autocovariance function is related to the variance of the RR intervals,

$$SDRR^2 = \phi_{RR}(0) \quad (\text{A-4})$$

and the variance of the delta-RR intervals,

$$SDRR^2 = 2(\phi_{RR}(0) - \phi_{RR}(1)) = 2(\gamma_{RR}(0) - \gamma_{RR}(1)) . \quad (\text{A-5})$$

APPENDIX B:

RECURRENCE PLOT STRUCTURES

B.1 Introduction

Recurrence is a fundamental property of dynamic systems, which can be exploited to characterise the system's behaviour in phase space. A powerful tool for their visualisation and analysis called the recurrence plot (RP) was introduced in the late 1980s by Eckmann *et al* [138]. An excellent review from Marwan *et al.* has introduced this powerful tool to a broad readership [173].

Suppose we have a trajectory $\{\vec{x}_i\}_{i=1}^N$ of a system in its phase space. The components of these vectors could be, e.g. the position and velocity of a pendulum or quantities such as temperature, air pressure, humidity and many others for the atmosphere. The development of the systems is then described by a series of these vectors, representing a trajectory in an abstract mathematical space. Then, the corresponding RP is based on the following recurrence matrix:

$$\mathbf{R}_{i,j} = \begin{cases} 1: \vec{x}_i \approx \vec{x}_j, \\ 0: \vec{x}_i \not\approx \vec{x}_j, \end{cases} \quad i, j = 1, \dots, N, \quad (\text{B-1})$$

where N is the number of considered states and \approx means equality up to an error (or distance) ε . Note that this ε is essential as systems often do not recur exactly to a formerly visited state but just approximately. Roughly speaking, the matrix compares the states of a system at times i and j . If the states are similar, this is indicated by a one in the matrix, i.e. $\mathbf{R}_{i,j}=1$. If on the other hand the states are rather different, the corresponding entry in the matrix is $\mathbf{R}_{i,j}=0$. So the matrix tells us when similar states

of the underlying system occur. Much more can be concluded from the recurrence matrix, equation (B-1).

As our focus is on recurrences of states of a dynamic system, we define now the tool which measures recurrences of a trajectory $\vec{x}_i \in \mathbb{R}^d$ in phase space: the *recurrence plot*, equation (B-1). The RP efficiently visualises recurrences and can be formally expressed by the matrix

$$\mathbf{R}_{i,j}(\varepsilon) = \Theta(\varepsilon - \|\vec{x}_i - \vec{x}_j\|), \quad i, j = 1, \dots, N, \quad (\text{B-2})$$

where N is the number of measured points \vec{x}_i ; ε is a threshold distance, $\Theta(\cdot)$ the Heaviside function (i.e. $\Theta(x) = 0$, if $x < 0$, and $\Theta(x) = 1$ otherwise) and $\|\cdot\|$ is a norm. For ε -recurrent states, i.e. for states which are in an ε -neighbourhood, we introduce the following notion:

$$\vec{x}_i \approx \vec{x}_j \Leftrightarrow \mathbf{R}_{i,j} \equiv 1 \quad (\text{B-3})$$

The RP is obtained by plotting the recurrence matrix, equation (B-2), and using different colours for its binary entries, e.g. plotting a black dot at the coordinates (i, j) , if $\mathbf{R}_{i,j} \equiv 1$, and a white dot, if $\mathbf{R}_{i,j} \equiv 0$. Both axes of the RP are time axes and show rightwards and upwards (convention). Since $\mathbf{R}_{i,j} \equiv 1 \big|_{i=1}^N$ by definition, the RP has always a black main diagonal line, the *line of identity* (LOI). Furthermore, the RP is symmetric by definition with respect to the main diagonal, i.e. $\mathbf{R}_{i,j} \equiv \mathbf{R}_{j,i}$.

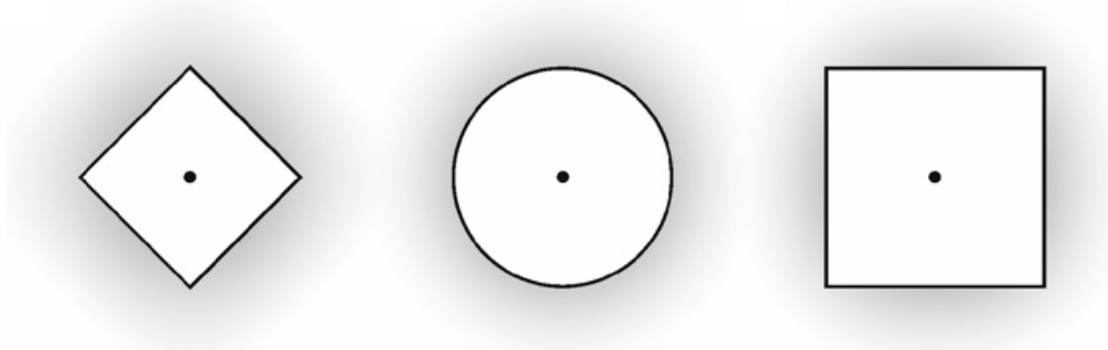


Figure B-1. Three commonly used norms for the neighbourhood with the same radius around a point (black dot) exemplarily shown for the two-dimensional phase space: (a) L_1 -norm, (b) L_2 -norm and (c) L_∞ -norm.

In order to compute an RP, an appropriate *norm* has to be chosen. The most frequently used norms are the L_1 -norm, the L_2 -norm (Euclidean norm) and the L_∞ -norm (Maximum or Supremum norm). Note that the neighbourhoods of these norms have different shapes (Figure B-1). Considering a fixed ε , the L_∞ -norm finds the most, the L_1 -norm the least and the L_2 -norm an intermediate amount of neighbours. To compute RPs, the L_∞ -norm is often applied, because it is computationally faster and allows to study some features in RPs analytically.

B.2 Structures in RPs

As already mentioned, the initial purpose of RPs was to visualise trajectories in phase space, which is especially advantageous in the case of high dimensional systems. RPs yield important insights into the time evolution of these trajectories, because typical patterns in RPs are linked to a specific behaviour of the system. Large scale patterns in RPs, designated in as *typology*, can be classified in *homogeneous*, *periodic*, *drift* and *disrupted* ones:

- *Homogeneous* RPs are typical of stationary systems in which the relaxation times are short in comparison with the time spanned by the RP. An example of such an RP is that of a stationary random time series (Figure B-2a).
- Periodic and quasi-periodic systems have RPs with diagonal oriented, *periodic* or *quasi-periodic* recurrent structures (diagonal lines, checkerboard structures). Figure B-2b shows the RP of a periodic system with two harmonic frequencies and with a frequency ratio of four (two and four short lines lie between the continuous diagonal lines). Irrational frequency ratios cause more complex quasi-periodic recurrent structures (the distances between the diagonal lines are different). However, even for oscillating systems whose oscillations are not easily recognisable, RPs can be useful.

- A *drift* is caused by systems with slowly varying parameters, i.e. non-stationary systems. The RP pales away from the LOI (Figure B-2c).
- Abrupt changes in the dynamics as well as extreme events cause *white areas or bands* in the RP (Figure B-2d). RPs allow finding and assessing extreme and rare events easily by using the frequency of their recurrences.

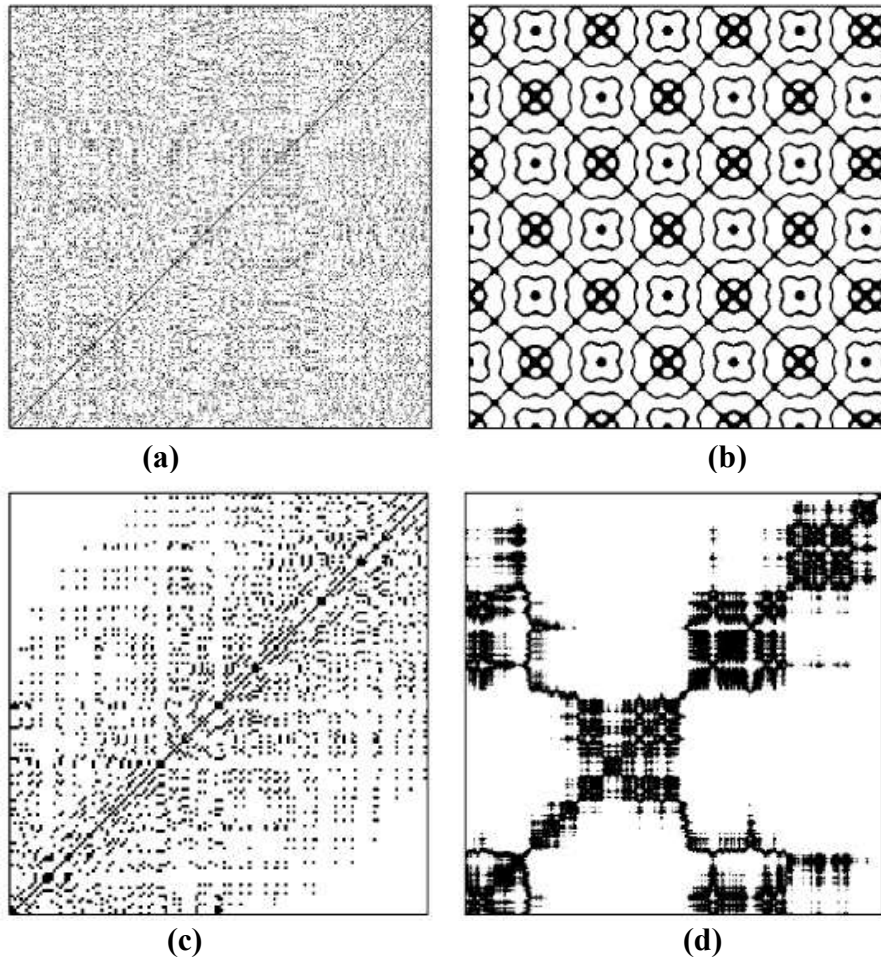


Figure B-2. Characteristic typology of recurrence plots: (a) homogeneous (uniformly distributed white noise), (b) periodic (super-positioned harmonic oscillations), (c) drift (logistic map corrupted with a linearly increasing term $x_{i+1}=4x_i(1-x_i)+0.01i$), and (d) disrupted (Brownian motion). These examples illustrate how different RPs can be. The used data have the length 400 (a, b, d) and 150 (c), respectively; RP parameters are $m=1$, $\epsilon=0.2$ (a, c, d) and $m=4$, $\tau=9$, $\epsilon=0.4$ (b); L_2 -norm.

A closer inspection of the RPs reveals also small-scale structures, the *texture*, which can be typically classified in *single dots*, *diagonal lines* as well as *vertical* and

Appendix B: Recurrence plot structures

horizontal lines (the combination of vertical and horizontal lines obviously forms rectangular clusters of recurrence points); in addition, even *bowed lines* may occur :

- *Single, isolated recurrence points* can occur if states are rare, if they persist only for a very short time, or fluctuate strongly.
- A *diagonal line* $\mathbf{R}_{i+k,j+k} \equiv 1 \big|_{k=0}^{l-1}$ (where l is the length of the diagonal line) occurs when a segment of the trajectory runs almost in parallel to another segment (i.e. through an ε -tube around the other segment) for l time units:

$$\vec{x}_i \approx \vec{x}_j, \vec{x}_{i+1} \approx \vec{x}_{j+1}, \dots, \vec{x}_{i+l-1} \approx \vec{x}_{j+l-1} \quad (\text{B-4})$$

A diagonal line of length l is then defined by

$$(1 - \mathbf{R}_{i-1,j-1})(1 - \mathbf{R}_{i+l,j+l}) \prod_{k=0}^{l-1} \mathbf{R}_{i+k,j+k} \equiv 1 \quad (\text{B-5})$$

The length of this diagonal line is determined by the duration of such similar local evolution of the trajectory segments. The direction of these diagonal structures is parallel to the LOI (slope one, angle $\pi/4$). They represent trajectories which evolve through the same ε -tube for a certain time. Since the definition of the Rényi entropy of second order K_2 uses the time how long trajectories evolve in an ε -tube, the existence of a relationship between the length of the diagonal lines and K_2 (and even the sum of the positive Lyapunov exponents) is plausible. Note that there might be also diagonal structures perpendicular to the LOI, representing parallel segments of the trajectory running with opposite time directions, i.e. $\vec{x}_i \approx \vec{x}_j, \vec{x}_{i+1} \approx \vec{x}_{j-1}, \dots$ (mirrored segments). This is often a hint for an inappropriate embedding.

- A *vertical (horizontal) line* $\mathbf{R}_{i,j+k} \equiv 1 \big|_{k=0}^{v-1}$ (with v the length of the vertical line) marks a time interval in which a state does not change or changes very slowly:

$$\vec{x}_i \approx \vec{x}_j, \vec{x}_i \approx \vec{x}_{j+1}, \dots, \vec{x}_i \approx \vec{x}_{j+v-1} \quad (\text{B-6})$$

The formal definition of a vertical line is

$$(1 - \mathbf{R}_{i,j-1})(1 - \mathbf{R}_{i,j+v}) \prod_{k=0}^{v-1} \mathbf{R}_{i,j+k} \equiv 1 \quad (\text{B-7})$$

Hence, the state is trapped for some time. This is a typical behaviour of laminar states (intermittency) [174].

- *Bowed lines* are lines with a non-constant slope. The shape of a bowed line depends on the local time relationship between the corresponding close trajectory segments.

To summarise the explanations about typology and texture, we present a list of features and their corresponding interpretation in Table 1.

Table B-1. Typical patterns in RPs and their meanings.

Pattern	Meaning
(1) Homogeneity	The process is stationary
(2) Fading to the upper left and lower right corners	Non-stationary data; the process contains a trend or a drift
(3) Disruptions (white bands)	Non-stationary data; some states are rare or far from the normal; transitions may have occurred
(4) Periodic/quasi-periodic patterns	Cyclicities in the process; the time distance between periodic patterns (e.g. lines) corresponds to the period; different distances between long diagonal lines reveal quasi-periodic processes
(5) Single isolated points	Strong fluctuation in the process; if only single isolated points occur, the process may be an uncorrelated random or even anti-correlated process
(6) Diagonal lines (parallel to the LOI)	The evolution of states is similar at different epochs; the process could be deterministic; if these diagonal lines occur beside single isolated points, the process could be chaotic (if these diagonal lines are periodic, unstable periodic orbits can be observed)
(7) Diagonal lines (orthogonal to the LOI)	The evolution of states is similar at different times but with reverse time; sometimes this is an indication for an insufficient embedding
(8) vertical and horizontal lines/clusters	Some states do not change or change slowly for some time; indication for laminar states
(9) Long bowed line structures	The evolution of states is similar at different epochs but with

APPENDIX C:

DESIGN OF INFINITE IMPULSE RESPONSE DIGITAL FILTER

C.1 Basic Features of infinite impulse response (IIR) filters

IIR digital filters are characterized by the following recursive equation:

$$y(n) = \sum_{k=0}^{\infty} h(k)x(n-k) = \sum_{k=0}^N b_k x(n-k) - \sum_{k=1}^M a_k y(n-k) \quad (\text{C-1})$$

where $h(k)$ is the impulse response of the filter which is theoretically infinite in duration, b_k and a_k are the coefficients of the filter, and $x(n)$ and $y(n)$ are the input and output to the filter. The transfer function for the IIR filter is given by

$$H(z) = \frac{b_0 + b_1 z^{-1} + \dots + b_N z^{-N}}{1 + a_1 z^{-1} + \dots + a_M z^{-M}} = \frac{\sum_{k=0}^N b_k z^{-k}}{1 + \sum_{k=1}^M a_k z^{-k}} \quad (\text{C-2})$$

An important part of the IIR filter design process is to find suitable values for the coefficients b_k and a_k such that some aspect of the filter characteristic, such as frequency response, behaves in a desired manner. Equations (C-1) and (C-2) are the characteristic equations for IIR filters.

In equation (C-1), the current output sample, $y(n)$, is a function of past outputs, $y(n-k)$, as well as present and past input samples, $x(n-k)$. IIR filter is a feedback system of some sort. The strength of IIR filters comes from the flexibility that the feedback arrangement provides. For example, an IIR filter normally requires fewer coefficients than an finite impulse response (FIR) filter for the same set of specifications, which is why IIR filters are used when sharp cut-off and high throughput are the important requirements.

B.2 Design stages for digital IIR filter

The design of IIR filter can be conveniently broken down into five main stages:

- (1) Filter specification, at which stage the designer gives the function of the filter (for example, lowpass) and the design performance.
- (2) Approximation or coefficient calculation, where we select one of a number of methods and calculate the values of the coefficients, b_k and a_k , in the transfer function, $H(z)$, such that the specification given in stage 1 are satisfied.
- (3) Realization, which is simply converting the transfer function into a suitable filter structure. Typical structures for IIR filters are parallel and cascade of second and/or first-order filter sections.
- (4) Analysis of errors that would arise from representing the filter coefficients and carrying out the arithmetic operations involved in filtering with only a finite number of bits.
- (5) Implementation, which involves building the hardware and/or writing the software codes, and carrying out the actual filtering operation.

B.3 Use of BZT and classical analogue filters to design IIR filters

In many practical cases, the analogue transfer function, $H(s)$, from which $H(z)$ is obtained, may not be available and will have to be determined from the specifications of the desired digital filters. For standard frequency selective digital filtering tasks, (i.e. involving lowpass, highpass, bandpass and bandstop filters), $H(s)$ can be derived from the classical filters with Butterworth, Chebyshev or elliptic characteristics.

Here, Butterworth filters is presented as an example. The lowpass Butterworth filters is characterized by the following magnitude-squared-frequency response:

$$|H(\omega)|^2 = \frac{1}{1 + \left(\frac{\omega}{\omega_p^p}\right)^{2N}} \quad (\text{C-3})$$

where N is the filter order and ω_p^p is the 3dB cutoff frequency of the lowpass filter (for the normalized prototype filter, $\omega_p^p = 1$). The magnitude-frequency response of a

typical Butterworth lowpass filter is depicted in Figure C-1, and is seen to be monotonic in both the passband and stopband. The response is said to be maximally flat because of its initial flatness (with a slope of zero at dc).

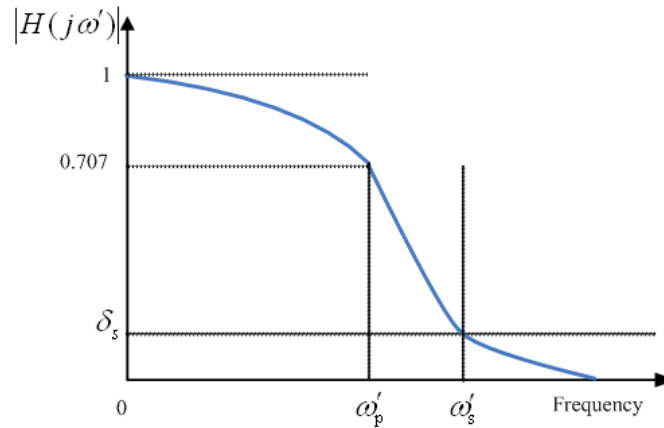


Figure C-1. Sketches of frequency responses of Butterworth filter.

The filter order, N , is given by

$$N \geq \frac{\log \left(\frac{10^{\frac{A_s}{10}} - 1}{10^{\frac{A_p}{10}} - 1} \right)}{2 \log \left(\frac{\omega_s^p}{\omega_p^p} \right)} \quad (\text{C-4})$$

where A_p and A_s are, respectively, the passband ripple and stopband attenuation in dB, and ω_s^p is the stopband edge frequency above. Only lowpass prototype filters are considered, since other filter types are normally derived from normalized lowpass filters.

Bilinear z -transform (BZT) is one of the most important method of obtaining IIR filter coefficients. The stages of the BZT method are:

- (1) Use the digital filter specifications to find a suitable normalized, prototype, analogue lowpass filter, $H(s)$.
- (2) Determine and prewarp the bandedge or critical frequencies of the desired filter. For lowpass or highpass filters there is just one bandedge or cutoff frequency, ω_p . For bandpass and bandstop filters, we have the lower and

upper passband edge frequencies, ω_{p1} and ω_{p2} , each of which needs to be prewarped:

$$\omega'_p = \tan\left(\frac{\omega_p T}{2}\right) \quad (C-5)$$

$$\omega'_{p1} = \tan\left(\frac{\omega_{p1} T}{2}\right); \quad \omega'_{p2} = \tan\left(\frac{\omega_{p2} T}{2}\right) \quad (C-6)$$

- (3) Denormalise the analogue prototype filter by replacing s in the transfer function, $H(s)$, using one of the following transformations, depending on the type of filter required:

$$s = \frac{s}{\omega'_p} \quad \text{lowpass to lowpass} \quad (C-7)$$

$$s = \frac{\omega'_p}{s} \quad \text{lowpass to highpass} \quad (C-8)$$

$$s = \frac{s^2 + \omega_0^2}{W_s} \quad \text{lowpass to bandpass} \quad (C-9)$$

$$s = \frac{W_s}{s^2 + \omega_0^2} \quad \text{lowpass to bandstop} \quad (C-10)$$

where $\omega_0^2 = \omega'_{p2} \omega'_{p1}$, $W = \omega'_{p2} - \omega'_{p1}$.

- (4) Apply the BZT to obtain the desired digital filter transfer function, $H(z)$, by replacing s in the frequency-scaled (i.e. denormalized) transfer function, $H'(s)$, as follows:

$$s = \frac{z-1}{z+1} \quad (C-11)$$

B.4 Application example

A lowpass, discrete-time filter, with Butterworth characteristics, is required to meet the following specifications: (1) cutoff frequency: 50 Hz; filter order: 10, and (3) sampling frequency: 1000Hz. Magnitude-frequency response for BZT is depicted in Figure C-2 with the aid of Matlab. The effect of this filter is shown in Figure C-3. The spectrum of the two signals, i.e. original signal and filtered signal, are presented in Figure C-4.

Matlab m-file for the design of the BZT filter.

```
Fs=1000;                                %Sampling frequency
FN=Fs/2;
fc=50;                                  %Cutoff frequency
N=10;
[z,p,k]=butter(N,fc/FN);
[h,f]=freqz(k*poly(z),poly(p),512,Fs);
plot(f,20*log10(abs(h))),grid
ylabel('Magnitude (dB)')
xlabel('Frequency (Hz)')
```

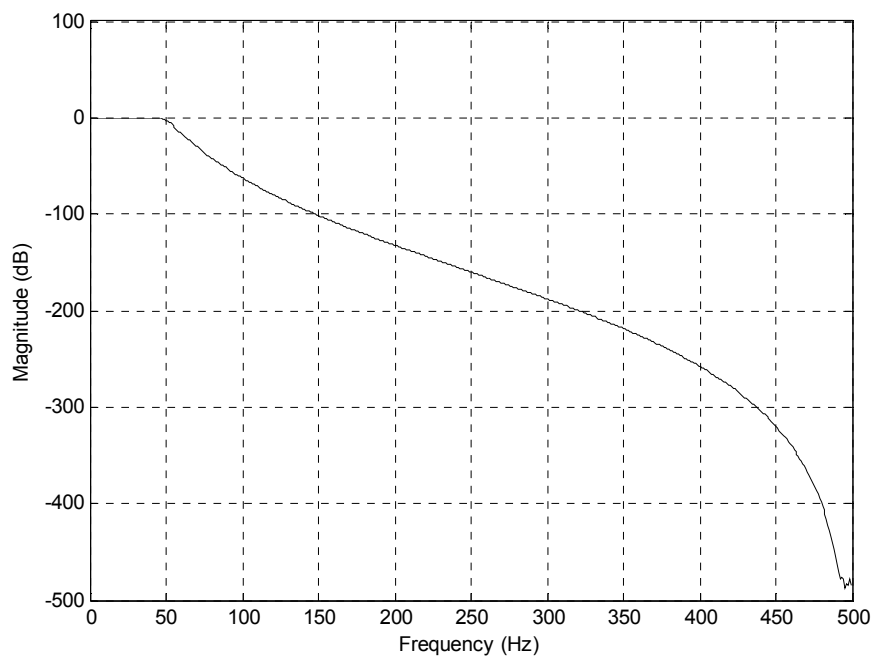


Figure C-2. Magnitude-frequency response for BZT.

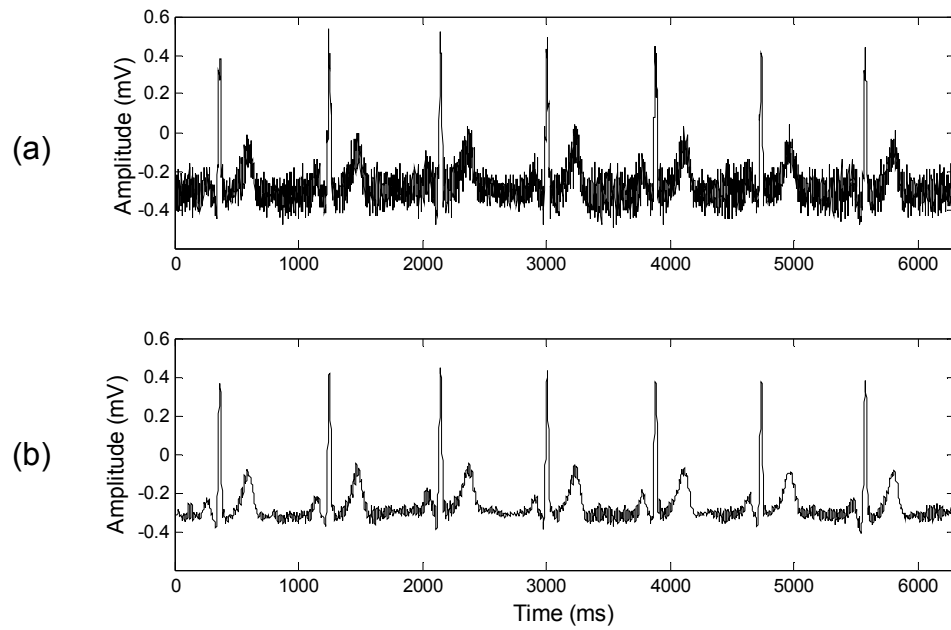


Figure C-3. (a) The original ECG signal. (b) The filtered ECG signal by using lowpass Butterworth filter.

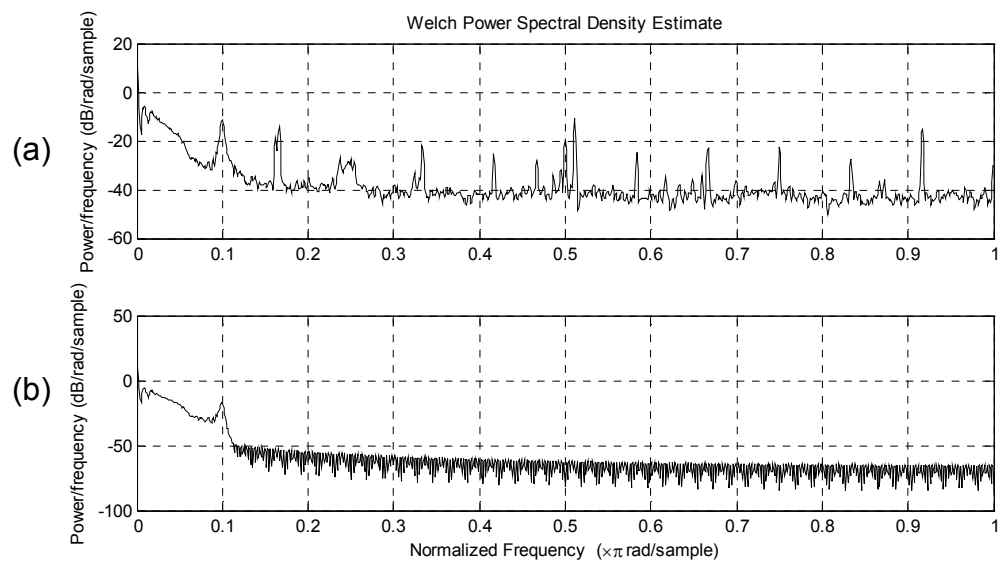


Figure C-4. (a) The spectrum of the original ECG signal. (b) The spectrum of the filtered ECG signal.

REFERENCES

1. Kamal AA, Harness JB, Irving G, Mearns AJ. Skin photoplethysmography--a review. *Comput Methods Programs Biomed.* 1989;28(4):257-269.
2. Arnett DK, Evans GW, Riley WA. Arterial stiffness: a new cardiovascular risk factor? *Am J Epidemiol.* 1994;140(8):669-682.
3. Laurent S, Cockcroft J, Van Bortel L, Boutouyrie P, Giannattasio C, Hayoz D, Pannier B, Vlachopoulos C, Wilkinson I, Struijker-Boudier H. Expert consensus document on arterial stiffness: methodological issues and clinical applications. *Eur Heart J.* 2006;27(21):2588-2605.
4. Glasser SP, Arnett DK, McVeigh GE, Finkelstein SM, Bank AK, Morgan DJ, Cohn JN. The importance of arterial compliance in cardiovascular drug therapy. *J Clin Pharmacol.* 1998;38(3):202-212.
5. Cohn JN. Arterial stiffness, vascular disease, and risk of cardiovascular events. *Circulation.* 2006;113(5):601-603.
6. Hertzman AB, Speelman CR. Observations on the finger volume pulse recorded photoelectrically. *Am J Physiol.* 1937;119:334-335.
7. Duprez DA, Kaiser DR, Whitwam W, Finkelstein S, Belalcazar A, Patterson R, Glasser S, Cohn JN. Determinants of radial artery pulse wave analysis in asymptomatic individuals. *Am J Hypertens.* 2004;17(8):647-653.
8. Takada H, Washino K, Harrell JS, Iwata H. Acceleration plethysmography to evaluate aging effect in cardiovascular system. Using new criteria of four wave patterns. *Med Prog Technol.* 1996;21(4):205-210.
9. Imanaga I, Hara H, Koyanagi S, Tanaka K. Correlation between wave components of the second derivative of plethysmogram and arterial distensibility. *Jpn Heart J.* 1998;39(6):775-784.
10. Takazawa K, Tanaka N, Fujita M, Matsuoka O, Saiki T, Aikawa M, Tamura S, Ibukiyama C. Assessment of vasoactive agents and vascular aging by the second derivative of photoplethysmogram waveform. *Hypertension.* 1998;32(2):365-370.

11. Bortolotto LA, Blacher J, Kondo T, Takazawa K, Safar ME. Assessment of vascular aging and atherosclerosis in hypertensive subjects: second derivative of photoplethysmogram versus pulse wave velocity. *Am J Hypertens*. 2000;13(2):165-171.
12. Allen J, Murray A. Prospective assessment of an artificial neural network for the detection of peripheral vascular disease from lower limb pulse waveforms. *Physiol Meas*. 1995;16(1):29-38.
13. Sherebrin MH, Sherebrin RZ. Frequency analysis of the peripheral pulse wave detected in the finger with a photoplethysmograph. *IEEE Trans Biomed Eng*. 1990;37(3):313-317.
14. Bhattacharya J, Kanjilal PP, Muralidhar V. Analysis and characterization of photo-plethysmographic signal. *IEEE Trans Biomed Eng*. 2001;48(1):5-11.
15. Kelly R, Hayward C, Avolio A, O'Rourke M. Noninvasive determination of age-related changes in the human arterial pulse. *Circulation*. 1989;80(6):1652-1659.
16. Dawber TR, Thomas HE, Jr., McNamara PM. Characteristics of the dicrotic notch of the arterial pulse wave in coronary heart disease. *Angiology*. 1973;24(4):244-255.
17. van Ravenswaaij-Arts CM, Kollee LA, Hopman JC, Stoeltinga GB, van Geijn HP. Heart rate variability. *Ann Intern Med*. 1993;118(6):436-447.
18. Task Force of the European Society of Cardiology and the North American Society of Pacing and Electrophysiology. Heart rate variability. Standards of measurement, physiological interpretation, and clinical use. *Eur Heart J*. 1996;17(3):354-381.
19. La Rovere MT, Pinna GD, Hohnloser SH, Marcus FI, Mortara A, Nohara R, Bigger JT, Jr., Camm AJ, Schwartz PJ. Baroreflex sensitivity and heart rate variability in the identification of patients at risk for life-threatening arrhythmias: implications for clinical trials. *Circulation*. 2001;103(16):2072-2077.
20. Yi G, Crook R, Guo XH, Staunton A, Camm AJ, Malik M. Exercise-induced changes in the QT interval duration and dispersion in patients with sudden cardiac death after myocardial infarction. *Int J Cardiol*. 1998;63(3):271-279.
21. Yi G, Guo XH, Reardon M, Gallagher MM, Hnatkova K, Camm AJ, Malik M. Circadian variation of the QT interval in patients with sudden cardiac death after myocardial infarction. *Am J Cardiol*. 1998;81(8):950-956.
22. Spargias KS, Lindsay SJ, Kawar GI, Greenwood DC, Cowan JC, Ball SG, Hall AS. QT dispersion as a predictor of long-term mortality in patients with acute myocardial infarction and clinical evidence of heart failure. *Eur Heart J*. 1999;20(16):1158-1165.

23. Rosenbaum DS, Jackson LE, Smith JM, Garan H, Ruskin JN, Cohen RJ. Electrical alternans and vulnerability to ventricular arrhythmias. *N Engl J Med.* 1994;330(4):235-241.
24. Guzik P, Schmidt G. A phenomenon of heart-rate turbulence, its evaluation, and prognostic value. *Card Electrophysiol Rev.* 2002;6(3):256-261.
25. Eckberg DL. Sympathovagal balance: a critical appraisal. *Circulation.* 1997;96(9):3224-3232.
26. Kleiger RE, Miller JP, Bigger JT, Jr., Moss AJ. Decreased heart rate variability and its association with increased mortality after acute myocardial infarction. *Am J Cardiol.* 1987;59(4):256-262.
27. Bigger JT, Jr., Fleiss JL, Rolnitzky LM, Steinman RC, Schneider WJ. Time course of recovery of heart period variability after myocardial infarction. *J Am Coll Cardiol.* 1991;18(7):1643-1649.
28. Huikuri HV, Koistinen MJ, Yli-Mayry S, Airaksinen KE, Seppanen T, Ikaheimo MJ, Myerburg RJ. Impaired low-frequency oscillations of heart rate in patients with prior acute myocardial infarction and life-threatening arrhythmias. *Am J Cardiol.* 1995;76(1):56-60.
29. Mueck-Weymann M, Rechlin T, Ehrengut F, Rauh R, Acker J, Dittmann RW, Czekalla J, Joraschky P, Musselman D. Effects of olanzapine and clozapine upon pulse rate variability. *Depress Anxiety.* 2002;16(3):93-99.
30. Srinivas K, Ram Gopal Reddy L, Srinivas R. Estimation of heart rate variability from peripheral pulse wave using PPG sensor Paper presented at: 3rd Kuala Lumpur International Conference on Biomedical Engineering, 2006; Kuala Lumpur, Malaysia
31. Hayes M. *Artefact reduction in photoplethysmography*, Doctoral Thesis: Loughborough University; 1998.
32. Cheang PYS. *Feasibility of non-contact photoplethysmography*, Doctoral Thesis: Loughborough University; 2008.
33. Jones DP. Medical electro-optics: measurements in the human microcirculation. *Physics in Technology* 1987;18:79-85.
34. Anderson RR, Parrish JA. The optics of human skin. *J Invest Dermatol.* 1981;77(1):13-19.
35. Twersky V. Multiple scattering of waves and optical phenomena. *J Opt Soc Am.* 1962;52:145-171.
36. Twersky V. Absorption and multiple scattering by biological suspensions. *J Opt Soc Am.* 1970;60(8):1084-1093.

37. de Kock JP, Tarassenko L. Pulse oximetry: theoretical and experimental models. *Med Biol Eng Comput.* 1993;31(3):291-300.
38. Hertzman AB. Photoelectric plethysmography of the fingers and toes in man. *Proc Soc Exp Biol Med.* 1937b;37:529-542.
39. Roberts VC. Photoplethysmography—fundamental aspects of the optical properties of blood in motion. *Trans Inst Meas Control.* 1982;4(2):101-106.
40. Challoner AVJ. *Photoelectric plethysmography for estimating cutaneous blood flow* Vol 1: London: Academic; 1979.
41. D'Agrosa LS, Hertzman AB. Opacity pulse of individual minute arteries. *J Appl Physiol.* 1967;23(5):613-620.
42. Parrish JA. New concepts in therapeutic photomedicine: photochemistry, optical targeting and the therapeutic window. *J Invest Dermatol.* 1981;77(1):45-50.
43. Molitor H, Kniazuk M. A new bloodless method for continuous recording of peripheral circulatory changes. *J Pharmacol Exp Ther.* 1936;57:6.
44. Hanzlik PJ, Deeds F, Terada B. A simple method of demonstrating changes in blood supply of the ear and effects of some measures. *J Pharmacol. Exp Ther.* 1936;56:194-204.
45. Hertzman AB. The blood supply of various skin areas as estimated by the photoelectric plethysmograph. *Am J Physiol.* 1938;124:328-340.
46. Hertzman AB, Roth LW. The vasomotor components in the vascular reactions in the finger to cold. *Am J Physiol.* 1942a;136:669-679.
47. Hertzman AB, Roth LW. The reactions of the digital artery and minute pad arteries to local cold. *Am J Physiol.* 1942b;136:680-691.
48. Hertzman AB, Roth LW. The absence of vasoconstrictor reflexes in the forehead circulation: effects of cold. *Am J Physiol.* 1942c;136:692-697.
49. Hertzman AB, Dillon JB. Distinction between arterial, venous and flow components in photoelectric plethysmography in man. *Am J Physiol.* 1940a;130:177-185.
50. Hertzman AB, Dillon JB. Applications of photoelectric plethysmography in peripheral vascular disease. *Am Heart J.* 1940b;20:750-761.
51. Senay LC, Jr., Christensen M, Hertzman AB. Cutaneous vascular responses in finger and forearm during rising ambient temperatures. *J Appl Physiol.* 1960;15:611-618.

52. Hertzman AB, Flath F. The continuous simultaneous registration of sweating and blood flow in a small skin area. *Aerosp Med.* 1963;34:710-713.
53. Ben-Hur N, Mahler Y, Shulman J, Neuman Z. A study of the peripheral blood flow in skin tubed flaps by photoconductive plethysmography. *Isr J Med Sci.* 1966;2(2):218-225.
54. Muir IF, Fox RH, Stranc WE, Stewart FS. The measurement of blood flow by a photoelectric technique and its application to the management of tubed skin pedicles. *Br J Plast Surg.* 1968;21(1):14-31.
55. Thorne FL, Georgiade NG, Wheeler WF, Mladick RA. Photoplethysmography as an aid in determining the viability of pedicle flaps. *Plast Reconstr Surg.* 1969 44(3):279-284.
56. Aoyagi T, Kiahi M, Yamaguchi K, Watanabe S. Improvement of the earpiece oximeter. *Abstracts of the 13th Annual Meeting of the Japanese Society of Medical Electronics and Biological Engineering.* 1974:90-91.
57. Yoshiya I, Shimada Y, Tanaka K. Spectrophotometric monitoring of arterial oxygen saturation in the fingertip. *Med Biol Eng Comput.* 1980;18(1):27-32.
58. Wieringa FP, Mastik F, van der Steen AF. Contactless multiple wavelength photoplethysmographic imaging: a first step toward "SpO2 camera" technology. *Ann Biomed Eng.* 2005;33(8):1034-1041.
59. Hu S, Zheng J, Chouliaras V, Summers R. Feasibility of imaging photoplethysmography. *International Conference on BioMedical Engineering and Informatics.* Sanya, Hainan, China; 2008:72-75.
60. Allen J. Photoplethysmography and its application in clinical physiological measurement. *Physiol Meas.* 2007;28(3):R1-39.
61. Webster JG. *Design of pulse oximeters.* Bristol: Institute of Physics Publishing; 1997.
62. Cheang PYS, Smith PR. An overview of non-contact photoplethysmography. *Loughborough University Department of Electrical and Electronic Engineering ESC Division Research Report.* 2003:57-59.
63. Kelleher JF. Pulse oximetry. *J Clin Monit.* 1989;5(1):37-62.
64. Severinghaus JW, Kelleher JF. Recent developments in pulse oximetry. *Anesthesiology.* 1992;76(6):1018-1038.
65. Kyriacou PA. Pulse oximetry in the oesophagus. *Physiol Meas.* 2006;27(1):R1-35.

66. Drummond GB, Park GR. Arterial Oxygen-Saturation before Intubation of the Trachea - an Assessment of Oxygenation Techniques. *Br J Anaesth*. 1984;56(9):987-993.
67. Short L, Hecker RB, Middaugh RE, Menk EJ. A comparison of pulse oximeters during helicopter flight. *J Emerg Med*. 1989;7(6):639-643.
68. Johnson N, Johnson VA, Fisher J, Jobbings B, Bannister J, Lilford RJ. Fetal monitoring with pulse oximetry. *Br J Obstet Gynaecol*. 1991;98(1):36-41.
69. Meierstaus P, Bucher HU, Hurlimann R, Konig V, Huch R. Pulse Oximetry Used for Documenting Oxygen-Saturation and Right-to-Left Shunting Immediately after Birth. *Eur J Pediatr*. 1990;149(12):851-855.
70. Hovagim AR, Vitkun SA, Manecke GR, Reiner R. Arterial oxygen desaturation in adult dental patients receiving conscious sedation. *J Oral Maxillofac Surg*. 1989;47(9):936-939.
71. Trang H, Boureghda S, Leske V. Sleep desaturation: Comparison of two oximeters. *Pediatric Pulmonology*. 2004;37(1):76-80.
72. Chan D, Hayes M, Smith PR. Venous Pulse Oximetry. *World Patent WO 03/063697*. 2003.
73. Echiadis A, Crabtree VP, Smith PR. VENOX technology implementation. *Loughborough University Department of Electrical and Electronic Engineering ESC Division Research Report*. 2005:31-34.
74. Peñáz J. Photoelectric measurement of blood pressure, volume, and flow in the finger. *Digest 10th Int Conf Med Biol Eng*. Dresden, Germany; 1973:104.
75. Chen W, Kobayashi T, Ichikawa S, Takeuchi Y, Togawa T. Continuous estimation of systolic blood pressure using the pulse arrival time and intermittent calibration. *Med Biol Eng Comput*. 2000;38(5):569-574.
76. Naschitz JE, Bezobchuk S, Mussafia-Priselac R, Sundick S, Dreyfuss D, Khorshidi I, Karidis A, Manor H, Nagar M, Peck ER, Peck S, Storch S, Rosner I, Gaitini L. Pulse transit time by R-wave-gated infrared photoplethysmography: review of the literature and personal experience. *J Clin Monit Comput*. 2004;18(5-6):333-342.
77. Kim JS, Chee YJ, Park JW, Choi JW, Park KS. A new approach for non-intrusive monitoring of blood pressure on a toilet seat. *Physiol Meas*. 2006;27(2):203-211.
78. Millasseau SC, Guigui FG, Kelly RP, Prasad K, Cockcroft JR, Ritter JM, Chowienczyk PJ. Noninvasive assessment of the digital volume pulse. Comparison with the peripheral pressure pulse. *Hypertension*. 2000;36(6):952-956.

79. Lindberg LG, Ugnell H, Oberg PA. Monitoring of respiratory and heart rates using a fiberoptic sensor. *Med Biol Eng Comput.* 1992;30(5):533-537.
80. Nilsson L, Johansson A, Kalman S. Monitoring of respiratory rate in postoperative care using a new photoplethysmographic technique. *J Clin Monit Comput.* 2000;16(4):309-315.
81. Johansson A. Neural network for photoplethysmographic respiratory rate monitoring. *Med Biol Eng Comput.* 2003;41(3):242-248.
82. Dorlas JC, Nijboer JA. Photo-electric plethysmography as a monitoring device in anaesthesia. Application and interpretation. *Br J Anaesth.* 1985;57(5):524-530.
83. Johansson A, Oberg PA. Estimation of respiratory volumes from the photoplethysmographic signal. Part 2: A model study. *Med Biol Eng Comput.* 1999;37(1):48-53.
84. Azabji Kenfack M, Lador F, Licker M, Moia C, Tam E, Capelli C, Morel D, Ferretti G. Cardiac output by Modelflow method from intra-arterial and fingertip pulse pressure profiles. *Clin Sci (Lond).* 2004;106(4):365-369.
85. Hyman C, Winsor T. History of plethysmography. *J Cardiovasc Surg (Torino).* 1961;2:506-518.
86. Heck AF, Hall VR. An on-line system for measurement of opacity pulse propagation times in atraumatic screening of patients for occlusive vascular disease. *Med Instrum.* 1975;9(2):88-92.
87. Osmundson PJ, O'Fallon WM, Clements IP, Kazmier FJ, Zimmerman BR, Palumbo PJ. Reproducibility of noninvasive tests of peripheral occlusive arterial disease. *J Vasc Surg.* 1985;2(5):678-683.
88. Kvernebo K, Megerman J, Hamilton G, Abbott WM. Response of skin photoplethysmography, laser Doppler flowmetry and transcutaneous oxygen tensiometry to stenosis-induced reductions in limb blood flow. *Eur J Vasc Surg.* 1989;3(2):113-120.
89. Allen J, Murray A. Age-related changes in peripheral pulse timing characteristics at the ears, fingers and toes. *J Hum Hypertens.* 2002;16(10):711-717.
90. Allen J, Murray A. Age-related changes in the characteristics of the photoplethysmographic pulse shape at various body sites. *Physiol Meas.* 2003;24(2):297-307.
91. Allen J, Oates CP, Lees TA, Murray A. Photoplethysmography detection of lower limb peripheral arterial occlusive disease: a comparison of pulse timing, amplitude and shape characteristics. *Physiol Meas.* 2005;26(5):811-821.

92. Allen J, Overbeck K, Stansby G, Murray A. Photoplethysmography assessments in cardiovascular disease. *Measurement & Control*. 2006;39(3):80-83.
93. Chowienczyk PJ, Kelly RP, MacCallum H, Millasseau SC, Andersson TL, Gosling RG, Ritter JM, Anggard EE. Photoplethysmographic assessment of pulse wave reflection: blunted response to endothelium-dependent beta2-adrenergic vasodilation in type II diabetes mellitus. *J Am Coll Cardiol*. 1999;34(7):2007-2014.
94. Gopaul NK, Manraj MD, Hebe A, Lee Kwai Yan S, Johnston A, Carrier MJ, Anggard EE. Oxidative stress could precede endothelial dysfunction and insulin resistance in Indian Mauritians with impaired glucose metabolism. *Diabetologia*. 2001;44(6):706-712.
95. Cooke ED, Bowcock SA, Smith AT. Photoplethysmography of the distal pulp in the assessment of the vasospastic hand. *Angiology*. 1985;36(1):33-40.
96. Abramowitz HB, Queral LA, Finn WR, Nora PF, Jr., Peterson LK, Bergan JJ, Yao JS. The use of photoplethysmography in the assessment of venous insufficiency: a comparison to venous pressure measurements. *Surgery*. 1979;86(3):434-441.
97. Murray WB, Foster PA. The peripheral pulse wave: information overlooked. *J Clin Monit*. 1996;12(5):365-377.
98. Rauh R, Posfay A, Muck-Weymann M. Quantification of inspiratory-induced vasoconstrictive episodes: a comparison of laser Doppler fluxmetry and photoplethysmography. *Clin Physiol Funct Imaging*. 2003;23(6):344-348.
99. Kistler A, Mariauzouls C, von Berlepsch K. Fingertip temperature as an indicator for sympathetic responses. *Int J Psychophysiol*. 1998;29(1):35-41.
100. Nasimi SG, Mearns AJ, Harness JB, Heath I. Quantitative measurement of sympathetic neuropathy in patients with diabetes mellitus. *J Biomed Eng*. 1991;13(3):203-208.
101. Nasimi SG, Harness JB, Marjanovic DZ, Knight T, Mearns AJ. Periodic posture stimulation of the baroreceptors and the local vasomotor reflexes. *J Biomed Eng*. 1992;14(4):307-312.
102. Linder SP, Wendelken SM, Wei E, McGrath SP. Using the morphology of photoplethysmogram peaks to detect changes in posture. *J Clin Monit Comput*. 2006;20(3):151-158.
103. Avnon Y, Nitzan M, Sprecher E, Rogowski Z, Yarnitsky D. Different patterns of parasympathetic activation in uni- and bilateral migraineurs. *Brain*. 2003;126(Pt 7):1660-1670.

104. Avnon Y, Nitzan M, Sprecher E, Rogowski Z, Yarnitsky D. Autonomic asymmetry in migraine: augmented parasympathetic activation in left unilateral migraineurs. *Brain*. 2004;127(Pt 9):2099-2108.
105. Komatsu K, Fukutake T, Hattori T. Fingertip photoplethysmography and migraine. *J Neurol Sci*. 2003;216(1):17-21.
106. Johansson A, Oberg PA, Sedin G. Monitoring of heart and respiratory rates in newborn infants using a new photoplethysmographic technique. *J Clin Monit Comput*. 1999;15(7-8):461-467.
107. Millasseau SC, Ritter JM, Takazawa K, Chowienczyk PJ. Contour analysis of the photoplethysmographic pulse measured at the finger. *J Hypertens*. 2006;24(8):1449-1456.
108. Dillon JB, Hertzman AB. The form of the volume pulse in the finger pad in health, arteriosclerosis, and hypertension. *Am Heart J*. 1941;21:172-190.
109. Miyai N, Miyashita K, Arita M, Morioka I, Kamiya K, Takeda S. Noninvasive assessment of arterial distensibility in adolescents using the second derivative of photoplethysmogram waveform. *Eur J Appl Physiol*. 2001;86(2):119-124.
110. Hashimoto J, Chonan K, Aoki Y, Nishimura T, Ohkubo T, Hozawa A, Suzuki M, Matsubara M, Michimata M, Araki T, Imai Y. Pulse wave velocity and the second derivative of the finger photoplethysmogram in treated hypertensive patients: their relationship and associating factors. *J Hypertens*. 2002;20(12):2415-2422.
111. Millasseau SC, Kelly RP, Ritter JM, Chowienczyk PJ. The vascular impact of aging and vasoactive drugs: comparison of two digital volume pulse measurements. *Am J Hypertens*. 2003;16(6):467-472.
112. Takazawa K, Fujita M, Yabe K, Sakai T, Kobayashi T, Maeda K, Yamashita Y, Hase M, Ibukiyama C. Clinical usefulness of the second derivative of a plethysmogram (acceleration plethysmogram). *J Cardiol*. 1993;23(suppl 37):207-217.
113. Allen J, Murray A. Development of a neural network screening aid for diagnosing lower limb peripheral vascular disease from photoelectric plethysmography pulse waveforms. *Physiol Meas*. 1993;14(1):13-22.
114. Allen J, Murray A. Comparison of three arterial pulse waveform classification techniques. *J Med Eng Technol*. 1996;20(3):109-114.
115. Friedman BH, Thayer JF. Autonomic balance revisited: panic anxiety and heart rate variability. *J Psychosom Res*. 1998;44(1):133-151.
116. Levy MN. Autonomic interactions in cardiac control. *Ann N Y Acad Sci*. 1990;601:209-221.

117. Rugh KS, Jiang B, Hatfield D, Garner HE, Hahn AW. Cardiac cycle length variability in ponies at rest and during exercise. *J Appl Physiol.* 1992;73(4):1572-1577.
118. Hon EH, Lee ST. Electronic Evaluation of the Fetal Heart Rate. Viii. Patterns Preceding Fetal Death, Further Observations. *Am J Obstet Gynecol.* 1963;87:814-826.
119. Sinnreich R, Kark JD, Friedlander Y, Sapoznikov D, Luria MH. Five minute recordings of heart rate variability for population studies: repeatability and age-sex characteristics. *Heart.* 1998;80(2):156-162.
120. Shannon DC, Carley DW, Benson H. Aging of modulation of heart rate. *Am J Physiol.* 1987;253(4 Pt 2):H874-877.
121. Liao D, Barnes RW, Chambless LE, Simpson RJ, Jr., Sorlie P, Heiss G. Age, race, and sex differences in autonomic cardiac function measured by spectral analysis of heart rate variability--the ARIC study. Atherosclerosis Risk in Communities. *Am J Cardiol.* 1995;76(12):906-912.
122. Nakagawa M, Iwao T, Ishida S, Yonemochi H, Fujino T, Saikawa T, Ito M. Circadian rhythm of the signal averaged electrocardiogram and its relation to heart rate variability in healthy subjects. *Heart.* 1998;79(5):493-496.
123. Yasuma F, Hayano J. Respiratory sinus arrhythmia: why does the heartbeat synchronize with respiratory rhythm? *Chest.* 2004;125(2):683-690.
124. Tulppo MP, Makikallio TH, Seppanen T, Laukkanen RT, Huikuri HV. Vagal modulation of heart rate during exercise: effects of age and physical fitness. *Am J Physiol.* 1998;274(2 Pt 2):H424-429.
125. Montano N, Ruscone TG, Porta A, Lombardi F, Pagani M, Malliani A. Power spectrum analysis of heart rate variability to assess the changes in sympathovagal balance during graded orthostatic tilt. *Circulation.* 1994;90(4):1826-1831.
126. Davy KP, Miniclier NL, Taylor JA, Stevenson ET, Seals DR. Elevated heart rate variability in physically active postmenopausal women: a cardioprotective effect? *Am J Physiol.* 1996;271(2 Pt 2):H455-460.
127. Coumel P, Hermida JS, Wennerblom B, Leenhardt A, Maison-Blanche P, Cauchemez B. Heart rate variability in left ventricular hypertrophy and heart failure, and the effects of beta-blockade. A non-spectral analysis of heart rate variability in the frequency domain and in the time domain. *Eur Heart J.* 1991;12(3):412-422.
128. Malik M, Farrell T, Cripps T, Camm AJ. Heart rate variability in relation to prognosis after myocardial infarction: selection of optimal processing techniques. *Eur Heart J.* 1989;10(12):1060-1074.

129. Malik M, Xia R, Odemuyiwa O, Staunton A, Poloniecki J, Camm AJ. Influence of the recognition artefact in automatic analysis of long-term electrocardiograms on time-domain measurement of heart rate variability. *Med Biol Eng Comput.* 1993;31(5):539-544.
130. Akselrod S, Gordon D, Ubel FA, Shannon DC, Berger AC, Cohen RJ. Power spectrum analysis of heart rate fluctuation: a quantitative probe of beat-to-beat cardiovascular control. *Science.* 1981;213(4504):220-222.
131. Pagani M, Lombardi F, Guzzetti S, Rimoldi O, Furlan R, Pizzinelli P, Sandrone G, Malfatto G, Dell'Orto S, Piccaluga E, et al. Power spectral analysis of heart rate and arterial pressure variabilities as a marker of sympatho-vagal interaction in man and conscious dog. *Circ Res.* 1986;59(2):178-193.
132. Malliani A, Pagani M, Lombardi F, Cerutti S. Cardiovascular neural regulation explored in the frequency domain. *Circulation.* 1991;84(2):482-492.
133. Woo MA, Stevenson WG, Moser DK, Trelease RB, Harper RM. Patterns of beat-to-beat heart rate variability in advanced heart failure. *Am Heart J.* 1992;123(3):704-710.
134. Kamen PW, Tonkin AM. Application of the Poincare plot to heart rate variability: a new measure of functional status in heart failure. *Aust N Z J Med.* 1995;25(1):18-26.
135. Huikuri HV, Seppanen T, Koistinen MJ, Airaksinen J, Ikaheimo MJ, Castellanos A, Myerburg RJ. Abnormalities in beat-to-beat dynamics of heart rate before the spontaneous onset of life-threatening ventricular tachyarrhythmias in patients with prior myocardial infarction. *Circulation.* 1996;93(10):1836-1844.
136. Kamen PW, Krum H, Tonkin AM. Poincare plot of heart rate variability allows quantitative display of parasympathetic nervous activity in humans. *Clin Sci (Lond).* 1996;91(2):201-208.
137. Tulppo MP, Makikallio TH, Takala TE, Seppanen T, Huikuri HV. Quantitative beat-to-beat analysis of heart rate dynamics during exercise. *Am J Physiol.* 1996;271(1 Pt 2):H244-252.
138. Eckmann JP, Kamphorst SO, Ruelle D. Recurrence Plots of Dynamic-Systems. *Europhysics Letters.* 1987;4(9):973-977.
139. Mendelson Y. Pulse oximetry: theory and applications for noninvasive monitoring. *Clin Chem.* 1992;38(9):1601-1607.
140. Feng S, Zeng F, Chance B. Photon migration in the presence of a single defect: a perturbation analysis. *Appl Opt.* 1995;34(19):3826-3837

141. Mitra SK. *Digital signal processing: a computer based approach*. Vol 1st edition: New York, McGraw Hill Companies; 1998.
142. Karakaya O, Barutcu I, Kaya D, Esen AM, Saglam M, Melek M, Onrat E, Turkmen M, Esen OB, Kaymaz C. Acute effect of cigarette smoking on heart rate variability. *Angiology*. 2007;58(5):620-624.
143. Welch PD. The use of fast Fourier transforms for the estimation of power spectra: A method based on time averaging over short modified periodograms. *IEEE Transactions on Audio and Electroacoustics*. 1967;15(2):70-73.
144. Brennan M, Palaniswami M, Kamen P. Do existing measures of Poincare plot geometry reflect nonlinear features of heart rate variability? *IEEE Trans Biomed Eng*. 2001;48(11):1342-1347.
145. Radespiel-Troger M, Rauh R, Mahlke C, Gottschalk T, Muck-Weymann M. Agreement of two different methods for measurement of heart rate variability. *Clin Auton Res*. 2003;13(2):99-102.
146. Bland JM, Altman DG. Statistical method for assessing agreement between two methods of clinical measurement. *The Lancet*. 1986;1:307-310.
147. Bland JM, Altman DG. Measuring agreement in method comparison studies. *Stat Methods Med Res*. 1999;8(2):135-160.
148. Woo MA, Stevenson WG, Moser DK, Middlekauff HR. Complex heart rate variability and serum norepinephrine levels in patients with advanced heart failure. *J Am Coll Cardiol*. 1994;23(3):565-569.
149. Qiu Y, Cai Y, Zhu Y, Cheang PYS, Crabtree V, Smith P, Hu S. Poincare plot analysis for pulse interval extracted from non-contact photoplethysmography. *Conf Proc IEEE Eng Med Biol Soc*. 2005;2:1964-1967.
150. Guzik P, Piskorski J, Krauze T, Schneider R, Wesseling KH, Wykretowicz A, Wysocki H. Correlations between the Poincare plot and conventional heart rate variability parameters assessed during paced breathing. *J Physiol Sci*. 2007;57(1):63-71.
151. Eliakim M, Sapoznikov D, Weinman J. Pulse wave velocity in healthy subjects and in patients with various disease states. *Am Heart J*. 1971;82(4):448-457.
152. Morikawa Y. Characteristic pulse wave caused by organic nitrates. *Nature*. 1967;213(5078):841-842.
153. Morikawa Y, Matsuzaka J, Kuratsune M, Tsukamoto S, Makisumi S. Plethysmographic study of effects of alcohol. *Nature*. 1968;220(5163):186-187.

154. Nichols WW, O'Rourke MF. *McDonald's blood flow in arteries. Theoretical, experimental and clinical principles*: London: Arnold; 1998.
155. Van Bortel LM, Struijker-Boudier HA, Safar ME. Pulse pressure, arterial stiffness, and drug treatment of hypertension. *Hypertension*. 2001;38(4):914-921.
156. Nichols WW. Clinical measurement of arterial stiffness obtained from noninvasive pressure waveforms. *Am J Hypertens*. 2005;18(1 Pt 2):3S-10S.
157. Millasseau SC, Kelly RP, Ritter JM, Chowienczyk PJ. Determination of age-related increases in large artery stiffness by digital pulse contour analysis. *Clin Sci (Lond)*. 2002;103(4):371-377.
158. Ahimastos AA, Formosa M, Dart AM, Kingwell BA. Gender differences in large artery stiffness pre- and post puberty. *J Clin Endocrinol Metab*. 2003;88(11):5375-5380.
159. Gangar KF, Vyas S, Whitehead M, Crook D, Meire H, Campbell S. Pulsatility index in internal carotid artery in relation to transdermal oestradiol and time since menopause. *Lancet*. 1991;338(8771):839-842.
160. Brumfield AM, Andrew ME. Digital pulse contour analysis: investigating age-dependent indices of arterial compliance. *Physiol Meas*. 2005;26(5):599-608.
161. Constant I, Laude D, Murat I, Elghozi JL. Pulse rate variability is not a surrogate for heart rate variability. *Clin Sci (Lond)*. 1999;97(4):391-397.
162. Miller IF, Yeates DB, Wong LB. Heart Rate Variability Analysis: Promise and Fulfilment. *Business Briefing: Global Healthcare—Advanced Medical Technologied*. 2004.
163. Chandra T, Yeates DB, Wong L. *Heart Rate Variability Analysis - Current and Future Trends*: World Medical Association (WMA) 2003.
164. Narkiewicz K, van de Borne PJ, Hausberg M, Cooley RL, Winniford MD, Davison DE, Somers VK. Cigarette smoking increases sympathetic outflow in humans. *Circulation*. 1998;98(6):528-534.
165. Mancia G, Groppelli A, Di Rienzo M, Castiglioni P, Parati G. Smoking impairs baroreflex sensitivity in humans. *Am J Physiol*. 1997;273(3 Pt 2):H1555-1560.
166. Hayano J, Yamada M, Sakakibara Y, Fujinami T, Yokoyama K, Watanabe Y, Takata K. Short- and long-term effects of cigarette smoking on heart rate variability. *Am J Cardiol*. 1990;65(1):84-88.

167. Lerma C, Infante O, Perez-Grovas H, Jose MV. Poincare plot indexes of heart rate variability capture dynamic adaptations after haemodialysis in chronic renal failure patients. *Clin Physiol Funct Imaging*. 2003;23(2):72-80.
168. Otzenberger H, Gronfier C, Simon C, Charloux A, Ehrhart J, Piquard F, Brandenberger G. Dynamic heart rate variability: a tool for exploring sympathovagal balance continuously during sleep in men. *Am J Physiol*. 1998;275(3 Pt 2):H946-950.
169. Brennan M, Palaniswami M, Kamen P. Poincare plot interpretation using a physiological model of HRV based on a network of oscillators. *Am J Physiol Heart Circ Physiol*. 2002;283(5):H1873-1886.
170. Barker SJ, Hyatt J, Shah NK, Kao YJ. The effect of sensor malpositioning on pulse oximeter accuracy during hypoxemia. *Anesthesiology*. 1993;79(2):248-254.
171. Okada E, Firbank M, Schweiger M, Arridge SR, Cope M, Delpy DT. Theoretical and experimental investigation of near-infrared light propagation in a model of the adult head. *Appl Opt*. 1997;36(1):21-31.
172. Teng XF, Zhang YT. The effect of contacting force on photoplethysmographic signals. *Physiol Meas*. 2004;25(5):1323-1335.
173. Marwan N, Romano MC, Thiel M, Kurths J. Recurrence plots for the analysis of complex systems. *Physics Reports-Review Section of Physics Letters*. 2007;438(5-6):237-329.
174. Marwan N, Wessel N, Meyerfeldt U, Schirdewan A, Kurths J. Recurrence-plot-based measures of complexity and their application to heart-rate-variability data. *Phys Rev E Stat Nonlin Soft Matter Phys*. 2002;66(2 Pt 2):026702.